

# Experimental Investigation of Fused Biconical Fiber Couplers for Measuring Refractive Index Changes in Aqueous Solutions

Marco V. Hernández-Arriaga, Miguel A. Bello-Jiménez, A. Rodríguez-Cobos,  
and Miguel V. Andrés, *Member, IEEE*

**Abstract**—A detailed experimental study of a simple and compact fiber optic sensor based on a fused biconical fiber coupler is presented, in which the sensitivity is improved by operating the coupler beyond the first coupling cycle. The sensor is demonstrated to perform high sensitivity measurements of refractive index changes by means of variation of sugar concentration in water. The device is operated to achieve a linear transmission response, allowing a linear relation between the sugar concentration and the output signal. The initial sensitivity was measured as 0.03 units of normalized transmission per unit of sugar concentration (g/100 mL), with a noise detection limit of a sugar concentration of 0.06 wt% of sugar concentration. Improvements in sensitivity were studied by operating the coupler beyond their first coupling cycles; achieving an improved sensitivity of 0.15 units of normalized transmission per unit of sugar concentration, and a minimum detection limit of 0.012 wt% of sugar concentration. From this result, the minimum detectable refractive index change is estimated as  $2 \times 10^{-5}$  refractive index unit.

**Index Terms**—Fiber optic sensor, fused biconical fiber coupler, refractive index sensor.

## I. INTRODUCTION

FIBER-OPTIC couplers have attracted considerable attention in recent years for their ability to detect small changes in the refractive index (RI) of liquid solutions. A fiber coupler is a four-port device with a transmission spectrum that is strongly affected by the refractive index of the surrounding medium due to the evanescent field that is generated along the coupling region [1]. This effect has proven to be useful for sensing applications [2]. Recent approaches of fiber-coupler based RI sensors include fused biconical fiber couplers [3]–[7], optical microfibers [8]–[12], photonic crystal fibers [13], [14], and specially designed

two-core optical fibers [15], [16], all of them offering the advantages of high sensitivity, *in situ* measurements, compact size, and immunity to external electromagnetic interference. Most of these sensors are codified in wavelength and the achieved sensitivities are in the range of 1,125 to 30,100 nanometer (nm) per refractive index unit (RIU), with a minimum detection limit of  $4 \times 10^{-4}$  to  $4 \times 10^{-7}$  RIU, respectively.

From the point of view of implementation, the necessity of expensive equipment, such as optical spectrum analyzers, for measuring the shift in wavelength heavily affects the use of fiber-coupler based RI sensors. Thus, it is worthwhile to consider an alternative scheme based on the dependence of the power coupling on the surrounding medium. The two complementary outputs of a fiber coupler enable a straightforward normalization, i.e. the ratio between the difference and the addition, which automatically compensates for power fluctuations. In earlier works the dependence of the power coupling of traditional fused biconical tapered couplers on the external RI has been presented and it has been proposed that it is possible to use such a structure to develop a fiber based refractometer [1], [17]. Tazawa et al. [2] have implemented this power measurement approach to demonstrate a biosensor with estimated  $4 \times 10^{-6}$  RIU detection limit. Recently, it has been demonstrated that modal interferometers based on integrated waveguides provide one of the best resolutions ever reported ( $2.5 \times 10^{-7}$  RIU) [18]. A fused biconical couplers is, in fact, a modal interferometer in which the phase difference between the symmetric and antisymmetric supermodes determine the power distribution at the output fibers. Small changes of the external RI do not modify substantially the coupling coefficient, but they generate a significant phase difference between supermodes. In terms of fiber-coupler based RI sensors, this last point deserves particular attention for the detection of slight changes in the refractive index of aqueous solutions. Although several schemes have reported this effect [1], [2], [17], they did not study the conditions for an optimal performance of the reported device. Here our purpose is the experimental analysis of a fused biconical fiber coupler, operated beyond the first coupling cycle, with a power transmission that depends on the surrounding medium.

The objective is not only to gain insights into the dynamics of this kind of device, but also looking forwards an improvement of its performance. Based on this motivation, the

Manuscript received July 10, 2015; revised August 26, 2015; accepted August 27, 2015. Date of publication September 16, 2015; date of current version December 10, 2015. This work was supported in part by Promep under Grant DSA/103.5/14/10476 and in part by the Consejo Nacional de Ciencia y Tecnología under Grant 206425 and Grant 222476. The associate editor coordinating the review of this paper and approving it for publication was Dr. Anna G. Mignani.

M. V. Hernández-Arriaga, M. A. Bello-Jiménez, and A. Rodríguez-Cobos are with the Instituto de Investigación en Comunicación Óptica, Universidad Autónoma de San Luis Potosí, San Luis Potosí 78210, Mexico (e-mail: dmxsol@hotmail.com; m.bello@cactus.iico.uaslp.mx; roca@cactus.iico.uaslp.mx).

M. V. Andrés is with the Departamento de Física Aplicada y Electromagnetismo, Institute of Materials Science, Universidad de Valencia, Valencia 46100, Spain (e-mail: miguel.andres@uv.es).

Digital Object Identifier 10.1109/JSEN.2015.2475320



# Nanostructure formation during relatively high temperature growth of Mn-doped GaAs by molecular beam epitaxy



A. Del Río-De Santiago<sup>a</sup>, V.H. Méndez-García<sup>a</sup>, I. Martínez-Velis<sup>b</sup>, Y.L. Casallas-Moreno<sup>b</sup>, E. López-Luna<sup>a</sup>, A. Yu Gorbachev<sup>c</sup>, M. López-López<sup>b</sup>, E. Cruz-Hernández<sup>a,\*</sup>

<sup>a</sup> CIACyT-UASLP, Sierra Leona Av. # 550, Lomas 2a Secc, San Luis Potosí, S.L.P. 78210, México

<sup>b</sup> Physics Department, CINVESTAV-IPN, Apdo. Postal 14470 D. F. México, México

<sup>c</sup> IICO-UASLP, Av. Karakorum 1470, Lomas 4a. Sección, San Luis Potosí, S.L.P. 78210, México

## ARTICLE INFO

### Article history:

Received 31 July 2014

Received in revised form 29 January 2015

Accepted 29 January 2015

Available online 7 February 2015

### Keywords:

MBE

GaMnAs

Nanostructures

Photoluminescence

Electrical properties

High temperature

## ABSTRACT

In the present work, we report on molecular beam epitaxy growth of Mn-doped GaAs films at the relatively high temperature (HT) of 530 °C. We found that by increasing the Mn atomic percent, Mn%, from 0.01 to 0.2, the surface morphology of the samples is strongly influenced and changes from planar to corrugated for Mn% values from 0.01 to 0.05, corresponding to nanostructures on the surface with dimensions of 200–300 nm and with the shape of leave, to nanowire-like structures for Mn% values above 0.05. From reflection high-energy electron diffraction patterns, we observed the growth mode transition from two- to three-dimensional occurring at a Mn% exceeding 0.05. The optical and electrical properties were obtained from photoluminescence (PL) and Hall effect measurements, respectively. For the higher Mn concentration, besides the Mn related transitions at approximately 1.41 eV, PL spectra sharp peaks are present between 1.43 and 1.49 eV, which we related to the coexistence of zinc blende and wurtzite phases in the nanowire-like structures of this sample. At Mn% of 0.04, an increase of the carrier mobility up to a value of  $1.1 \times 10^3 \text{ cm}^2/\text{Vs}$  at 77 K was found, then decreases as Mn% is further increased due to the strengthening of the ionized impurity scattering.

© 2015 Elsevier B.V. All rights reserved.

## 1. Introduction

Since the first successful growth of GaMnAs by molecular-beam epitaxy (MBE) showing ferromagnetic behavior [1–3], this diluted magnetic semiconductor (DMS) has received extensive attention because of the interest in the integration of both carrier induced ferromagnetism and spin-electronics with the existing semiconductor technology. However, these potential applications have been limited because of the low solubility of the Mn atoms, on the order of  $10^{18} \text{ cm}^{-3}$  or less, in the GaAs semiconductor matrix [4,5]. So far, the low-temperature (LT) MBE technique, below 300 °C, is the best method for the preparation of such materials with Mn concentrations many times higher than solubility. Unfortunately, LT-MBE and a high Mn concentration are characterized by a high content of point defects, such as As antisites and Mn interstitials [6,7] and by the poor crystallinity. Even when these defects can be reduced by optimizing the growth LT conditions or by post-growth annealing processes [7,8], the number of defects remains

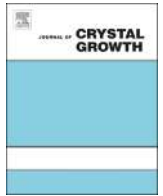
elevated relative to GaAs films grown at relatively high temperature (HT) MBE (>500 °C). Successful growth of high crystalline quality GaMnAs at HT possesses a high potential for incorporating the ferromagnetic GaMnAs layers into GaAs-based microelectronic and optoelectronic devices. However, by growing at HT, precipitation of MnAs clusters in a GaMnAs matrix has been observed [9,10]. In addition, due to the inherent inhibition of uniform growth of GaMnAs with high Mn concentrations, little work has been published regarding HT MBE [11–13]. Despite this drawback, the number of As<sub>Ga</sub> in GaMnAs has been found to be reduced by increasing the substrate temperature ( $T_S$ ) [12,13]. Moreover, by growing at intermediate temperatures (IT), from 325 to 500 °C, some authors have been able to improve the optical properties of Mn-doped GaAs layers compared to LT GaMnAs [14,15]. In this paper, to gain more insight into relatively HT GaMnAs, we present a study of Mn-doped GaAs layers prepared by varying the nominal Mn atomic percent (Mn%) from 0.01 to 0.2 at a temperature of 530 °C.

## 2. Experimental

The samples were grown by MBE using solid sources onto epitaxial GaAs (001) substrates. After growing a five-period AlAs

\* Corresponding author. Tel.: +52 4448262300.

E-mail address: [esteban.cruz@uaslp.mx](mailto:esteban.cruz@uaslp.mx) (E. Cruz-Hernández).



## Si-doped AlGaAs/GaAs(6 3 1)A heterostructures grown by MBE as a function of the As-pressure



Víctor-Hugo Méndez-García<sup>a,\*</sup>, S. Shimomura<sup>b</sup>, A.Yu. Gorbachev<sup>c</sup>,  
E. Cruz-Hernández<sup>a</sup>, D. Vázquez-Cortés<sup>b</sup>

<sup>a</sup> Center for the Innovation and Application of Science and Technology, Universidad Autónoma de San Luis Potosí, Av. Sierra Leona # 550, Col. Lomas 2a Sección, C.P. 78210 San Luis Potosí, Mexico

<sup>b</sup> Graduate School of Science and Engineering, Ehime University, 3 Bukyo-cho, Matsuyama 790-8577, Ehime, Japan

<sup>c</sup> Instituto de Investigación en Comunicación Óptica, Universidad Autónoma de San Luis Potosí, Av. Karakorum # 1470, Col. Lomas 2a Secc., C.P. 78210 San Luis Potosí, Mexico

### ARTICLE INFO

Available online 2 April 2015

#### Keywords:

A1. Atomic force microscopy  
A1. Impurities  
A1. Characterization  
A3. Molecular beam epitaxy  
B2. Semiconducting gallium compounds

### ABSTRACT

The effects of doping with silicon (Si) AlGaAs layers grown by molecular beam epitaxy on GaAs (6 3 1)-oriented substrates as a function of the arsenic pressure ( $P_{As}$ ) is presented and compared with layers grown on (1 0 0) oriented substrates. The surface texture of the AlGaAs (6 3 1) films is composed by nanogrooves, whose dimensions depend on  $P_{As}$ . On the contrary, the MBE growth on the (1 0 0) plane resulted on rough surfaces, without evidence of formation of terraces. Mobility and carrier density of AlGaAs:Si layers grown on substrates (6 3 1) were studied as a function of  $P_{As}$ . The doping type conversion from p-type to n-type as a function of the As pressure is corroborated for high index samples. All the films grown on (1 0 0) exhibited silicon n-type doping. These observations were related with the amphotericity of Si, where it acts as a donor impurity occupying Al or Ga-sites or as an acceptor when it takes an As-site, depending on the competition that the Si atoms encounters with As for any of these sites. The acceptor and donor lines close to the AlGaAs transition observed by photoluminescence spectroscopy (PL) were affected by the incorporation of Si. When increasing  $P_{As}$  the energy of the main PL peak is redshifted for n-type AlGaAs layers, but it is shifted back towards high energy once the conduction type conversion takes place. X-ray diffraction patterns revealed high crystalline quality for samples grown at the highest  $P_{As}$ .

© 2015 Elsevier B.V. All rights reserved.

### 1. Introduction

Recently nanotechnology is generating new technological developments and it is envisaged as the most powerful and promising engine for the development of the society. In this emerging area, nanostructured materials are investigated for applications in electronics, optoelectronic and electro-mechanical devices. For example, semiconductor nanowires (NWRs) have emerged as one of the most versatile building blocks for integration of nanoscale devices with current technology. In addition, NWRs has been used for the investigation of basic aspects of one-dimensional systems (1D) [1–4]. In this direction, the growth of semiconductor materials on high-index substrates is a very important subject since it has been proved that, under suitable growth conditions, nanoscale step arrays and

nanogrooves can be self-assembled and later employed as templates for the synthesis of high quality semiconductor NWRs. Recently, highly ordered nanoscale step arrays were obtained in the homoepitaxial growth of GaAs on (6 3 1) oriented substrates [5], opening opportunities to the self-assembling of 1D arrays. Nevertheless, for the further application of these 1D systems, several challenges must be overcome. For example, the obtaining of n- and p-type doped AlGaAs layers is an essential step for the application of NWRs in optoelectronic devices. Si is known to be amphoteric dopant in III–V compounds [6,7]. For example in GaAs, Si behaves as donor or acceptor depending on the lattice site occupation: a Si atom occupying an As (Ga) site acts like an acceptor (donor). In the growth on high index substrates, the doping type strongly depends on both, growth conditions and on the particular substrate orientation [6–11].

In this work the Si doping of AlGaAs layers grown on (6 3 1)-oriented substrates as a function of the  $As_4$ -beam equivalent pressure ( $P_{As}$ ) is studied. The electrical properties obtained by

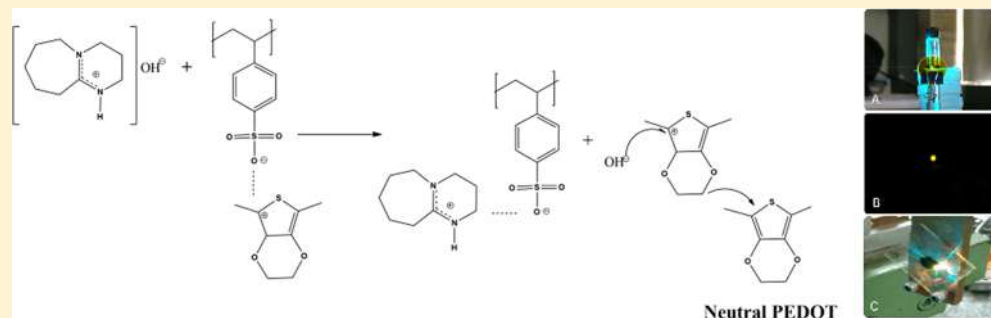
\* Corresponding author.

E-mail address: [victor.mendez@uaslp.mx](mailto:victor.mendez@uaslp.mx) (V.-H. Méndez-García).

## Visible Luminescence of Dedoped DBU-Treated PEDOT:PSS Films

Isidro Cruz-Cruz,<sup>†,‡</sup> Marisol Reyes-Reyes,<sup>†</sup> Israel A. Rosales-Gallegos,<sup>†</sup> Andrei Yu Gorbachev,<sup>†</sup> José M. Flores-Camacho,<sup>†</sup> and Román López-Sandoval<sup>\*,‡</sup><sup>†</sup>Instituto de Investigación en Comunicación Óptica, Universidad Autónoma de San Luis Potosí, Álvaro Obregón 64, San Luis Potosí 78000, Mexico<sup>‡</sup>Advanced Materials Department, IPICYT, Camino a la Presa San José 2055, Col. Lomas 4a sección, San Luis Potosí 78216, Mexico

## Supporting Information



**ABSTRACT:** Dedoping of PEDOT:PSS by a simple and physical process has been performed by the addition of 1,8-diazabicyclo[5.4.0]undec-7-ene (DBU), a strong organic base, in the PEDOT:PSS aqueous dispersion. The DBU-treated PEDOT:PSS samples showed a strong absorption band at 600 nm ( $\pi-\pi^*$  transition) and a small band at 900 nm (polaronic band), which indicates that some PEDOT chains were being reduced. The dedoping efficiency depended of the amount of DBU added to the aqueous PEDOT:PSS dispersion. The DBU-treated PEDOT:PSS aqueous dispersions and films showed a strong yellow emission, visible with the naked eye, when they were excited with a 488 nm laser. In addition, the same emission features were observed using another reducing agent like sodium hydroxide (NaOH), which indicates that the emission originates from neutral PEDOT chains rather than artifacts. Finally, Raman and FTIR spectroscopies were used to figure out the mechanism responsible for the PEDOT reduction. The reduction of PEDOT chains is due to the formation of hydroxide anions, which come from the interaction of DBU with water present in the PEDOT:PSS aqueous solution and interact with the oxidized thiophene molecules, resulting in a neutralization of the PEDOT backbone.

## INTRODUCTION

Organic compounds have attracted a great interest over the past years due to the possibility of obtaining flexible, stable, and low-cost electronic devices.<sup>1</sup> One of these compounds that have attracted great interest is the conductive material poly(3,4-ethylenedioxythiophene) doped with the counteranion poly(styrenesulfonate) (PEDOT:PSS).<sup>2</sup> As is well-known, PEDOT is considered a promising material in applications where the electronic transport is crucial since, in its oxidized state, it has excellent conductivity and high transparency in the visible spectrum, among other properties.<sup>3,4</sup> In the case of the polymeric complex PEDOT:PSS, which is available commercially as an aqueous dispersion, PSS improves its processability for the fabrication of thin films, but reduces the conductivity down to around 0.1 S/cm. In this regard, many efforts have been performed in order to improve its conductivity and the importance of the molecular rearrangement in the thin films was discussed widely,<sup>5–22</sup> because better molecular arrangement promotes an increase in the crystallinity degree and improves the charge carriers delocalization. In particular, oxidizing agents have been used to increase the PEDOT:PSS

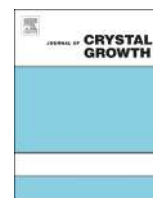
conductivity by the partial replacement of some segments of PSS<sup>-1</sup> by ionic groups such as SO<sub>4</sub><sup>-2</sup> or HSO<sub>4</sub><sup>-1</sup> and the corresponding elimination of the insulating PSS from the thin films.<sup>20,21</sup> Thus, the majority of the applications are related with PEDOT in its oxidized state (*p*-doped). However, in this work, we performed the partial reduction of this polymer to its neutral state (PEDOT<sup>0</sup>), which shows enough stability.

As reported in the literature, it is possible to modulate the electrical, thermoelectric, and optical properties of PEDOT:PSS<sup>23–26</sup> by using reducing agents like polyethylenimine,<sup>24</sup> hydrazine,<sup>25</sup> and sodium hydroxide (NaOH).<sup>26</sup> In the former two cases, it was possible to obtain a low oxidized form of PEDOT,<sup>24,25</sup> whereas, in the latter, no change in the doped state of the polymer was observed, but only a change in the relative population between polarons and bipolarons.<sup>26</sup> In the present work, the use of 1,8-diazabicyclo[5.4.0]undec-7-ene (DBU) as a reducing agent in PEDOT:PSS is reported. DBU is

Received: April 27, 2015

Revised: July 23, 2015

Published: August 11, 2015



# Bulk lattice parameter and band gap of cubic $\text{In}_x\text{Ga}_{1-x}\text{N}$ (001) alloys on MgO (100) substrates



V.D. Compeán García<sup>a</sup>, I.E. Orozco Hinostroza<sup>b</sup>, A. Escobosa Echavarría<sup>c</sup>, E. López Luna<sup>a</sup>, A.G. Rodríguez<sup>a</sup>, M.A. Vidal<sup>a,\*</sup>

<sup>a</sup> Coordinación para la Innovación y Aplicación de la Ciencia y Tecnología (CIACyT), Universidad Autónoma de San Luis Potosí (UASLP), Álvaro Obregón 64, 78000 San Luis Potosí, Mexico

<sup>b</sup> Instituto Potosino de Investigación Científica y Tecnológica, Camino a la Presa San José 2055, Col. Lomas 4<sup>a</sup> Sección, 78216 San Luis Potosí, Mexico

<sup>c</sup> Electric Engineering Department, Centro de Investigación y Estudios Avanzados del IPN, Apartado Postal 14-740, 07000 México D.F., Mexico

## ARTICLE INFO

### Article history:

Received 9 September 2014

Received in revised form

11 February 2015

Accepted 13 February 2015

Communicated by: M. Weyers

Available online 25 February 2015

### Keywords:

A3. Molecular beam epitaxy

B1. Nitrides

B2. Semiconducting III–V materials

## ABSTRACT

$\text{In}_x\text{Ga}_{1-x}\text{N}$  (001) ternary alloys were grown on GaN/MgO (100) substrates in a plasma assisted molecular beam epitaxy system. We determined the in-plane [001] and in-growth [110] lattice parameters, as well as the bulk lattice parameter of the alloys for different In concentrations by high resolution X-ray diffraction. The In concentration was determined assuming Vegard's law for the alloy lattice parameter. The optical energy gap of  $\text{In}_x\text{Ga}_{1-x}\text{N}$  has been determined by transmittance measurements from absorption edges for several In concentrations. Our results show that the alloys have a direct band gap for all In concentrations and a bowing parameter  $b=1.84$ .

© 2015 Elsevier B.V. All rights reserved.

## 1. Introduction

GaN and InN in cubic phase have a band gap of 3.2 and 0.61 eV at room temperature [1,2] and a lattice parameters  $a=4.51$  Å [1] and 5.01 Å [2,3], respectively. The ternary alloy between GaN and InN has a great potential, among other wide and narrow bandgap III–V semiconductors, for fabrication of devices emitting in the blue–green–red spectral region [4–7] and multijunction solar cell devices. Therefore, InGaN has attracted attention in recent years due to the possibility of tuning its bandgap energy from UV (GaN) to IR (InN) only by varying the In molar fraction.

While the most stable and studied phase of III–N compounds is the hexagonal (wurtzite) structure, GaN and InN can also have the cubic zincblende structure as a metastable phase [8,9]. Nitrides with the cubic structure have several advantages compared to those with the hexagonal phase, for instance, a higher crystalline symmetry of the cubic nitrides that results in more isotropic properties and no spontaneous polarization induced–electric fields in the direction parallel to the  $c$ -axis. In addition, it is expected that cubic nitrides have superior electronic properties such as higher carrier mobilities, higher drift velocities, better doping efficiencies. Since the bandgap of  $\beta$ -InGaN is lower than that of

hexagonal InGaN with the same In molar fraction, it is possible to achieve visible light emission at a given wavelength with lower In molar fraction using  $\beta$ -InGaN.

Although several research groups have grown  $\beta$ -InGaN with low In content [10–17], the growth of cubic  $\beta$ -InGaN over the complete range of In concentration has not been accomplished. These limitations can be stem from several factors: (i) very narrow range of Ga, In and N fluxes to obtain ternary alloys for different In concentrations, in a plasma assisted molecular beam epitaxial system (PA-MBE), (ii) instability of molecular fluxes during the growth that leads to changes in the arrival rate of surface atoms species and therefore change of concentration or stoichiometry of layers, (iii) the strong tendency to incorporate the more stable hexagonal phase in the growth process, especially when dealing with substrates with high lattice-mismatch.

In this work, we report the growth of cubic  $\beta$ -InGaN(001) homogeneous epilayers on MgO (100) substrates by PA-MBE, and the characterization of the optical band gap and structural properties for several In concentrations in all range from  $x=0$  to  $x=1$ .

## 2. Experimental details.

Before growing  $\beta$ -InGaN ternary alloys, the MgO (100) substrate was cleaned in a sequential trichloroethylene and acetone ultrasonic

\* Corresponding author.

# Determination of the Thermal Expansion Coefficient of Single-Wall Carbon Nanotubes by Raman Spectroscopy

L. I. ESPINOSA-VEGA, A. G. RODRÍGUEZ, H. NAVARRO-CONTRERAS, and M. A. VIDAL

*Coordinación para la Innovación y la Aplicación de la Ciencia y la Tecnología (CIACYT) Universidad Autónoma de San Luis Potosí, San Luis Potosí, México*

Received 20 September 2013, Accepted 24 October 2013

We have examined the effect of high temperature on single-wall carbon nanotubes under air and nitrogen ambient by Raman spectroscopy. We observe the temperature dependence of the radial breathing mode and the G-band modes. The thermal expansion coefficient ( $\beta$ ) of the bundled nanotubes is obtained experimentally using the estimated volume from Raman scattering.  $\beta$  behaves linearly with temperature from  $0.33 \times 10^{-5} \text{ K}^{-1}$  to  $0.28 \times 10^{-5} \text{ K}^{-1}$  in air and from  $0.58 \times 10^{-5} \text{ K}^{-1}$  to  $0.47 \times 10^{-5} \text{ K}^{-1}$  in nitrogen ambient, respectively. The temperature dependence of the radial breathing mode Raman frequencies is consistent with a pure temperature effect.

**Keywords:** nanotubes, Raman spectroscopy, thermal expansion

## Introduction

Research on single-wall carbon nanotubes (SWCNTs) has been of great interest due to their potential applications given their electronic, mechanical, and thermal properties.<sup>[1]</sup> For certain applications, it is important to know the effect of high temperature on the properties of nanotubes. Raman scattering is one of the useful analysis techniques for the characterization of carbon nanostructures and investigation of their properties.<sup>[2–7]</sup> The Raman spectra from the SWCNTs have unique features, such as the G-band, D-band, and the radial breathing mode (RBM) peaks, which are related to the conductivity, the quality, and the diameter distribution of the SWCNTs. These measurements are usually obtained at room temperature but the temperature-dependent Raman frequency shift of carbon nanomaterials has also been reported.<sup>[2–7]</sup> The Raman spectra of SWCNTs can present some significant changes with increasing temperature such as frequency shifts, increase or decrease of the modes intensity, and the G-peaks broadening. A few authors have noted that the frequency decreases with increasing temperature for all the Raman peaks of straight nanotubes and rings in SWCNT bundles.<sup>[4]</sup> Raravikar et al. report a softening of the radial and tangential band frequencies with temperature and estimate the contribution of the factors that may be responsible for the observed temperature dependence of

the RBM frequency.<sup>[2]</sup> Maoshuai et al. obtain the Raman spectra of carbon nanobuds and compare them to those of SWCNT and show the thermal stability of these nanostructures.<sup>[8]</sup>

In this paper, we present the Raman Spectroscopy of SWCNTs when heated under two different ambient conditions: air and nitrogen. We show that the experimental data of the Raman shifts allow us to determine the thermal expansion coefficient of the nanotubes. The experimental coefficient is in good agreement with calculated values of the linear thermal expansion coefficient and X-ray measurements.<sup>[2,9]</sup> In air, the process is reversible up to a critical temperature between 855 and 875 K. If the nanotubes are heated above this temperature, the RBM and G phonon line-shapes change abruptly, and the process is no longer reversible. On the other hand, if the nanotubes are heated in nitrogen the phonon line-shapes of the Raman spectra do not deteriorate permanently with temperature, and the process remains reversible up to 1075 K. The irreversibility may be caused by oxygen adsorption when the nanotubes are heated in air, as revealed energy-dispersive X-ray spectroscopy (EDS) measurements.

## Experimental Details

The SWCNT bundles under study were purchased from Nano-Lab, Waltham, MA, USA. According to the vendor specifications, the nanotubes diameter is 1–1.5 nm with an average length of 1  $\mu\text{m}$  and approximately 90% pure. Raman scattering measurements were carried out in SWCNTs at different temperatures. The Raman scattering measurements were done using a Jobin-Yvon T64000 spectrometer

---

Address correspondence to A. G. Rodríguez, Coordinación para la Innovación y la Aplicación de la Ciencia y la Tecnología (CIACYT) Universidad Autónoma de San Luis Potosí, Álvaro Obregón 64, San Luis Potosí, S. L. P. 78000, México. E-mail: angel.rodriguez@uaslp.mx

## Raman scattering from $\text{Ge}_{1-x}\text{Sn}_x$ ( $x \leq 0.14$ ) alloys

H. Navarro-Contreras, A.G. Rodríguez, and M.A. Vidal

*Coordinación para la Innovación y la Aplicación de la Ciencia y la Tecnología, Universidad Autónoma de San Luis Potosí, Álvaro Obregón 64, San Luis Potosí, S.L.P. 78000, México.*

H. Pérez-Ladrón de Guevara

*Centro Universitario de los Lagos, Universidad de Guadalajara, Av. Enrique Díaz de León 1144, Col. Paseos de la Montaña, Lagos de Moreno, Jal. 47460, México.*

Received 5 November 2014; accepted 18 August 2015

$\text{Ge}_{1-x}\text{Sn}_x$  alloys with  $x$  concentration up to 0.14 were grown on Ge(001) and GaAs(001) substrates in a conventional R. F. Magnetron Sputtering system at low substrate temperatures. The structural characteristics of these alloys were studied for different Sn concentrations between 1 to 14 % by high resolution X ray diffraction, and Raman spectroscopy. Contrasting characteristics of the grown layers are observed if the Sn concentration is larger or smaller than 6 % as revealed by X-ray diffraction and Raman spectroscopy.

*Keywords:* Raman; space correlation model.

PACS: 68; 68.35.bg

### 1. Introduction

$\text{Ge}_{1-x}\text{Sn}_x$  alloys, pertaining to the IV-IV column of the periodic table, have been a subject of interest for the last two decades, due to the very attractive possibility to fabricate with them materials consisting of elements of the column IV that may have a direct electronic band gap tunable from 0 to near 0.55 eV [1]. The study is driven by the interest to apply them as systems to produce far and medium infrared diodes, photodetectors [2,3] and lasers [4,5]; hence, as a very convenient substitute for the Hg-Cd-Te system [6]. These alloys have also been used as buffer layers for a complete integration between Ge or the ternary alloy  $\text{Ge}_{1-x-y}\text{Si}_x\text{Sn}_y$  on Si substrates, instead of  $\text{Si}_{1-x}\text{Ge}_x$  alloys [7-9]. Calculations in the strong bonding models [10] and from pseudopotential methods [11] in the virtual crystal approximation, have predicted that  $\text{Ge}_{1-x}\text{Sn}_x$  alloys must exhibit a direct band gap somewhere in the tin composition range between  $x = 0.2$  to 0.5 eV in non-stressed films [12]. Additionally, due to the prevalence of covalent bonding of both Ge and Sn, and similar external electronic configurations, it has been predicted in the same set of theoretical works, that  $\text{Ge}_{1-x}\text{Sn}_x$  must have higher carrier mobility's than other semiconductor compounds or alloys, with band gaps in the same energy range, due to the absence of polar phononic dispersion [6].

When the alloy is prepared starting from Ge, a direct gap material is eventually obtained, that evolves from indirect to direct electronic band gap as a result of the fact that the  $\Gamma$ -point conduction-band minimum decreases in energy value more rapidly than the  $L$ -point valleys at the [111] points at the border of the Brillouin Zone [10,11,14,15]. Moreover, as  $\text{Ge}_{1-x}\text{Sn}_x$  alloys are always prepared as strained films grown mainly either on Si or Ge substrates, the presence of compressive strain is expected to decrease the Sn concentration at which the indirect  $L_6 \rightarrow \Gamma_8$  to direct  $L_7 \rightarrow \Gamma_8$  band-gap crossover is observed [7,12,15-18].

The growth of these  $\text{Ge}_{1-x}\text{Sn}_x$  alloys, however, has been limited because it presents severe difficulties, that have to be overcome, stemming from to the following three factors: (a) limited Sn miscibility in the Ge (less than 1%) or of the Ge in Sn (less than 0.6%) [19]; (b) the tendency of the diamond tin phase ( $\alpha$ -Sn) to spontaneously suffer a transition to the metallic phase ( $\beta$ -Sn) at temperatures higher than 13.2 °C [20]; (c) with increasing Sn composition, the high diffusivity of Sn into Ge and the free energy difference among the metastable state and the equilibrium state of the two phases causes a phase separation and promotes the transformation from the meta stable to the stable phase  $\alpha \rightarrow \beta$  [20]. Low temperature deposition is then needed. An additional obstacle to overcome in the epitaxial growth of  $\text{Ge}_{1-x}\text{Sn}_x$  on Ge, the preferred substrate, is that the lattice constant mismatch between  $\alpha$ -Sn ( $a_{\text{Sn}} = 6.4892 \text{ \AA}$ ) and Ge ( $a_{\text{Ge}} = 5.6579 \text{ \AA}$ ) is 14.7% [21].

The difficulties to prepare  $\text{Ge}_{1-x}\text{Sn}_x$  on either Ge or Sn or any other substrate, have resulted in a notorious scarcity of data in the literature for almost all of their physical properties, as well as the interest mentioned to use it as a column IV direct bandgap material in the far and medium infrared. We find this facts as a challenge for synthesize, study and determine as many of the physical properties of  $\text{Ge}_{1-x}\text{Sn}_x$  as possible.

In this article, we present a study of  $\text{Ge}_{1-x}\text{Sn}_x$  alloys of low Sn concentration  $0.01 \leq x \leq 0.14$  samples grown on either Ge(001) or GaAs(001) by radio frequency sputtering [22]. GaAs substrates were chosen, in addition to Ge, because of the very similar lattice constants of GaAs and Ge ( $a_{\text{GaAs}} = 5.6535 \text{ \AA}$ ). The samples with  $0.01 \leq x < 0.06$  have a highly heterogeneous structural conformation, with a thin superficial layer of contrasting concentration. The study reveals that for higher Sn concentrations this phenomenon is not detected and the samples grow partially or totally relaxed with a high density of dislocations and a more homogenous Sn con-

# Towards Precision Measurements at UASLP

**S Hamzeloui, N Arias, V Abediyeh, D Martínez, M Gutiérrez, E Uruñuela, E del Rio, E Cerda-Méndez, E Gomez**

Instituto de Física, Universidad Autónoma de San Luis Potosí (UASLP), San Luis Potosí 78290, México

E-mail: [egomez@ifisica.uaslp.mx](mailto:egomez@ifisica.uaslp.mx)

**V M Valenzuela**

Facultad de Ciencias Físico Matemáticas, Universidad Autónoma de Sinaloa, Sinaloa 80000, México

**Abstract.** Atomic interferometry is a very sensitive technique to measure small forces. Here we present an overview of the progress towards interferometric measurements in our laboratory. We characterize the magnetic field noise and describe the strategies to minimize the sensitivity to magnetic field fluctuations. We introduce as well a system for Raman excitation with minimum phase noise and the frequency filtering needed to implement it. Finally, we demonstrate atomic interferometry with a frequency sensitivity of 3 Hz.

## 1. Introduction

Laser cooling is a widely used technique nowadays. The control achieved over the atomic sample improves the precision of different measurements in physics. The best example is that of atomic clocks where 18 digits of precision have been achieved in the determination of time [1]. The use of interferometric techniques is largely responsible for the continuous improvement of measurements. Cold atoms are well suited for such techniques since they allow for coherence times of several seconds [2,3]. In our group we are particularly interested in the measurement of small forces. Here cold atoms have been used to study the gravitational force [4], variations of gravity at short distances [5], interactions of atoms with surfaces [6,7] and the weak force [8,9].

The separated oscillatory fields method of Ramsey is at the heart of an atomic interferometer [10]. In this method a  $\pi/2$  pulse creates a coherent superposition between two hyperfine levels. The system is then left to evolve for a time  $T$ , and a second  $\pi/2$  pulse is applied to read the relative phase between the two levels. An ideal atomic interferometer must have high sensitivity and it should not be affected by environmental perturbations. Magnetic field variations are often a concern, but it is possible to choose energy levels that remain unperturbed by those fluctuations.

Here we present our progress on atomic interferometry. We explore different ways to suppress the sensitivity to magnetic field fluctuations. Also, the use of a phase modulator allows for the excitation of Raman transitions with a minimum of phase noise. The flexibility of the system opens the door to complex excitation schemes.





## Spatial Patterns of Dissipative Polariton Solitons in Semiconductor Microcavities

J. K. Chana,<sup>1</sup> M. Sich,<sup>1,\*</sup> F. Frasn,<sup>1,2</sup> A. V. Gorbach,<sup>3</sup> D. V. Skryabin,<sup>3,4</sup> E. Cancellieri,<sup>1</sup> E. A. Cerda-Méndez,<sup>5</sup> K. Biermann,<sup>5</sup> R. Hey,<sup>5</sup> P. V. Santos,<sup>5</sup> M. S. Skolnick,<sup>1</sup> and D. N. Krizhanovskii<sup>1,†</sup>

<sup>1</sup>*Department of Physics and Astronomy, The University of Sheffield, Sheffield S3 7RH, United Kingdom*

<sup>2</sup>*IPCMS UMR 7504, CNRS and Université de Strasbourg, Strasbourg 67084, France*

<sup>3</sup>*Department of Physics, University of Bath, Bath BA2 7AY, United Kingdom*

<sup>4</sup>*ITMO University, Kronverksky Avenue 49, St. Petersburg 197101, Russian Federation*

<sup>5</sup>*Paul-Drude-Institut für Festkörperelektronik, Berlin 10117, Germany*

(Received 1 December 2014; revised manuscript received 23 July 2015; published 15 December 2015)

We report propagating bound microcavity polariton soliton arrays consisting of multipeak structures either along ( $x$ ) or perpendicular ( $y$ ) to the direction of propagation. Soliton arrays of up to five solitons are observed, with the number of solitons controlled by the size and power of the triggering laser pulse. The breakup along the  $x$  direction occurs when the effective area of the trigger pulse exceeds the characteristic soliton size determined by polariton-polariton interactions. Narrowing of soliton emission in energy-momentum space indicates phase locking between adjacent solitons, consistent with numerical modeling which predicts stable multihump soliton solutions. In the  $y$  direction, the breakup originates from inhomogeneity across the wave front in the transverse direction which develops into a stable array only in the solitonic regime via phase-dependent interactions of propagating fronts.

DOI: [10.1103/PhysRevLett.115.256401](https://doi.org/10.1103/PhysRevLett.115.256401)

PACS numbers: 71.36.+c, 05.45.Yv, 78.67.Pt

Solitons occur when dispersive spreading of wave packets is compensated through nonlinear interactions. They have been observed in numerous systems including nonlinear crystals and optical fibers [1,2], atomic Bose-Einstein condensates [3], and natural processes including signal propagation in neurons [4], cloud formation [5], and large-amplitude waves [6,7]. In many aspects, solitons behave like artificial particles. They may repel or attract depending on their relative phase as was shown in optical fibers [8] and cold atom systems [9]. Multisoliton complexes can form when localized initial perturbations split into multiple peaks [10,11]. Furthermore, solitons can self-organize into stable patterns with an equilibrium spacing [12] or can scatter in a collision [13].

Recently, polaritons, hybrid light-matter particles forming in the strong coupling regime in semiconductor microcavities [14,15], have been shown to exhibit many interesting nonlinear hydrodynamic phenomena such as superfluidity [16] and integer [17] and half vortices [18]. Microcavity polaritons are an open system far from equilibrium. Bright polariton solitons have been observed [19], which exist when an external pump fully compensates photonic losses and the decay of the excitonic coherence and are therefore termed dissipative. Polariton solitons can be manipulated on a picosecond time scale, which is promising for the development of miniature polaritonic

circuits and logic gates [20]. Dark soliton trains in a 1D conservative microcavity system (no pump) were recently predicted theoretically [21], whereas dissipative polariton soliton patterns in microcavities remain unexplored.

Semiconductor optical resonators are prone to growth defects and imperfections [22], and, in contrast to atomic condensates [11], the observation of multiple solitons in such systems is a challenging task, even in well-studied systems such as vertical-cavity surface-emitting lasers (VCSELs) [23,24]. In contrast to solitons in VCSELs, microcavity polariton solitons are excited at high momenta. Combined with large energy blueshifts due to the giant optical nonlinearity, this makes polariton solitons less sensitive to photonic disorder, enabling our observation of stable multisoliton patterns.

Here we demonstrate the formation of dissipative polariton soliton patterns. The interplay between bistability of the external pump field, polariton-polariton scattering, and polariton negative effective mass along the propagation direction enables the formation of  $x$ -soliton arrays, i.e., bound solitons following one another in space and time. The  $k$ -space emission patterns observed indicate phase locking between adjacent solitons. Up to five stable bound solitons are observed in agreement with numerical modeling predicting stable multihump solutions. Soliton separations in a time of  $\approx 10$  ps are observed in the  $x$  arrays, potentially promising for the development of polaritonic devices operating at  $\approx 100$  Gbit/s. We also observe stable  $y$ -soliton arrays formed perpendicular to the propagation direction, arising from changes of the front velocity across the propagating beam profile.

---

Published by the American Physical Society under the terms of the [Creative Commons Attribution 3.0 License](https://creativecommons.org/licenses/by/3.0/). Further distribution of this work must maintain attribution to the author(s) and the published article's title, journal citation, and DOI.



# Nanostructure formation during relatively high temperature growth of Mn-doped GaAs by molecular beam epitaxy



A. Del Río-De Santiago<sup>a</sup>, V.H. Méndez-García<sup>a</sup>, I. Martínez-Velis<sup>b</sup>, Y.L. Casallas-Moreno<sup>b</sup>, E. López-Luna<sup>a</sup>, A. Yu Gorbachev<sup>c</sup>, M. López-López<sup>b</sup>, E. Cruz-Hernández<sup>a,\*</sup>

<sup>a</sup> CIACyT-UASLP, Sierra Leona Av. # 550, Lomas 2a Secc, San Luis Potosí, S.L.P. 78210, México

<sup>b</sup> Physics Department, CINVESTAV-IPN, Apdo. Postal 14470 D. F. México, México

<sup>c</sup> IICO-UASLP, Av. Karakorum 1470, Lomas 4a. Sección, San Luis Potosí, S.L.P. 78210, México

## ARTICLE INFO

### Article history:

Received 31 July 2014

Received in revised form 29 January 2015

Accepted 29 January 2015

Available online 7 February 2015

### Keywords:

MBE

GaMnAs

Nanostructures

Photoluminescence

Electrical properties

High temperature

## ABSTRACT

In the present work, we report on molecular beam epitaxy growth of Mn-doped GaAs films at the relatively high temperature (HT) of 530 °C. We found that by increasing the Mn atomic percent, Mn%, from 0.01 to 0.2, the surface morphology of the samples is strongly influenced and changes from planar to corrugated for Mn% values from 0.01 to 0.05, corresponding to nanostructures on the surface with dimensions of 200–300 nm and with the shape of leave, to nanowire-like structures for Mn% values above 0.05. From reflection high-energy electron diffraction patterns, we observed the growth mode transition from two- to three-dimensional occurring at a Mn% exceeding 0.05. The optical and electrical properties were obtained from photoluminescence (PL) and Hall effect measurements, respectively. For the higher Mn concentration, besides the Mn related transitions at approximately 1.41 eV, PL spectra sharp peaks are present between 1.43 and 1.49 eV, which we related to the coexistence of zinc blende and wurtzite phases in the nanowire-like structures of this sample. At Mn% of 0.04, an increase of the carrier mobility up to a value of  $1.1 \times 10^3 \text{ cm}^2/\text{Vs}$  at 77 K was found, then decreases as Mn% is further increased due to the strengthening of the ionized impurity scattering.

© 2015 Elsevier B.V. All rights reserved.

## 1. Introduction

Since the first successful growth of GaMnAs by molecular-beam epitaxy (MBE) showing ferromagnetic behavior [1–3], this diluted magnetic semiconductor (DMS) has received extensive attention because of the interest in the integration of both carrier induced ferromagnetism and spin-electronics with the existing semiconductor technology. However, these potential applications have been limited because of the low solubility of the Mn atoms, on the order of  $10^{18} \text{ cm}^{-3}$  or less, in the GaAs semiconductor matrix [4,5]. So far, the low-temperature (LT) MBE technique, below 300 °C, is the best method for the preparation of such materials with Mn concentrations many times higher than solubility. Unfortunately, LT-MBE and a high Mn concentration are characterized by a high content of point defects, such as As antisites and Mn interstitials [6,7] and by the poor crystallinity. Even when these defects can be reduced by optimizing the growth LT conditions or by post-growth annealing processes [7,8], the number of defects remains

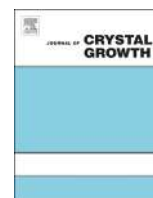
elevated relative to GaAs films grown at relatively high temperature (HT) MBE (>500 °C). Successful growth of high crystalline quality GaMnAs at HT possesses a high potential for incorporating the ferromagnetic GaMnAs layers into GaAs-based microelectronic and optoelectronic devices. However, by growing at HT, precipitation of MnAs clusters in a GaMnAs matrix has been observed [9,10]. In addition, due to the inherent inhibition of uniform growth of GaMnAs with high Mn concentrations, little work has been published regarding HT MBE [11–13]. Despite this drawback, the number of As<sub>Ga</sub> in GaMnAs has been found to be reduced by increasing the substrate temperature ( $T_S$ ) [12,13]. Moreover, by growing at intermediate temperatures (IT), from 325 to 500 °C, some authors have been able to improve the optical properties of Mn-doped GaAs layers compared to LT GaMnAs [14,15]. In this paper, to gain more insight into relatively HT GaMnAs, we present a study of Mn-doped GaAs layers prepared by varying the nominal Mn atomic percent (Mn%) from 0.01 to 0.2 at a temperature of 530 °C.

## 2. Experimental

The samples were grown by MBE using solid sources onto epitaxial GaAs (001) substrates. After growing a five-period AlAs

\* Corresponding author. Tel.: +52 4448262300.

E-mail address: [esteban.cruz@uaslp.mx](mailto:esteban.cruz@uaslp.mx) (E. Cruz-Hernández).



# Bulk lattice parameter and band gap of cubic $\text{In}_x\text{Ga}_{1-x}\text{N}$ (001) alloys on MgO (100) substrates



V.D. Compeán García<sup>a</sup>, I.E. Orozco Hinostroza<sup>b</sup>, A. Escobosa Echavarría<sup>c</sup>, E. López Luna<sup>a</sup>, A.G. Rodríguez<sup>a</sup>, M.A. Vidal<sup>a,\*</sup>

<sup>a</sup> Coordinación para la Innovación y Aplicación de la Ciencia y Tecnología (CIACyT), Universidad Autónoma de San Luis Potosí (UASLP), Álvaro Obregón 64, 78000 San Luis Potosí, Mexico

<sup>b</sup> Instituto Potosino de Investigación Científica y Tecnológica, Camino a la Presa San José 2055, Col. Lomas 4<sup>a</sup> Sección, 78216 San Luis Potosí, Mexico

<sup>c</sup> Electric Engineering Department, Centro de Investigación y Estudios Avanzados del IPN, Apartado Postal 14-740, 07000 México D.F., Mexico

## ARTICLE INFO

### Article history:

Received 9 September 2014

Received in revised form

11 February 2015

Accepted 13 February 2015

Communicated by: M. Weyers

Available online 25 February 2015

### Keywords:

A3. Molecular beam epitaxy

B1. Nitrides

B2. Semiconducting III–V materials

## ABSTRACT

$\text{In}_x\text{Ga}_{1-x}\text{N}$  (001) ternary alloys were grown on GaN/MgO (100) substrates in a plasma assisted molecular beam epitaxy system. We determined the in-plane [001] and in-growth [110] lattice parameters, as well as the bulk lattice parameter of the alloys for different In concentrations by high resolution X-ray diffraction. The In concentration was determined assuming Vegard's law for the alloy lattice parameter. The optical energy gap of  $\text{In}_x\text{Ga}_{1-x}\text{N}$  has been determined by transmittance measurements from absorption edges for several In concentrations. Our results show that the alloys have a direct band gap for all In concentrations and a bowing parameter  $b=1.84$ .

© 2015 Elsevier B.V. All rights reserved.

## 1. Introduction

GaN and InN in cubic phase have a band gap of 3.2 and 0.61 eV at room temperature [1,2] and a lattice parameters  $a=4.51$  Å [1] and 5.01 Å [2,3], respectively. The ternary alloy between GaN and InN has a great potential, among other wide and narrow bandgap III–V semiconductors, for fabrication of devices emitting in the blue–green–red spectral region [4–7] and multijunction solar cell devices. Therefore, InGaN has attracted attention in recent years due to the possibility of tuning its bandgap energy from UV (GaN) to IR (InN) only by varying the In molar fraction.

While the most stable and studied phase of III–N compounds is the hexagonal (wurtzite) structure, GaN and InN can also have the cubic zincblende structure as a metastable phase [8,9]. Nitrides with the cubic structure have several advantages compared to those with the hexagonal phase, for instance, a higher crystalline symmetry of the cubic nitrides that results in more isotropic properties and no spontaneous polarization induced–electric fields in the direction parallel to the  $c$ -axis. In addition, it is expected that cubic nitrides have superior electronic properties such as higher carrier mobilities, higher drift velocities, better doping efficiencies. Since the bandgap of  $\beta$ -InGaN is lower than that of

hexagonal InGaN with the same In molar fraction, it is possible to achieve visible light emission at a given wavelength with lower In molar fraction using  $\beta$ -InGaN.

Although several research groups have grown  $\beta$ -InGaN with low In content [10–17], the growth of cubic  $\beta$ -InGaN over the complete range of In concentration has not been accomplished. These limitations can be stem from several factors: (i) very narrow range of Ga, In and N fluxes to obtain ternary alloys for different In concentrations, in a plasma assisted molecular beam epitaxial system (PA-MBE), (ii) instability of molecular fluxes during the growth that leads to changes in the arrival rate of surface atoms species and therefore change of concentration or stoichiometry of layers, (iii) the strong tendency to incorporate the more stable hexagonal phase in the growth process, especially when dealing with substrates with high lattice-mismatch.

In this work, we report the growth of cubic  $\beta$ -InGaN(001) homogeneous epilayers on MgO (100) substrates by PA-MBE, and the characterization of the optical band gap and structural properties for several In concentrations in all range from  $x=0$  to  $x=1$ .

## 2. Experimental details.

Before growing  $\beta$ -InGaN ternary alloys, the MgO (100) substrate was cleaned in a sequential trichloroethylene and acetone ultrasonic

\* Corresponding author.

Article

## Design and Fabrication of Interdigital Nanocapacitors Coated with HfO<sub>2</sub>

Gabriel González <sup>1,2</sup>, Eleazar Samuel Kolosovas-Machuca <sup>2</sup>, Edgar López-Luna <sup>2</sup>, Heber Hernández-Arriaga <sup>2</sup> and Francisco Javier González <sup>2,\*</sup>

<sup>1</sup> Cátedras Conacyt, Universidad Autónoma de San Luis Potosí, 78000 San Luis Potosí, Mexico; E-Mail: gabriel.gonzalez@uaslp.mx

<sup>2</sup> Coordinación para la Innovación y la Aplicación de la Ciencia y la Tecnología, Universidad Autónoma de San Luis Potosí, 78000 San Luis Potosí, Mexico; E-Mails: samuel.kolosovas@uaslp.mx (E.S.K.-M.); edgar.luna@uaslp.mx (E.L.-L.); heber.hernandez@uaslp.mx (H.H.-A.)

\* Author to whom correspondence should be addressed; E-Mail: javier.gonzalez@uaslp.mx; Tel.: +52-444-826-2300 (ext. 8416).

Academic Editor: Manh-Huong Phan

Received: 5 November 2014 / Accepted: 19 December 2014 / Published: 16 January 2015

---

**Abstract:** In this article nickel interdigital capacitors were fabricated on top of silicon substrates. The capacitance of the interdigital capacitor was optimized by coating the electrodes with a 60 nm layer of HfO<sub>2</sub>. An analytical solution of the capacitance was compared to electromagnetic simulations using COMSOL and with experimental measurements. Results show that modeling interdigital capacitors using Finite Element Method software such as COMSOL is effective in the design and electrical characterization of these transducers.

**Keywords:** interdigital nanocapacitors; finite element method; capacitance

---

### 1. Introduction

Interdigital capacitors (IDCs) are one of the most used transducers in chemical and biological sensors where a change in capacitance or impedance is measured as a response to the interaction between the analyte and a sensitive layer [1]. Interdigital capacitors are used also for the evaluation of near-surface

## On the growth of directed complex networks with preferential attachment: Effect upon the prohibition of multiple links

J. Esquivel-Gómez\* and R. E. Balderas-Navarro†

*Instituto de Investigación en Comunicación Óptica  
Universidad Autónoma de San Luis Potosí (UASLP), Mexico*

\*jesquivel@fc.uaslp.mx

†rbn@cactus.iico.uaslp.mx

Edgardo Ugalde

*Instituto de Física*

*Universidad Autónoma de San Luis Potosí (UASLP), Mexico*

ugalde@ifisica.uaslp.mx

J. Acosta-Eliás

*Facultad de Ciencias*

*Universidad Autónoma de San Luis Potosí (UASLP), Mexico*

jacosta@uaslp.mx

Received 22 July 2014

Accepted 15 October 2014

Published 25 November 2014

Several real-world directed networks do not have multiple links. For example, in a paper citation network a paper does not cite two identical references, and in a network of friends there exists only a single link between two individuals. This suggests that the growth and evolution models of complex networks should take into account such feature in order to approximate the topological properties of this class of networks. The aim of this paper is to propose a growth model of directed complex networks that takes into account the prohibition of the existence multiple links. It is shown through numerical experiments that when multiple links are forbidden, the exponent  $\gamma$  of the in-degree connectivity distribution,  $P(k_{\text{in}}) \sim k_{\text{in}}^{-\gamma}$ , takes values ranging from 1 to  $\infty$ . In particular, the proposed multi-link free (MLF) model is able to predict exponents occurring in real-world complex networks, which range  $1.05 < \gamma < 3.51$ . As an example, the MLF reproduces some topological properties exhibited by the network of flights between airports of the world (NFAW); i.e.  $\gamma \approx 1.74$ . With this result, we believe that the multiple links prohibition might be one of the local processes accounting for the existence of exponents  $\gamma < 2$  found in some real complex networks.

*Keywords:* Complex networks; power-laws; preferential attachment.

PACS Nos.: 11.25.Hf, 123.1K.

## PROJECTIVE DISTANCE AND $g$ -MEASURES

LILIANA TREJO-VALENCIA AND EDGARDO UGALDE

Instituto de Física, Universidad Autónoma de San Luis Potosí  
Avenida Manuel Nava 6, Zona Universitaria  
78290 San Luis Potosí, México

ABSTRACT. We introduce a distance in the space of fully-supported probability measures on one-dimensional symbolic spaces. We compare this distance to the  $\bar{d}$ -distance and we prove that in general they are not comparable. Our projective distance is inspired on Hilbert's projective metric, and in the framework of  $g$ -measures, it allows to assess the continuity of the entropy at  $g$ -measures satisfying uniqueness. It also allows to relate the speed of convergence and the regularity of sequences of locally finite  $g$ -functions, to the preservation at the limit, of certain ergodic properties for the associate  $g$ -measures.

### 1. Introduction.

1.1. In [12] Hilbert introduced the so called projective distance, for which the geodesic are precisely the straight lines. It was later used by G. Birkhoff to prove the existence and uniqueness of positive eigenvectors for positive linear transformations on Banach spaces [1]. Birkhoff's strategy goes as follows: uniformly positive bounded linear transformations map the positive cone of a Banach space into itself. This transformation is non-expansive with respect to the projective distance, and if the image cone has finite diameter, then the transformation is a projective contraction. In this case Banch's fixed point Theorem ensures the existence and uniqueness of a projective fixed point for the linear transformation, and projective fixed points are nothing but positive eigenvectors. Furthermore, the contractiveness ensures that the iterations of the linear transformation on any positive vector converge exponentially fast, in the projective sense, towards to the fixed point. Birkhoff's strategy has been successfully employed in the solution of a variety of problems, in particular to prove existence and uniqueness of invariant measures, and the exponential decay of correlations of convenient observables. This has been done for symbolic systems [10, 23], for suitable one-dimensional maps [18, 19], and for general maps with some degree of hyperbolicity [17, 24].

Ornstein's  $\bar{d}$ -distance was introduced in [26] to give a topological characterization to the Bernoulli processes. This distance generates a topological structure well adapted to the study of important ergodic properties. For instance,  $\bar{d}$ -limits of sequences of mixing processes are mixing, the class of Bernoulli processes is  $\bar{d}$ -closed, as well as the class of  $K$ -processes. Bressaud and coauthors, in a study of Markov approximation to  $g$ -measures (chains of complete connection in their nomenclature), found an upper bound for the speed of  $\bar{d}$ -convergence of the approximations related

---

2010 *Mathematics Subject Classification.* Primary: 58F15, 58F17; Secondary: 53C35.

*Key words and phrases.*  $\bar{d}$ -distance, projective distance, Markov approximations,  $g$ -measures, entropy convergence.



# Nanostructure formation during relatively high temperature growth of Mn-doped GaAs by molecular beam epitaxy



A. Del Río-De Santiago<sup>a</sup>, V.H. Méndez-García<sup>a</sup>, I. Martínez-Velis<sup>b</sup>, Y.L. Casallas-Moreno<sup>b</sup>, E. López-Luna<sup>a</sup>, A. Yu Gorbachev<sup>c</sup>, M. López-López<sup>b</sup>, E. Cruz-Hernández<sup>a,\*</sup>

<sup>a</sup> CIACyT-UASLP, Sierra Leona Av. # 550, Lomas 2a Secc, San Luis Potosí, S.L.P. 78210, México

<sup>b</sup> Physics Department, CINVESTAV-IPN, Apdo. Postal 14470 D. F. México, México

<sup>c</sup> IICO-UASLP, Av. Karakorum 1470, Lomas 4a. Sección, San Luis Potosí, S.L.P. 78210, México

## ARTICLE INFO

### Article history:

Received 31 July 2014

Received in revised form 29 January 2015

Accepted 29 January 2015

Available online 7 February 2015

### Keywords:

MBE

GaMnAs

Nanostructures

Photoluminescence

Electrical properties

High temperature

## ABSTRACT

In the present work, we report on molecular beam epitaxy growth of Mn-doped GaAs films at the relatively high temperature (HT) of 530 °C. We found that by increasing the Mn atomic percent, Mn%, from 0.01 to 0.2, the surface morphology of the samples is strongly influenced and changes from planar to corrugated for Mn% values from 0.01 to 0.05, corresponding to nanostructures on the surface with dimensions of 200–300 nm and with the shape of leave, to nanowire-like structures for Mn% values above 0.05. From reflection high-energy electron diffraction patterns, we observed the growth mode transition from two- to three-dimensional occurring at a Mn% exceeding 0.05. The optical and electrical properties were obtained from photoluminescence (PL) and Hall effect measurements, respectively. For the higher Mn concentration, besides the Mn related transitions at approximately 1.41 eV, PL spectra sharp peaks are present between 1.43 and 1.49 eV, which we related to the coexistence of zinc blende and wurtzite phases in the nanowire-like structures of this sample. At Mn% of 0.04, an increase of the carrier mobility up to a value of  $1.1 \times 10^3 \text{ cm}^2/\text{Vs}$  at 77 K was found, then decreases as Mn% is further increased due to the strengthening of the ionized impurity scattering.

© 2015 Elsevier B.V. All rights reserved.

## 1. Introduction

Since the first successful growth of GaMnAs by molecular-beam epitaxy (MBE) showing ferromagnetic behavior [1–3], this diluted magnetic semiconductor (DMS) has received extensive attention because of the interest in the integration of both carrier induced ferromagnetism and spin-electronics with the existing semiconductor technology. However, these potential applications have been limited because of the low solubility of the Mn atoms, on the order of  $10^{18} \text{ cm}^{-3}$  or less, in the GaAs semiconductor matrix [4,5]. So far, the low-temperature (LT) MBE technique, below 300 °C, is the best method for the preparation of such materials with Mn concentrations many times higher than solubility. Unfortunately, LT-MBE and a high Mn concentration are characterized by a high content of point defects, such as As antisites and Mn interstitials [6,7] and by the poor crystallinity. Even when these defects can be reduced by optimizing the growth LT conditions or by post-growth annealing processes [7,8], the number of defects remains

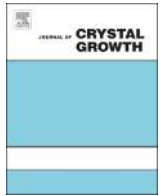
elevated relative to GaAs films grown at relatively high temperature (HT) MBE (>500 °C). Successful growth of high crystalline quality GaMnAs at HT possesses a high potential for incorporating the ferromagnetic GaMnAs layers into GaAs-based microelectronic and optoelectronic devices. However, by growing at HT, precipitation of MnAs clusters in a GaMnAs matrix has been observed [9,10]. In addition, due to the inherent inhibition of uniform growth of GaMnAs with high Mn concentrations, little work has been published regarding HT MBE [11–13]. Despite this drawback, the number of As<sub>Ga</sub> in GaMnAs has been found to be reduced by increasing the substrate temperature ( $T_S$ ) [12,13]. Moreover, by growing at intermediate temperatures (IT), from 325 to 500 °C, some authors have been able to improve the optical properties of Mn-doped GaAs layers compared to LT GaMnAs [14,15]. In this paper, to gain more insight into relatively HT GaMnAs, we present a study of Mn-doped GaAs layers prepared by varying the nominal Mn atomic percent (Mn%) from 0.01 to 0.2 at a temperature of 530 °C.

## 2. Experimental

The samples were grown by MBE using solid sources onto epitaxial GaAs (001) substrates. After growing a five-period AlAs

\* Corresponding author. Tel.: +52 4448262300.

E-mail address: [esteban.cruz@uaslp.mx](mailto:esteban.cruz@uaslp.mx) (E. Cruz-Hernández).



## Si-doped AlGaAs/GaAs(6 3 1)A heterostructures grown by MBE as a function of the As-pressure



Víctor-Hugo Méndez-García<sup>a,\*</sup>, S. Shimomura<sup>b</sup>, A.Yu. Gorbachev<sup>c</sup>,  
E. Cruz-Hernández<sup>a</sup>, D. Vázquez-Cortés<sup>b</sup>

<sup>a</sup> Center for the Innovation and Application of Science and Technology, Universidad Autónoma de San Luis Potosí, Av. Sierra Leona # 550, Col. Lomas 2a Sección, C.P. 78210 San Luis Potosí, Mexico

<sup>b</sup> Graduate School of Science and Engineering, Ehime University, 3 Bukyo-cho, Matsuyama 790-8577, Ehime, Japan

<sup>c</sup> Instituto de Investigación en Comunicación Óptica, Universidad Autónoma de San Luis Potosí, Av. Karakorum # 1470, Col. Lomas 2a Secc., C.P. 78210 San Luis Potosí, Mexico

### ARTICLE INFO

Available online 2 April 2015

#### Keywords:

A1. Atomic force microscopy  
A1. Impurities  
A1. Characterization  
A3. Molecular beam epitaxy  
B2. Semiconducting gallium compounds

### ABSTRACT

The effects of doping with silicon (Si) AlGaAs layers grown by molecular beam epitaxy on GaAs (6 3 1)-oriented substrates as a function of the arsenic pressure ( $P_{As}$ ) is presented and compared with layers grown on (1 0 0) oriented substrates. The surface texture of the AlGaAs (6 3 1) films is composed by nanogrooves, whose dimensions depend on  $P_{As}$ . On the contrary, the MBE growth on the (1 0 0) plane resulted on rough surfaces, without evidence of formation of terraces. Mobility and carrier density of AlGaAs:Si layers grown on substrates (6 3 1) were studied as a function of  $P_{As}$ . The doping type conversion from p-type to n-type as a function of the As pressure is corroborated for high index samples. All the films grown on (1 0 0) exhibited silicon n-type doping. These observations were related with the amphotericity of Si, where it acts as a donor impurity occupying Al or Ga-sites or as an acceptor when it takes an As-site, depending on the competition that the Si atoms encounters with As for any of these sites. The acceptor and donor lines close to the AlGaAs transition observed by photoluminescence spectroscopy (PL) were affected by the incorporation of Si. When increasing  $P_{As}$  the energy of the main PL peak is redshifted for n-type AlGaAs layers, but it is shifted back towards high energy once the conduction type conversion takes place. X-ray diffraction patterns revealed high crystalline quality for samples grown at the highest  $P_{As}$ .

© 2015 Elsevier B.V. All rights reserved.

### 1. Introduction

Recently nanotechnology is generating new technological developments and it is envisaged as the most powerful and promising engine for the development of the society. In this emerging area, nanostructured materials are investigated for applications in electronics, optoelectronic and electro-mechanical devices. For example, semiconductor nanowires (NWRs) have emerged as one of the most versatile building blocks for integration of nanoscale devices with current technology. In addition, NWRs has been used for the investigation of basic aspects of one-dimensional systems (1D) [1–4]. In this direction, the growth of semiconductor materials on high-index substrates is a very important subject since it has been proved that, under suitable growth conditions, nanoscale step arrays and

nanogrooves can be self-assembled and later employed as templates for the synthesis of high quality semiconductor NWRs. Recently, highly ordered nanoscale step arrays were obtained in the homoepitaxial growth of GaAs on (6 3 1) oriented substrates [5], opening opportunities to the self-assembling of 1D arrays. Nevertheless, for the further application of these 1D systems, several challenges must be overcome. For example, the obtaining of n- and p-type doped AlGaAs layers is an essential step for the application of NWRs in optoelectronic devices. Si is known to be amphoteric dopant in III–V compounds [6,7]. For example in GaAs, Si behaves as donor or acceptor depending on the lattice site occupation: a Si atom occupying an As (Ga) site acts like an acceptor (donor). In the growth on high index substrates, the doping type strongly depends on both, growth conditions and on the particular substrate orientation [6–11].

In this work the Si doping of AlGaAs layers grown on (6 3 1)-oriented substrates as a function of the  $As_4$ -beam equivalent pressure ( $P_{As}$ ) is studied. The electrical properties obtained by

\* Corresponding author.

E-mail address: [victor.mendez@uaslp.mx](mailto:victor.mendez@uaslp.mx) (V.-H. Méndez-García).



## A Hydrogen detectors Wireless network for monitoring the gas ambient in a laboratory.

F Sánchez-Niño<sup>1</sup>, F J. De Anda Salazar<sup>1</sup>

<sup>1</sup>IICO-UASLP, Av. Karakorum 1470 Lomas 4a sección  
San Luis Potosí, S.L.P, 78210, México

E-mail: franciscosanchezn@gmail.com

**Abstract.** A system to monitor the hydrogen contents in the atmosphere present in the various sections of a crystal growth laboratory has been built. When hydrogen is used in the processes carried out in a laboratory it is important to monitor its content because the oxygen-hydrogen mixture is highly flammable and/or explosive. The system emits a warning when the Hydrogen concentration increases and if the concentration rises above 1 % in vol. it shuts down automatically any process that is using hydrogen. The design and performance of the system is reported here.

### 1. Introduction.

Hydrogen is necessary in many industrial and laboratory processes but there is the problem that when its concentration in the atmosphere is higher than normal the mixture is highly flammable and if its concentration reaches 4 % in vol. the mixture explodes if its temperature reaches 80 °C., the explosion can be triggered by a spark produced by a short circuit or the opening of a switch in an electric circuit [1, 2, 3, 4, 5].

It is then highly desirable to have a system to permanently monitor the hydrogen concentration in the ambient atmosphere if a small rise in the concentration is detected it is a sign that a Hydrogen is leaking somewhere in the process and if it is detected at an early stage the leakage can be found and stopped before the Hydrogen concentrations reaches dangerous values. Also, if somehow the Hydrogen concentration rises above a certain threshold an automatic shut-off of any hydrogen flow or electric circuit could prevent an explosion [1, 2, 3, 4, 5].

### 2. Design of the detectors wireless network.

A block diagram of the network is shown in Fig. 1 it consists of three boards containing a Hydrogen sensor, the signal of the sensor is connected directly to one of the internal ADC converters of a PIC16F877A microcontroller [6]. Depending on the value of the signal the microcontroller sends one of three different commands and an identification signal through a radiofrequency transmitter. There are two reception boards one located outside the laboratory and the other, inside the laboratory, is connected to a PC that controls the experiment where hydrogen is being used.



# Bolometric Properties of Semiconducting and Metallic Single-Walled Carbon Nanotube Composite Films

Trevor J. Simmons,<sup>†,‡</sup> Gustavo Vera-Reveles,<sup>‡,§</sup> Gabriel González,<sup>‡,||</sup> José Manuel Gutiérrez-Hernández,<sup>‡</sup> Robert J. Linhardt,<sup>‡,#,○,□,△</sup> Hugo Navarro-Contreras,<sup>‡</sup> and Francisco J. González<sup>\*,‡</sup>

<sup>†</sup>Center for Future Energy Systems, <sup>‡</sup>Department of Chemistry and Chemical Biology, <sup>#</sup>Center for Biotechnology and Interdisciplinary Studies, <sup>○</sup>Department of Chemical and Biological Engineering, <sup>□</sup>Department of Biomedical Engineering, and <sup>△</sup>Department of Biology, Rensselaer Polytechnic Institute, 110 Eighth Street, Troy, New York 12180, United States

<sup>‡</sup>Coordinación para la Innovación y la Aplicación de la Ciencia y la Tecnología, Universidad Autónoma de San Luis Potosí, San Luis Potosí 78000, México

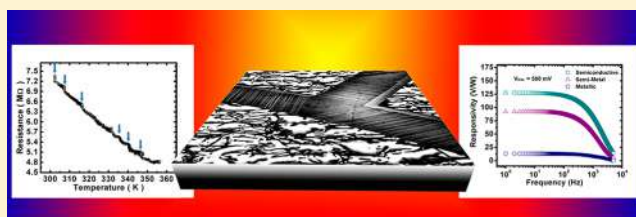
<sup>§</sup>Departamento de Ciencias Básicas, Instituto Tecnológico de San Luis Potosí, Soledad de Graciano Sánchez, 78437 México

<sup>||</sup>Cátedras CONACYT/Universidad Autónoma de San Luis Potosí, San Luis Potosí 78000, México

## Supporting Information

**ABSTRACT:** Single-walled carbon nanotubes (SWNTs) have shown interesting bolometric properties, making them good candidates for the detection of infrared and terahertz radiation. However, little has been reported on the bolometric characteristics of SWNT as a function of their chirality or the possible influence of composite morphology on these properties. The separation of SWNTs based on chirality allows for almost purely semiconductive or metallic SWNTs to be studied. The current study focuses on the bolometric performance of self-assembled composite films of SWNTs. The dependence of these properties on the chirality of the SWNTs was evaluated. To this end, metallic, semiconducting, and a 1:1 mixture of metallic and semiconductive were studied. Also, a theoretical model based on the Wiedemann–Franz law is used to explain the resistance of the SWNT composite films as a function of temperature. Results show that the composite morphology has a significant impact on bolometer performance, with cracked composite films containing highly aligned SWNT arrays suspended over a silicon substrate showing superior responsivity values due to higher thermal isolation. Uncracked composite films showed superior thermal coefficient of resistance values ( $\alpha = -6.5\%/K$ ), however, the responsivity was lower due to lower thermal isolation.

**KEYWORDS:** bolometer, carbon nanotube, chirality, composite, infrared detector



Carbon nanotubes (CNTs) are cylindrical tubes of  $sp^2$ -hybridized carbon. These structures have been studied extensively over the past two decades and continue to find new applications. The optoelectronic properties of single-walled carbon nanotubes (SWNTs) make them an attractive candidate for infrared sensors.<sup>1–3</sup> Uncooled microbolometers, which are a specific class of infrared detectors,<sup>4</sup> represent a promising application for SWNTs. Previous work has shown that self-assembled arrays of highly aligned SWNTs in a polymer–surfactant matrix can achieve bolometric properties superior to those reported in prior CNT-bolometer studies.<sup>5</sup> The current work evaluates how the SWNT composite morphology along with intrinsic SWNT properties affect the performance of these microbolometer devices.

Single-walled carbon nanotubes (SWNTs) may exist as either metallic or semiconductive, depending on their chirality, and in general, the bulk synthesis of SWNTs results in one-third having metallic character and two-thirds having semiconductive character.<sup>6,7</sup> Recent advances in CNT processing have allowed for the separation of these nanotubes based on chirality.<sup>8</sup> These

nanotube separations exhibit almost purely semiconductive or metallic properties, depending on the sample preparation, and have recently become commercially available.

Microbolometers are devices that can detect infrared radiation through a change in their electrical resistance. When the bolometer material absorbs infrared radiation, its temperature increases, and there is a commensurate change in the electrical resistance known as the temperature coefficient of resistance (TCR or  $\alpha$ ), which is measured in percent change of resistance per degree Kelvin (%/K). In the case of semiconductors, increasing temperature due to incident infrared radiation will promote valence electrons into the conduction band, thus, reducing the electrical resistance of the material. In the case of metals, increasing temperature due to incident infrared radiation will increase the electrical resistance of the material. The conversion of incident radiation to electrical signals is known as the responsivity ( $R_v$ ) and is measured in

Received: August 5, 2014

Published: January 28, 2015

Article

## Design and Fabrication of Interdigital Nanocapacitors Coated with HfO<sub>2</sub>

Gabriel González <sup>1,2</sup>, Eleazar Samuel Kolosovas-Machuca <sup>2</sup>, Edgar López-Luna <sup>2</sup>, Heber Hernández-Arriaga <sup>2</sup> and Francisco Javier González <sup>2,\*</sup>

<sup>1</sup> Cátedras Conacyt, Universidad Autónoma de San Luis Potosí, 78000 San Luis Potosí, Mexico; E-Mail: gabriel.gonzalez@uaslp.mx

<sup>2</sup> Coordinación para la Innovación y la Aplicación de la Ciencia y la Tecnología, Universidad Autónoma de San Luis Potosí, 78000 San Luis Potosí, Mexico; E-Mails: samuel.kolosovas@uaslp.mx (E.S.K.-M.); edgar.luna@uaslp.mx (E.L.-L.); heber.hernandez@uaslp.mx (H.H.-A.)

\* Author to whom correspondence should be addressed; E-Mail: javier.gonzalez@uaslp.mx; Tel.: +52-444-826-2300 (ext. 8416).

Academic Editor: Manh-Huong Phan

Received: 5 November 2014 / Accepted: 19 December 2014 / Published: 16 January 2015

---

**Abstract:** In this article nickel interdigital capacitors were fabricated on top of silicon substrates. The capacitance of the interdigital capacitor was optimized by coating the electrodes with a 60 nm layer of HfO<sub>2</sub>. An analytical solution of the capacitance was compared to electromagnetic simulations using COMSOL and with experimental measurements. Results show that modeling interdigital capacitors using Finite Element Method software such as COMSOL is effective in the design and electrical characterization of these transducers.

**Keywords:** interdigital nanocapacitors; finite element method; capacitance

---

### 1. Introduction

Interdigital capacitors (IDCs) are one of the most used transducers in chemical and biological sensors where a change in capacitance or impedance is measured as a response to the interaction between the analyte and a sensitive layer [1]. Interdigital capacitors are used also for the evaluation of near-surface

## Electric radiation mapping of silver/zinc oxide nanoantennas by using electron holography

J. E. Sanchez,<sup>1</sup> F. Mendoza Santoyo,<sup>1,a)</sup> J. Cantu Valle,<sup>1</sup> J. Velazquez-Salazar,<sup>1</sup> M. José Yacaman,<sup>1</sup> F. J. González,<sup>2</sup> R. Diaz de Leon,<sup>3</sup> and A. Ponce<sup>1</sup>

<sup>1</sup>Department of Physics and Astronomy, University of Texas at San Antonio, San Antonio 78249, USA

<sup>2</sup>Coordinación para la Innovación y la Aplicación de la Ciencia y la Tecnología, Universidad Autónoma de San Luis Potosí, San Luis Potosí 78210, Mexico

<sup>3</sup>Instituto Tecnológico de San Luis Potosí, San Luis Potosí 78437, Mexico

(Received 3 October 2014; accepted 17 December 2014; published online 16 January 2015)

In this work, we report the fabrication of self-assembled zinc oxide nanorods grown on pentagonal faces of silver nanowires by using microwaves irradiation. The nanostructures resemble a hierarchical nanoantenna and were used to study the far and near field electrical metal-semiconductor behavior from the electrical radiation pattern resulting from the phase map reconstruction obtained using off-axis electron holography. As a comparison, we use electric numerical approximations methods for a finite number of ZnO nanorods on the Ag nanowires and show that the electric radiation intensities maps match closely the experimental results obtained with electron holography. The time evolution of the radiation pattern as generated from the nanostructure was recorded under *in-situ* radio frequency signal stimulation, in which the generated electrical source amplitude and frequency were varied from 0 to 5 V and from 1 to 10 MHz, respectively. The phase maps obtained from electron holography show the change in the distribution of the electric radiation pattern for individual nanoantennas. The mapping of this electrical behavior is of the utmost importance to gain a complete understanding for the metal-semiconductor (Ag/ZnO) heterojunction that will help to show the mechanism through which these receiving/transmitting structures behave at nanoscale level. © 2015 AIP Publishing LLC. [<http://dx.doi.org/10.1063/1.4906102>]

### I. INTRODUCTION

Intermetallics-semiconductor nanostructures have developed are promising active elements that emulate a metallic nanostructure, which will act as a transmission line "electrically" connected to a semiconductor material that can be used as building blocks for nanoantennas.<sup>1-4</sup> Moreover, the frequency response for these systems is known to be useful in the design of nanoantennas, solar cells, optoelectronic detectors, and nonlinear optical devices.<sup>5-7</sup> In particular, zinc oxide (ZnO) has become one of the most promissory semiconductor materials to be used in metal-semiconductor alloys due to the fact that its structure and morphological arrangements can be controlled in a precise way to match a particular metal-semiconductor configuration. The combination of a metal with ZnO has demonstrated interesting physic-electrical properties that could be manipulated when acting in a particular optoelectronic application.<sup>8-10</sup> Furthermore, it has been reported that using different ensemble mechanisms for the metal-semiconductor structure, it is possible to integrate highly ordered silver-zinc oxide (Ag/ZnO) nanostructure systems.<sup>8</sup> It is worth pointing out here that most of the ZnO nanostructure production methods are based on chemical reactions involving synthesis and thermal treatments at high temperatures (around 400–500 °C) with reactions times around 48 h.<sup>11</sup> Despite the fact that these methods lead to well aligned nanostructures, normally in a

preferential c-axis direction and with high stability, it is well known that they are time consuming with high production costs a major drawback in profitable market industries, where mass production has to be considered. An alternative chemical synthesis process is the microwave irradiation process (MIP), which has demonstrated a significant time reduction compared with the thermal chemical synthesis methods.<sup>11-14</sup> Besides, the MIP method also stimulates the growth with precise control and distribution of well-aligned crystalline nanostructures. One of the most important characteristics in this growing process for Ag/ZnO systems is the control of their morphological distribution that is associated to their electrical properties observed due to the metal-semiconductor junction. In order to theoretically study the influence of the geometrical arrangement on the electrical properties in a variety of similar systems, several approaches on numerical electromagnetic code techniques are used to understand the electrical and its time evolution response in this type of high order nanostructures.<sup>15,16</sup> An experimental approach worth noticing uses specific optical techniques that allow the mapping of the electrical response of metal-semiconductor junctions. Specifically, using near field optical microscopy as well as Fourier microphotoluminescence measurements, it is possible to scan the near and far electric fields using polarized light that induces a charge distribution on the metal-semiconductor junction, enabling to study the electric near/far field behavior.<sup>17-19</sup>

Today's available literature contains many reports on fundamental theory related to furthering the understanding

<sup>a)</sup>On sabbatical leave Centro de Investigaciones en Óptica, León, Guanajuato 37150, Mexico.

Available online at [www.sciencedirect.com](http://www.sciencedirect.com)

# Journal of Applied Research and Technology



Journal of Applied Research and Technology xxx (2015) xxx–xxx

[www.jart.ccadet.unam.mx](http://www.jart.ccadet.unam.mx)

Original

## Enhancement of antenna-coupled microbolometers response by impedance matching<sup>☆</sup>

Jorge Simón<sup>a,\*</sup>, Eleazar Samuel Kolosovas-Machuca<sup>b</sup>, Gustavo Vera-Reveles<sup>b</sup>, Edgar Briones<sup>b</sup>,  
Jorge Flores-Troncoso<sup>c</sup>, Francisco Javier González<sup>b</sup><sup>a</sup> Cátedras CONACYT, Centro de Investigación y Desarrollo en Telecomunicaciones Espaciales, Unidad Académica de Ingeniería Eléctrica, Universidad Autónoma de Zacatecas<sup>b</sup> Coordinación para la Innovación y la Aplicación de la Ciencia y la Tecnología, Universidad Autónoma de San Luis Potosí<sup>c</sup> Centro de Investigación y Desarrollo en Telecomunicaciones Espaciales, Unidad Académica de Ingeniería Eléctrica, Universidad Autónoma de Zacatecas

Received 14 January 2015; accepted 7 September 2015

### Abstract

Metallic structures were evaluated to determine the one best matches impedance between lithographic antennas and microbolometers. The best was a  $0.28\lambda$  transmission line section between the antenna and the microbolometer, 12% longer than what RF theory sets, whose behaviour was compared with other structures. The response was 360% higher.

All Rights Reserved © 2015 Universidad Nacional Autónoma de México, Centro de Ciencias Aplicadas y Desarrollo Tecnológico. This is an open access item distributed under the Creative Commons CC License BY-NC-ND 4.0.

**Keywords:** Enhancement; Antenna-coupled; Microbolometer; Response; Impedance; Matching

### 1. Introduction

Terahertz antennas (lithographic antennas) are devices which had opened a new route for the sensing and manipulation of the mid-infrared electromagnetic radiation free in the space, founding in last years applications in the field of infrared image acquisition (Gonzalez, Ilic, Alda, & Boreman, 2005) and solar energy harvesting (Briones, Alda, & González, 2013). Terahertz antennas work by using the wave nature of the THz radiation in order to induce a resonant alternate current along the antennas arms (with the same frequency of the incoming wave) which is exploited to sense or recover the optical energy of radiation.

In imaging applications, these types of antennas have been coupled with success to niobium microbolometers to capture images with infrared cameras containing hundreds of these elements (González, Gritz, Fumeaux, & Boreman, 2002). The presence of current in antennas heats the microbolometers

loaded to them, leading to an increase of its temperature what in turns changes the resistance of bolometers, defining this way the detection mechanism (Codreanu, Gonzalez, & Boreman, 2003). In the field of solar energy harvesting, lithographic antennas have been used to capture radiation coming from the sun and to build solar energy panels (Bareisß et al., 2011) when coupled to THz rectifiers based on metal-oxide–metal diodes, allowing the recovering of the optical energy into Direct Current (DC) Power.

In spite of the attractive properties of the THz antennas as thermal devices, the principal reason that they have not been yet employed in commercial applications it is their low performance, arising from impedance matching or energy transfer problems between the THz antennas and the load elements; being a topic of current interest (Krenz et al., 2012; Mandviwala, Boreman, & Lail, 2008; Mandviwala, Lail, & Boreman, 2005). Some coupling methods commonly used with the radio and microwave antennas have recently been scaled to the THz regime in order to better match the diodes to the antennas. In this context, transmission lines have been used as impedance-matching elements between a thermocouple and a bow-tie antenna tuned to absorb in the mid-infrared region, obtaining a substantially

<sup>☆</sup> Peer Review under the responsibility of Universidad Nacional Autónoma de México.

\* Corresponding author.

E-mail address: [jsimonr@gmail.com](mailto:jsimonr@gmail.com) (J. Simón).

<http://dx.doi.org/10.1016/j.jart.2015.10.005>

1665-6423/All Rights Reserved © 2015 Universidad Nacional Autónoma de México, Centro de Ciencias Aplicadas y Desarrollo Tecnológico. This is an open access item distributed under the Creative Commons CC License BY-NC-ND 4.0.

Wednesday, July 9 between 10:00-20:00 GMT we'll be busy making things better. You'll still be able to search, browse and read our articles, but you won't be able to register, edit your account, post content, or activate tokens or eprints during that period.



Journal

**Journal of Immunoassay and Immunochemistry** >

Volume 36, 2015 - Issue 2

Enter keywords, authors, DOI etc.

This Journal

117

Views

0


CrossRef citations

0

Altmetric


Original Articles

# Resistance-Based Biosensor of Multi-Walled Carbon Nanotubes

E. S. Kolosovas-Machuca , G. Vera-Reveles, M. C. Rodríguez-Aranda, L. C. Ortiz-Dosal, Emmanuel Segura-Cardenas & Francisco J. Gonzalez

Pages 142-148 | Accepted author version posted online: 01 Apr 2014, Published online: 01 Apr 2014

 Download citation

 <http://dx.doi.org/10.1080/15321819.2014.908129>

 Check for updates

 Full Article

 Figures & data

 References

 Citations

 Metrics

 Reprints & Permissions

Get access



## Abstract

Multi-Walled Carbon Nanotubes (MWNTs) are a good choice for resistive biosensors due to their great resistance changes when immunoreactions take place, they are also low-cost, more biocompatible than single-walled carbon nanotubes, and resistive measurement equipment is usually not expensive and readily available. In this work a novel resistive biosensor based on the immobilization of an antigen through a silanization process over the surface of Multi-Walled Carbon Nanotubes (MWNTs) is reported. Results show that the biosensor increases its conductivity when adding the antigen and

Seleccionar idioma

Translator disclaimer

Sample Our  
Physical Science journals



# Resonance properties of Ag-ZnO nanostructures at terahertz frequencies

John E. Sanchez,<sup>1</sup> Ramón Díaz de León,<sup>2</sup> Fernando Mendoza-Santoyo,<sup>1</sup>  
Gabriel González,<sup>3</sup> Miguel José-Yacaman,<sup>1</sup> Arturo Ponce,<sup>1</sup>  
and Francisco Javier González<sup>3,\*</sup>

<sup>1</sup> Department of Physics and Astronomy, University of Texas at San Antonio, San Antonio 78249, USA

<sup>2</sup> Instituto Tecnológico de San Luis Potosí, San Luis Potosí 78437, Mexico

<sup>3</sup> Coordinación para la Innovación y la Aplicación de la Ciencia y la Tecnología, Universidad Autónoma de San Luis Potosí, San Luis Potosí, 78210, Mexico

\*javier.gonzalez@uaslp.mx

**Abstract:** Nanoantennas have been fabricated by scaling down traditional antenna designs using nanolithographic techniques and testing them at different optical wavelengths, these particular nanoantennas have shown responses in a broad range of frequencies going from visible wavelengths to the range of the terahertz. Some self-assembled nanostructures exist that exhibit similar shapes and properties to those of traditional antenna structures. In this work the emission and absorption properties of self-assembled nanostructures made of zinc oxide nanorods on silver nanowires, which resemble traditional dipole antennas, were measured and simulated in order to test their antenna performance. These structures show resonant properties in the 10-120 THz range, with the main resonance at 60 THz. The radiation pattern of these nanostructures was also obtained by numerical simulations, and it is shown that it can be tailored to increase or decrease its directivity as a function of the location of the energy source of excitation. Experimental measurements were performed by Raman spectroscopy and Fourier Transform Infrared Spectroscopy (FTIR) in order to show existing vibrational frequencies at the resonant frequencies of the nanostructures, measurements were made from ~9 to 103 THz and the results were in agreement with the simulations. These characteristics make these metal-semiconductor Ag/ZnO nanostructures useful as self-assembled nanoantennas in applications such as terahertz spectroscopy and sensing at terahertz frequencies.

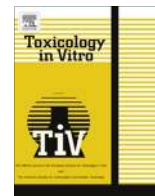
©2015 Optical Society of America

OCIS codes: (040.2235) Far infrared or terahertz; (160.4236) Nanomaterials.

---

## References and links

1. T. H. Taminiau, F. D. Stefani, F. B. Segerink, and N. F. van Hulst, "Optical antennas direct single-molecule emission," *Nat. Photonics* **2**(4), 234–237 (2008).
2. F. J. González and G. D. Boreman, "Comparison of dipole, bowtie, spiral and log-periodic IR antennas," *Infrared Phys. Technol.* **46**(5), 418–428 (2005).
3. J. E. Sanchez, F. Mendoza-Santoyo, J. Cantu-Valle, J. Velazquez-Salazar, M. José Yacaman, F. J. González, R. Díaz de León, and A. Ponce, "Electric radiation mapping of silver/zinc oxide nanoantennas by using electron holography," *J. Appl. Phys.* **117**(3), 034306 (2015).
4. S. Kim, J. Jin, Y.-J. Kim, I.-Y. Park, Y. Kim, and S.-W. Kim, "High-harmonic generation by resonant plasmon field enhancement," *Nature* **453**(7196), 757–760 (2008).
5. R. M. Bakker, V. P. Drachev, Z. Liu, H.-K. Yuan, R. H. Pedersen, A. Boltasseva, J. Chen, J. Irudayaraj, A. V. Kildishev, and V. M. Shalaev, "Nanoantenna array-induced fluorescence enhancement and reduced lifetimes," *New J. Phys.* **10**(12), 125022 (2008).
6. P. Anger, P. Bharadwaj, and L. Novotny, "Enhancement and quenching of single-molecule fluorescence," *Phys. Rev. Lett.* **96**(11), 113002 (2006).
7. K. Kneipp, Y. Wang, H. Kneipp, L. T. Perelman, I. Itzkan, R. R. Dasari, and M. S. Feld, "Single molecule detection using surface-enhanced Raman scattering (SERS)," *Phys. Rev. Lett.* **78**(9), 1667–1670 (1997).



## Brief communication

## Single-walled carbon nanotubes (SWCNTs) induce vasodilation in isolated rat aortic rings



J.M. Gutiérrez-Hernández<sup>a,1</sup>, M.A. Ramirez-Lee<sup>b,1</sup>, H. Rosas-Hernandez<sup>b</sup>, S. Salazar-García<sup>b</sup>, D.A. Maldonado-Ortega<sup>b</sup>, F.J. González<sup>a</sup>, C. Gonzalez<sup>b,\*</sup>

<sup>a</sup> Universidad Autonoma de San Luis Potosi, Coordinacion para la Innovacion y la Aplicacion de la Ciencia y la Tecnologia, San Luis Potosi, Mexico

<sup>b</sup> Universidad Autonoma de San Luis Potosi, Facultad de Ciencias Quimicas, San Luis Potosi, Mexico

## ARTICLE INFO

## Article history:

Received 14 August 2014

Accepted 3 February 2015

Available online 11 February 2015

## Keywords:

Aorta

Endothelium

Single walled carbon nanotubes

Vascular tone

Smooth muscle

Vasodilation

## ABSTRACT

Single-walled carbon nanotubes (SWCNTs) are used in biological systems with impact in biomedicine in order to improve diagnostics and treatment of diseases. However, their effects upon the vascular system, are not fully understood. Endothelium and smooth muscle cells (SMC) communicate through release of vasoactive factors as nitric oxide (NO) to maintain vascular tone. The aim of this study was to evaluate the effect of SWCNTs on vascular tone using isolated rat aortic rings, which were exposed to SWCNTs (0.1, 1 and 10 µg/mL) in presence and absence of endothelium. SWCNTs induced vasodilation in both conditions, indicating that this effect was independent on endothelium; moreover that vasodilation was NO-independent, since its blockage with L-NAME did not modify the observed effect. Together, these results indicate that SWCNTs induce vasodilation in the macrovasculature, may be through a direct interaction with SMC rather than endothelium independent of NO production. Further investigation is required to fully understand the mechanisms of action and mediators involved in the signaling pathway induced by SWCNTs on the vascular system.

© 2015 Elsevier Ltd. All rights reserved.

## 1. Introduction

Recently, the advancement of nanotechnology has led to the generation of materials with unique physicochemical properties, known as nanomaterials (NMs), structures that have one or more external dimensions within the size range of 1–100 nm (Fiorino, 2010). Among all NMs, carbon nanotubes (CNTs) confer potential biological applications, due to their mechanical and optical properties (Wu et al., 2008; Tang et al., 2012). Single-walled CNTs (SWCNTs) are made of single graphene cylindrically folded sheet (Zhu et al., 2003; Bianco et al., 2011; Wang et al., 2011), and have several biomedical applications (Wu et al., 2008; Liu et al., 2009; Kang et al., 2008; Yang et al., 2010; Sridharan et al., 2009; Harrison et al., 2007; Sinha et al., 2006). It has been demonstrated that SWCNTs can deposit in lungs inducing inflammatory mediators release and activating thrombogenic proteins (Erdely et al., 2009), altering the structures of the cardiovascular system,

including the endothelium, that coats the intimal surface of the vessels (Vallance, 1992; Bauer and Sotníková, 2010), playing a pivotal role in the vascular tone regulation through the release of vasoconstrictive (tromboxane and endothelin-1), or vasodilator factors (nitric oxide (NO), prostacyclin) (Sandoo et al., 2010; Giles et al., 2012). It has been reported that SWCNTs combined with iron and gadolinium, promote dual effect upon vascular tone of murine small arterioles, vasodilation in presence of aggregated SWCNTs, and vasoconstriction in non-aggregated state (Frame et al., 2014). Despite the current and controversial reports of SWCNTs in circulatory system, there still a lack of information about their direct effects on this system. The aim of this study was to evaluate the direct effect of purified SWCNTs on vascular tone using an isolated rat aortic rings model.

## 2. Materials and methods

## 2.1. Chemicals

SWCNTs were purchased from Thomas Swan, Advanced Materials (United Kingdom). Other compounds such as phenylephrine (Phe), N-(1-Naphthyl) ethylenediamine dihydrochlorid, sulfanilamide, vanadium (III) chloride, N<sup>G</sup>-nitro-L-arginine methyl

\* Corresponding author at: Universidad Autonoma de San Luis Potosi, Facultad de Ciencias Quimicas, Av. Manuel Nava Num. 6, Col. Universitaria, Zip Code 78210, San Luis Potosi, Mexico. Tel.: +52 444 8262440x6521.

E-mail addresses: [cgonzalez.uaslp@gmail.com](mailto:cgonzalez.uaslp@gmail.com), [gonzalez.castillocarmen@fcq.uaslp.mx](mailto:gonzalez.castillocarmen@fcq.uaslp.mx) (C. Gonzalez).

<sup>1</sup> These authors contributed equally in the realization of this work.



# On the Decay of Crossing Numbers of Sparse Graphs

————— József Balogh,<sup>1,\*</sup> Jesus Leños,<sup>2</sup> and Gelasio Salazar<sup>3</sup>

<sup>1</sup>DEPARTMENT OF MATHEMATICAL SCIENCES  
UNIVERSITY OF ILLINOIS AT URBANA-CHAMPAIGN  
ILLINOIS  
E-mail: jobal@math.uiuc.edu

<sup>2</sup>UNIDAD ACADÉMICA DE MATEMÁTICAS  
UAZ. ZACATECAS, MEXICO  
E-mail: jleanos@mate.reduaz.mx

<sup>3</sup>INSTITUTO DE FÍSICA  
UASLP. SAN LUIS POTOSI, MEXICO  
E-mail: gsalazar@ifisica.uaslp.mx

Received March 2, 2012; Revised September 24, 2014

Published online 19 December 2014 in Wiley Online Library (wileyonlinelibrary.com).

DOI 10.1002/jgt.21848

**Abstract:** Richter and Thomassen proved that every graph has an edge  $e$  such that the crossing number  $\text{cr}(G - e)$  of  $G - e$  is at least  $(2/5)\text{cr}(G) - O(1)$ . Fox and Cs. Tóth proved that dense graphs have large sets of edges (proportional in the total number of edges) whose removal leaves a graph

---

\*Contract grant sponsor: NSF CAREER; Contract grant number: DMS-0745185; Contract grant sponsor: UIUC Campus Research Board; Contract grant number: 11067; Contract grant sponsor: OTKA; Contract grant number: K76099 (to J. B.) Supported by the European Union and co-funded by the European Social Fund under the project “Telemedicine-focused research activities on the field of Mathematics, Informatics and Medical sciences” of project number “TÁMOP-4.2.2.A-11/1/KONV-2012-0073”.

Contract grant sponsor: CONACYT; Contract grant number: 179867 (to J. L.).  
Contract grant sponsor: CONACYT; Contract grant number: 106432 (to G. S.).

Journal of Graph Theory  
© 2015 Wiley Periodicals, Inc.

# Analysis of cytotoxic effects of silver nanoclusters on human peripheral blood mononuclear cells 'in vitro'

Sandra Teresa Orta-García<sup>a,b</sup>, Germán Plascencia-Villa<sup>c</sup>,  
Angeles Catalina Ochoa-Martínez<sup>a,b</sup>, Tania Ruiz-Vera<sup>a,b</sup>,  
Francisco Javier Pérez-Vázquez<sup>a,b</sup>, J Jesús Velázquez-Salazar<sup>c</sup>,  
Miguel José Yacamán<sup>c</sup>, Hugo Ricardo Navarro-Contreras<sup>a</sup>  
and Iván N. Pérez-Maldonado<sup>a,b,d,\*</sup>

**ABSTRACT:** The antimicrobial properties of silver nanoparticles (AgNPs) have made these particles one of the most used nanomaterials in consumer products. Therefore, an understanding of the interactions (unwanted toxicity) between nanoparticles and human cells is of significant interest. The aim of this study was to assess the *in vitro* cytotoxicity effects of silver nanoclusters (AgNC, < 2 nm diameter) on peripheral blood mononuclear cells (PBMC). Using flow cytometry and comet assay methods, we demonstrate that exposure of PBMC to AgNC induced intracellular reactive oxygen species (ROS) generation, DNA damage and apoptosis at 3, 6 and 12 h, with a dose-dependent response (0.1, 1, 3, 5 and 30  $\mu\text{g ml}^{-1}$ ). Advanced electron microscopy imaging of complete and ultrathin-sections of PBMC confirmed the cytotoxic effects and cell damage caused by AgNC. The present study showed that AgNC produced without coating agents induced significant cytotoxic effects on PBMC owing to their high aspect ratio and active surface area, even at much lower concentrations (<1  $\mu\text{g ml}^{-1}$ ) than those applied in previous studies, resembling what would occur under real exposure conditions to nanosilver-functionalized consumer products. Copyright © 2015 John Wiley & Sons, Ltd.

**Keywords:** apoptosis; comet assay; cytotoxicity; nanoparticles; oxidative stress; PBMC; silver nanoclusters

## Introduction

Nanotechnology has been an actively expanding research area during recent years. The novel physical and chemical properties of materials at the nanoscale (1–100 nm) have been exploited in different consumer products and applications in life sciences. However, the increasing use of nanomaterials has identified some concerns regarding their possible adverse effects, especially cell toxicity (Cedervall *et al.*, 2007; Dawson *et al.*, 2009; Donaldson and Poland, 2009; Elder, 2009; Kane and Hurt, 2008; Mitchell *et al.*, 2009; Myllynen, 2009; Keelan, 2011; Mahmoudi *et al.*, 2011; Samuel, 2011).

Among all the nanomaterials currently used in consumer products, silver nanoparticles (AgNP) have the highest degree of commercialization, with more than 1000 products currently in the market (Henig, 2007; Nanotechproject, 2013). Different AgNP formulations have been developed and applied as effective antimicrobial and viricidal agents (Chen and Schluesener, 2008; Klaine *et al.*, 2008), particularly in functionalization of nanofiber mats, bandages, wound dressings and ointments, among others (Melaiye *et al.*, 2005; Margaret *et al.*, 2006). Additionally, AgNP prevents bacterial colonization of surfaces, such in catheters (Samuel and Guggenbichler, 2004), prostheses (Gosheger *et al.*, 2004) and clothing (Vigneshwaran *et al.*, 2007). Thus, humans can be constantly exposed to AgNP from many different sources. Nanoparticles may enter the human body through inhalation, ingestion, injection and dermal contact (Wijnhoven *et al.*, 2009).

Consequently AgNP are translocated to the circulatory system to be in direct contact with blood cells, and eventually distributed and accumulated throughout the main organs, especially the kidneys, liver, spleen and brain (Tang *et al.*, 2009).

Despite the increasing use of AgNP in many products, there is a serious lack of quantitative analysis of potential cytotoxicity and cellular responses of human blood cells to AgNP. Although several studies have observed the cytotoxic effects of AgNP, most of them were performed on mammalian and human immortalized cell lines (Braydich-Stolle *et al.*, 2005; Hussain *et al.*, 2005; Park *et al.*,

\*Correspondence to: Ivan Nelinho Pérez-Maldonado. Avenida Sierra Leona No. 550, Colonia Lomas Segunda Sección, San Luis Potosí 78210, SLP, México.  
E-mail: ivan.perez@uaslp.mx

<sup>a</sup>Laboratorio de Toxicología Molecular, Centro de Investigación Aplicada en Ambiente y Salud (CIAAS), Coordinación para la Innovación y Aplicación de la Ciencia y la Tecnología (CIACYT), Universidad Autónoma de San Luis Potosí, San Luis Potosí, México

<sup>b</sup>Facultad de Medicina, Universidad Autónoma de San Luis Potosí, San Luis Potosí, México

<sup>c</sup>Department of Physics & Astronomy, The University of Texas at San Antonio (UTSA), San Antonio, Texas, USA

<sup>d</sup>Unidad Académica Multidisciplinaria Zona Media, Universidad Autónoma de San Luis Potosí San Luis Potosí, México

# Bolometric Properties of Semiconducting and Metallic Single-Walled Carbon Nanotube Composite Films

Trevor J. Simmons,<sup>†,‡</sup> Gustavo Vera-Reveles,<sup>‡,§</sup> Gabriel González,<sup>‡,||</sup> José Manuel Gutiérrez-Hernández,<sup>‡</sup> Robert J. Linhardt,<sup>‡,#,○,□,△</sup> Hugo Navarro-Contreras,<sup>‡</sup> and Francisco J. González<sup>\*,‡</sup>

<sup>†</sup>Center for Future Energy Systems, <sup>‡</sup>Department of Chemistry and Chemical Biology, <sup>#</sup>Center for Biotechnology and Interdisciplinary Studies, <sup>○</sup>Department of Chemical and Biological Engineering, <sup>□</sup>Department of Biomedical Engineering, and <sup>△</sup>Department of Biology, Rensselaer Polytechnic Institute, 110 Eighth Street, Troy, New York 12180, United States

<sup>‡</sup>Coordinación para la Innovación y la Aplicación de la Ciencia y la Tecnología, Universidad Autónoma de San Luis Potosí, San Luis Potosí 78000, México

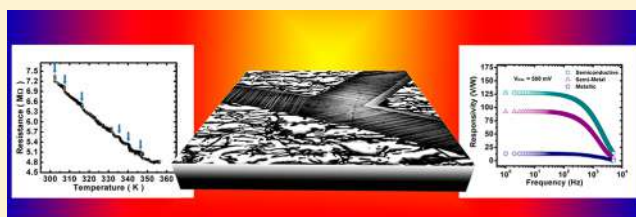
<sup>§</sup>Departamento de Ciencias Básicas, Instituto Tecnológico de San Luis Potosí, Soledad de Graciano Sánchez, 78437 México

<sup>||</sup>Cátedras CONACYT/Universidad Autónoma de San Luis Potosí, San Luis Potosí 78000, México

## Supporting Information

**ABSTRACT:** Single-walled carbon nanotubes (SWNTs) have shown interesting bolometric properties, making them good candidates for the detection of infrared and terahertz radiation. However, little has been reported on the bolometric characteristics of SWNT as a function of their chirality or the possible influence of composite morphology on these properties. The separation of SWNTs based on chirality allows for almost purely semiconductive or metallic SWNTs to be studied. The current study focuses on the bolometric performance of self-assembled composite films of SWNTs. The dependence of these properties on the chirality of the SWNTs was evaluated. To this end, metallic, semiconducting, and a 1:1 mixture of metallic and semiconductive were studied. Also, a theoretical model based on the Wiedemann–Franz law is used to explain the resistance of the SWNT composite films as a function of temperature. Results show that the composite morphology has a significant impact on bolometer performance, with cracked composite films containing highly aligned SWNT arrays suspended over a silicon substrate showing superior responsivity values due to higher thermal isolation. Uncracked composite films showed superior thermal coefficient of resistance values ( $\alpha = -6.5\%/K$ ), however, the responsivity was lower due to lower thermal isolation.

**KEYWORDS:** bolometer, carbon nanotube, chirality, composite, infrared detector



Carbon nanotubes (CNTs) are cylindrical tubes of  $sp^2$ -hybridized carbon. These structures have been studied extensively over the past two decades and continue to find new applications. The optoelectronic properties of single-walled carbon nanotubes (SWNTs) make them an attractive candidate for infrared sensors.<sup>1–3</sup> Uncooled microbolometers, which are a specific class of infrared detectors,<sup>4</sup> represent a promising application for SWNTs. Previous work has shown that self-assembled arrays of highly aligned SWNTs in a polymer–surfactant matrix can achieve bolometric properties superior to those reported in prior CNT-bolometer studies.<sup>5</sup> The current work evaluates how the SWNT composite morphology along with intrinsic SWNT properties affect the performance of these microbolometer devices.

Single-walled carbon nanotubes (SWNTs) may exist as either metallic or semiconductive, depending on their chirality, and in general, the bulk synthesis of SWNTs results in one-third having metallic character and two-thirds having semiconductive character.<sup>6,7</sup> Recent advances in CNT processing have allowed for the separation of these nanotubes based on chirality.<sup>8</sup> These

nanotube separations exhibit almost purely semiconductive or metallic properties, depending on the sample preparation, and have recently become commercially available.

Microbolometers are devices that can detect infrared radiation through a change in their electrical resistance. When the bolometer material absorbs infrared radiation, its temperature increases, and there is a commensurate change in the electrical resistance known as the temperature coefficient of resistance (TCR or  $\alpha$ ), which is measured in percent change of resistance per degree Kelvin ( $\%/K$ ). In the case of semiconductors, increasing temperature due to incident infrared radiation will promote valence electrons into the conduction band, thus, reducing the electrical resistance of the material. In the case of metals, increasing temperature due to incident infrared radiation will increase the electrical resistance of the material. The conversion of incident radiation to electrical signals is known as the responsivity ( $R_v$ ) and is measured in

Received: August 5, 2014

Published: January 28, 2015

# Determination of the Thermal Expansion Coefficient of Single-Wall Carbon Nanotubes by Raman Spectroscopy

L. I. ESPINOSA-VEGA, A. G. RODRÍGUEZ, H. NAVARRO-CONTRERAS, and M. A. VIDAL

*Coordinación para la Innovación y la Aplicación de la Ciencia y la Tecnología (CIACYT) Universidad Autónoma de San Luis Potosí, San Luis Potosí, México*

Received 20 September 2013, Accepted 24 October 2013

We have examined the effect of high temperature on single-wall carbon nanotubes under air and nitrogen ambient by Raman spectroscopy. We observe the temperature dependence of the radial breathing mode and the G-band modes. The thermal expansion coefficient ( $\beta$ ) of the bundled nanotubes is obtained experimentally using the estimated volume from Raman scattering.  $\beta$  behaves linearly with temperature from  $0.33 \times 10^{-5} \text{ K}^{-1}$  to  $0.28 \times 10^{-5} \text{ K}^{-1}$  in air and from  $0.58 \times 10^{-5} \text{ K}^{-1}$  to  $0.47 \times 10^{-5} \text{ K}^{-1}$  in nitrogen ambient, respectively. The temperature dependence of the radial breathing mode Raman frequencies is consistent with a pure temperature effect.

**Keywords:** nanotubes, Raman spectroscopy, thermal expansion

## Introduction

Research on single-wall carbon nanotubes (SWCNTs) has been of great interest due to their potential applications given their electronic, mechanical, and thermal properties.<sup>[1]</sup> For certain applications, it is important to know the effect of high temperature on the properties of nanotubes. Raman scattering is one of the useful analysis techniques for the characterization of carbon nanostructures and investigation of their properties.<sup>[2–7]</sup> The Raman spectra from the SWCNTs have unique features, such as the G-band, D-band, and the radial breathing mode (RBM) peaks, which are related to the conductivity, the quality, and the diameter distribution of the SWCNTs. These measurements are usually obtained at room temperature but the temperature-dependent Raman frequency shift of carbon nanomaterials has also been reported.<sup>[2–7]</sup> The Raman spectra of SWCNTs can present some significant changes with increasing temperature such as frequency shifts, increase or decrease of the modes intensity, and the G-peaks broadening. A few authors have noted that the frequency decreases with increasing temperature for all the Raman peaks of straight nanotubes and rings in SWCNT bundles.<sup>[4]</sup> Raravikar et al. report a softening of the radial and tangential band frequencies with temperature and estimate the contribution of the factors that may be responsible for the observed temperature dependence of

the RBM frequency.<sup>[2]</sup> Maoshuai et al. obtain the Raman spectra of carbon nanobuds and compare them to those of SWCNT and show the thermal stability of these nanostructures.<sup>[8]</sup>

In this paper, we present the Raman Spectroscopy of SWCNTs when heated under two different ambient conditions: air and nitrogen. We show that the experimental data of the Raman shifts allow us to determine the thermal expansion coefficient of the nanotubes. The experimental coefficient is in good agreement with calculated values of the linear thermal expansion coefficient and X-ray measurements.<sup>[2,9]</sup> In air, the process is reversible up to a critical temperature between 855 and 875 K. If the nanotubes are heated above this temperature, the RBM and G phonon line-shapes change abruptly, and the process is no longer reversible. On the other hand, if the nanotubes are heated in nitrogen the phonon line-shapes of the Raman spectra do not deteriorate permanently with temperature, and the process remains reversible up to 1075 K. The irreversibility may be caused by oxygen adsorption when the nanotubes are heated in air, as revealed energy-dispersive X-ray spectroscopy (EDS) measurements.

## Experimental Details

The SWCNT bundles under study were purchased from Nano-Lab, Waltham, MA, USA. According to the vendor specifications, the nanotubes diameter is 1–1.5 nm with an average length of 1  $\mu\text{m}$  and approximately 90% pure. Raman scattering measurements were carried out in SWCNTs at different temperatures. The Raman scattering measurements were done using a Jobin-Yvon T64000 spectrometer

Address correspondence to A. G. Rodríguez, Coordinación para la Innovación y la Aplicación de la Ciencia y la Tecnología (CIACYT) Universidad Autónoma de San Luis Potosí, Álvaro Obregón 64, San Luis Potosí, S. L. P. 78000, México. E-mail: angel.rodriguez@uaslp.mx

## Raman scattering from $\text{Ge}_{1-x}\text{Sn}_x$ ( $x \leq 0.14$ ) alloys

H. Navarro-Contreras, A.G. Rodríguez, and M.A. Vidal

*Coordinación para la Innovación y la Aplicación de la Ciencia y la Tecnología, Universidad Autónoma de San Luis Potosí, Álvaro Obregón 64, San Luis Potosí, S.L.P. 78000, México.*

H. Pérez-Ladrón de Guevara

*Centro Universitario de los Lagos, Universidad de Guadalajara, Av. Enrique Díaz de León 1144, Col. Paseos de la Montaña, Lagos de Moreno, Jal. 47460, México.*

Received 5 November 2014; accepted 18 August 2015

$\text{Ge}_{1-x}\text{Sn}_x$  alloys with  $x$  concentration up to 0.14 were grown on Ge(001) and GaAs(001) substrates in a conventional R. F. Magnetron Sputtering system at low substrate temperatures. The structural characteristics of these alloys were studied for different Sn concentrations between 1 to 14 % by high resolution X ray diffraction, and Raman spectroscopy. Contrasting characteristics of the grown layers are observed if the Sn concentration is larger or smaller than 6 % as revealed by X-ray diffraction and Raman spectroscopy.

*Keywords:* Raman; space correlation model.

PACS: 68; 68.35.bg

### 1. Introduction

$\text{Ge}_{1-x}\text{Sn}_x$  alloys, pertaining to the IV-IV column of the periodic table, have been a subject of interest for the last two decades, due to the very attractive possibility to fabricate with them materials consisting of elements of the column IV that may have a direct electronic band gap tunable from 0 to near 0.55 eV [1]. The study is driven by the interest to apply them as systems to produce far and medium infrared diodes, photodetectors [2,3] and lasers [4,5]; hence, as a very convenient substitute for the Hg-Cd-Te system [6]. These alloys have also been used as buffer layers for a complete integration between Ge or the ternary alloy  $\text{Ge}_{1-x-y}\text{Si}_x\text{Sn}_y$  on Si substrates, instead of  $\text{Si}_{1-x}\text{Ge}_x$  alloys [7-9]. Calculations in the strong bonding models [10] and from pseudopotential methods [11] in the virtual crystal approximation, have predicted that  $\text{Ge}_{1-x}\text{Sn}_x$  alloys must exhibit a direct band gap somewhere in the tin composition range between  $x = 0.2$  to 0.5 eV in non-stressed films [12]. Additionally, due to the prevalence of covalent bonding of both Ge and Sn, and similar external electronic configurations, it has been predicted in the same set of theoretical works, that  $\text{Ge}_{1-x}\text{Sn}_x$  must have higher carrier mobility's than other semiconductor compounds or alloys, with band gaps in the same energy range, due to the absence of polar phononic dispersion [6].

When the alloy is prepared starting from Ge, a direct gap material is eventually obtained, that evolves from indirect to direct electronic band gap as a result of the fact that the  $\Gamma$ -point conduction-band minimum decreases in energy value more rapidly than the  $L$ -point valleys at the [111] points at the border of the Brillouin Zone [10,11,14,15]. Moreover, as  $\text{Ge}_{1-x}\text{Sn}_x$  alloys are always prepared as strained films grown mainly either on Si or Ge substrates, the presence of compressive strain is expected to decrease the Sn concentration at which the indirect  $L_6 \rightarrow \Gamma_8$  to direct  $L_7 \rightarrow \Gamma_8$  band-gap crossover is observed [7,12,15-18].

The growth of these  $\text{Ge}_{1-x}\text{Sn}_x$  alloys, however, has been limited because it presents severe difficulties, that have to be overcome, stemming from to the following three factors: (a) limited Sn miscibility in the Ge (less than 1%) or of the Ge in Sn (less than 0.6%) [19]; (b) the tendency of the diamond tin phase ( $\alpha$ -Sn) to spontaneously suffer a transition to the metallic phase ( $\beta$ -Sn) at temperatures higher than 13.2 °C [20]; (c) with increasing Sn composition, the high diffusivity of Sn into Ge and the free energy difference among the metastable state and the equilibrium state of the two phases causes a phase separation and promotes the transformation from the meta stable to the stable phase  $\alpha \rightarrow \beta$  [20]. Low temperature deposition is then needed. An additional obstacle to overcome in the epitaxial growth of  $\text{Ge}_{1-x}\text{Sn}_x$  on Ge, the preferred substrate, is that the lattice constant mismatch between  $\alpha$ -Sn ( $a_{\text{Sn}} = 6.4892 \text{ \AA}$ ) and Ge ( $a_{\text{Ge}} = 5.6579 \text{ \AA}$ ) is 14.7% [21].

The difficulties to prepare  $\text{Ge}_{1-x}\text{Sn}_x$  on either Ge or Sn or any other substrate, have resulted in a notorious scarcity of data in the literature for almost all of their physical properties, as well as the interest mentioned to use it as a column IV direct bandgap material in the far and medium infrared. We find this facts as a challenge for synthesize, study and determine as many of the physical properties of  $\text{Ge}_{1-x}\text{Sn}_x$  as possible.

In this article, we present a study of  $\text{Ge}_{1-x}\text{Sn}_x$  alloys of low Sn concentration  $0.01 \leq x \leq 0.14$  samples grown on either Ge(001) or GaAs(001) by radio frequency sputtering [22]. GaAs substrates were chosen, in addition to Ge, because of the very similar lattice constants of GaAs and Ge ( $a_{\text{GaAs}} = 5.6535 \text{ \AA}$ ). The samples with  $0.01 \leq x < 0.06$  have a highly heterogeneous structural conformation, with a thin superficial layer of contrasting concentration. The study reveals that for higher Sn concentrations this phenomenon is not detected and the samples grow partially or totally relaxed with a high density of dislocations and a more homogenous Sn con-

## Forced synchronization of autonomous dynamical Boolean networks

R. R. Rivera-Durón,<sup>1,a)</sup> E. Campos-Cantón,<sup>1,b)</sup> I. Campos-Cantón,<sup>2</sup> and Daniel J. Gauthier<sup>3</sup>

<sup>1</sup>*División de Matemáticas Aplicadas, Instituto Potosino de Investigación Científica y Tecnológica A. C., Camino a la Presa San José 2055, Col. Lomas 4 Sección, C.P. 78216, San Luis Potosí, S.L.P., Mexico*

<sup>2</sup>*Facultad de Ciencias, Universidad Autónoma de San Luis Potosí, Álvaro Obregón 64, C.P. 78000, San Luis Potosí, S.L.P., Mexico*

<sup>3</sup>*Department of Physics and Center for Nonlinear and Complex Systems, Duke University, Box 90305, Durham, North Carolina 27708, USA*

(Received 29 January 2015; accepted 6 August 2015; published online 18 August 2015)

We present the design of an autonomous time-delay Boolean network realized with readily available electronic components. Through simulations and experiments that account for the detailed nonlinear response of each circuit element, we demonstrate that a network with five Boolean nodes displays complex behavior. Furthermore, we show that the dynamics of two identical networks display near-instantaneous synchronization to a periodic state when forced by a common periodic Boolean signal. A theoretical analysis of the network reveals the conditions under which complex behavior is expected in an individual network and the occurrence of synchronization in the forced networks. This research will enable future experiments on autonomous time-delay networks using readily available electronic components with dynamics on a slow enough time-scale so that inexpensive data collection systems can faithfully record the dynamics. © 2015 AIP Publishing LLC.

[<http://dx.doi.org/10.1063/1.4928739>]

In real-world, there exist many situations in which simple objects are interconnected in a network, such as power grids, ecosystems, communication systems, human relationships, economic trading, and biological neural networks. In the network approach for analyzing these systems, the individual simple systems are represented as nodes and their interactions are represented as links. Mathematically, a network is represented as a collection of points and ordered pairs describing their connections, this mathematical object is called a graph. However, it is often difficult to find a graph that represents a complex real-world system, especially when signals travelling along the links experience a delay time that is long in comparison to the response time of the nodes. To simplify the problem for the case when the nodes display a switching-like behavior, a Boolean approximation for the nodes is appropriate and allows for progress on a theoretical analysis of the dynamics. Boolean networks are a particularly simple form of a complex system and have been found to be useful in the research of a wide range of systems, including gene regulatory systems, circuit theory, and computer science. A particularly interesting behavior is when networks synchronize their behavior. Here, we present the design of a Boolean network that displays complex behavior and shows that the networks can synchronize their behavior when they are forced by a common periodic Boolean signal. This research lays the foundation for future experimental research on time-delay Boolean networks that will help to guide theoretical research on these systems difficult to analyze.

### I. INTRODUCTION

Boolean networks were first proposed by Kauffman in 1969 as a mathematical framework for studying gene regulatory networks.<sup>1</sup> Boolean networks have received a great deal of attention across many disciplines because they are an approximate model of any network system where the network nodes display switch-like behavior. Examples include electronic logic circuits or gene regulatory networks, and it is often useful to assume that for these systems, the state variables take only two values (e.g., “high” and “low”), updated according to specified Boolean functions.<sup>2–6</sup>

There are three ways in which the state variables can be updated in Boolean networks: synchronously, asynchronously, or autonomously. Synchronous update rules assume that an external process, such as a clock, synchronizes all the updates or a device that selects a particular order of individual gate updates.<sup>7</sup> Because there are only a finite number of total states, the network must eventually visit a state that it has been before, and because the update rules are deterministic, the network settles into a periodic attractor or fixed point. For asynchronous updating rules, the Boolean states of the nodes are updated according to their logic functions simultaneously successively with randomly chosen updating order. In autonomous updating, the future behavior is determined by the history of the past network switching events, and the time-delays along the network links must be taken into account. In other words, a node in an autonomous Boolean network (ABN) updates its Boolean state whenever Boolean transitions are present at its inputs. The mathematics describing autonomous time-delay Boolean networks is much less developed, although it is known that they can display aperiodic patterns if the logic elements have instantaneous response times, the link time delays are incommensurate,

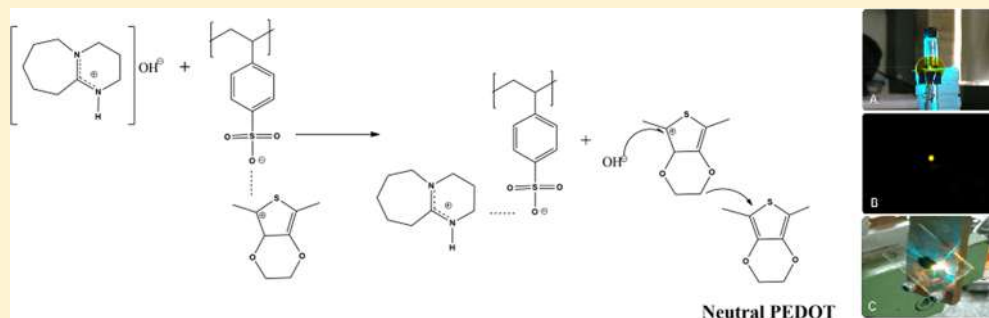
<sup>a)</sup>Electronic mail: roberto.rivera@ipicyt.edu.mx

<sup>b)</sup>Electronic mail: eric.campos@ipicyt.edu.mx

## Visible Luminescence of Dedoped DBU-Treated PEDOT:PSS Films

Isidro Cruz-Cruz,<sup>†,‡</sup> Marisol Reyes-Reyes,<sup>†</sup> Israel A. Rosales-Gallegos,<sup>†</sup> Andrei Yu Gorbachev,<sup>†</sup> José M. Flores-Camacho,<sup>†</sup> and Román López-Sandoval<sup>\*,‡</sup><sup>†</sup>Instituto de Investigación en Comunicación Óptica, Universidad Autónoma de San Luis Potosí, Álvaro Obregón 64, San Luis Potosí 78000, Mexico<sup>‡</sup>Advanced Materials Department, IPICYT, Camino a la Presa San José 2055, Col. Lomas 4a sección, San Luis Potosí 78216, Mexico

## Supporting Information



**ABSTRACT:** Dedoping of PEDOT:PSS by a simple and physical process has been performed by the addition of 1,8-diazabicyclo[5.4.0]undec-7-ene (DBU), a strong organic base, in the PEDOT:PSS aqueous dispersion. The DBU-treated PEDOT:PSS samples showed a strong absorption band at 600 nm ( $\pi-\pi^*$  transition) and a small band at 900 nm (polaronic band), which indicates that some PEDOT chains were being reduced. The dedoping efficiency depended of the amount of DBU added to the aqueous PEDOT:PSS dispersion. The DBU-treated PEDOT:PSS aqueous dispersions and films showed a strong yellow emission, visible with the naked eye, when they were excited with a 488 nm laser. In addition, the same emission features were observed using another reducing agent like sodium hydroxide (NaOH), which indicates that the emission originates from neutral PEDOT chains rather than artifacts. Finally, Raman and FTIR spectroscopies were used to figure out the mechanism responsible for the PEDOT reduction. The reduction of PEDOT chains is due to the formation of hydroxide anions, which come from the interaction of DBU with water present in the PEDOT:PSS aqueous solution and interact with the oxidized thiophene molecules, resulting in a neutralization of the PEDOT backbone.

## INTRODUCTION

Organic compounds have attracted a great interest over the past years due to the possibility of obtaining flexible, stable, and low-cost electronic devices.<sup>1</sup> One of these compounds that have attracted great interest is the conductive material poly(3,4-ethylenedioxythiophene) doped with the counteranion poly(styrenesulfonate) (PEDOT:PSS).<sup>2</sup> As is well-known, PEDOT is considered a promising material in applications where the electronic transport is crucial since, in its oxidized state, it has excellent conductivity and high transparency in the visible spectrum, among other properties.<sup>3,4</sup> In the case of the polymeric complex PEDOT:PSS, which is available commercially as an aqueous dispersion, PSS improves its processability for the fabrication of thin films, but reduces the conductivity down to around 0.1 S/cm. In this regard, many efforts have been performed in order to improve its conductivity and the importance of the molecular rearrangement in the thin films was discussed widely,<sup>5–22</sup> because better molecular arrangement promotes an increase in the crystallinity degree and improves the charge carriers delocalization. In particular, oxidizing agents have been used to increase the PEDOT:PSS

conductivity by the partial replacement of some segments of PSS<sup>-1</sup> by ionic groups such as SO<sub>4</sub><sup>-2</sup> or HSO<sub>4</sub><sup>-1</sup> and the corresponding elimination of the insulating PSS from the thin films.<sup>20,21</sup> Thus, the majority of the applications are related with PEDOT in its oxidized state (*p*-doped). However, in this work, we performed the partial reduction of this polymer to its neutral state (PEDOT<sup>0</sup>), which shows enough stability.

As reported in the literature, it is possible to modulate the electrical, thermoelectric, and optical properties of PEDOT:PSS<sup>23–26</sup> by using reducing agents like polyethylenimine,<sup>24</sup> hydrazine,<sup>25</sup> and sodium hydroxide (NaOH).<sup>26</sup> In the former two cases, it was possible to obtain a low oxidized form of PEDOT,<sup>24,25</sup> whereas, in the latter, no change in the doped state of the polymer was observed, but only a change in the relative population between polarons and bipolarons.<sup>26</sup> In the present work, the use of 1,8-diazabicyclo[5.4.0]undec-7-ene (DBU) as a reducing agent in PEDOT:PSS is reported. DBU is

Received: April 27, 2015

Revised: July 23, 2015

Published: August 11, 2015

# FPGA implementation of a reconfigurable image encryption system

M.T. Ramírez-Torres *IICO, UASLP*, J. S. Murguía *Facultad de ciencias, UASLP*, and M. Mejía-Carlos, *IICO, UASLP*

**Abstract**—This paper presents the hardware implementation of a cryptographic algorithm using a matrix approach, named ESCA (encryption by synchronization of cellular automata). The ESCA system is a symmetric key algorithm, which is based on the rule-90 cellular automaton to implement all their components. In the hardware implementation of the ESCA system was used the soft processor core Microblaze in a Virtex-5 VC5VLX110T FPGA. With this embedded system we can have a reconfigurable encryption system that allows to the user select among different configurations without the need to program the FPGA every time. With the different options to configure the ESCA system, we may increase the security or have a customized system for a faster performance. With this implementation we carry out the encryption of grayscale and RGB color images. In addition, a sparse matrix format was implemented to reduce the latency, and to prove the security of the algorithm, different tests were applied exhibiting good results.

**Keywords**—Encryption, cellular automata, FPGA, Microblaze.

## I. INTRODUCTION

THE digital image encryption is an area of interest, because there are digital visual data stored on different media and exchanged over different networks nowadays. This task is required in many applications, such as pay-TV, medical imaging systems, military image communications, surveillance and confidential video conferences. Classic encryption algorithms like Data Encryption Standard (DES), Advanced Encryption Standard (AES), International Data Encryption Algorithm (IDEA)[1] among others present a poor performance for images, due to some of their intrinsic features such as high redundancy, bulk data capacity, high correlation among pixels and others[1].

There are numerous image encryption methods that have been proposed through the last few decades. For instance many encryption systems have been implemented with a chaotic approach[2] because of their chaotic properties such as ergodicity and sensitive dependence on initial conditions and on system parameters. Also, some cryptography techniques are based on the application of cellular automata (CA), such cryptosystems have used CA in the encryption algorithm, as a pseudo-random generator, or as a combination of them[3][4]. Our proposed encryption system, ESCA, is based on the synchronization phenomenon of CA using the rule-90 cellular automaton[5]. In such a work is considered as a class of block cryptosystems that comprises two indexed families of permutations and an asymptotically perfect pseudo-random number generator (PRNG). Moreover, taking into account, in order to have a simple implementation, Murguía et al.[6] have used a matrix approach to implement the ESCA system. In

ref. [7] the ESCA system was improved to fit with the formats of the present digital technology, and the second improvement makes the cryptosystem secure against cryptanalysis attacks.

On the other hand, the hardware implementation of cryptographic algorithms allows to improve its efficiency using dedicated architectures. For this case the reconfigurable logic devices are a suitable solution to implement cryptographic algorithms for embedded systems or high speed applications. In these days, the capacity and features of FPGA devices have increased so that it is possible to implement on them an entire cryptographic system based on a soft processor core.

## II. ESCA SYSTEM

In this hardware implementation we consider the encryption scheme used in Ref. [5],[6],[7] where the synchronization phenomenon of CA has been applied to devise the two families of permutations and an asymptotically perfect PRNG. The encryption system is based on the usage of CA that evolves according to the local rule  $x_i^{t+1} = (x_{i-1}^t + x_{i+1}^t) \bmod 2$  which corresponds to the rule 90. The phenomenon of synchronization in coupled pairs of CA is described in detail in Ref. [5], where it was found that a pair of coupled CA can synchronize if every pair of consecutive coordinates is separated by a block of  $(2^n - 1)$  uncoupled sites, for  $n = 1, 2, 3, \dots$

Such cryptosystem comprises the sets  $M$ ,  $C$  and  $K$  of binary words,  $M$  and  $C$  correspond to the plain-texts and cipher-texts respectively, the length of these words is  $J = 2^j$ , for  $j = 1, 2, 3, \dots$ . The set  $K$  corresponds to the enciphering keys of length  $N = 2^n - 1$ , for a complete encryption  $n > j$  such that  $N$  must be larger than  $J$ . The two indexed families of permutations  $\Psi = \{\psi_k : k \in K\}$  and  $\Phi = \{\phi_k : k \in K\}$  are called encryption and decryption functions respectively. Basically, the cryptosystem transforms a plain-text sequence  $\mathbf{m}$  to a cipher-text sequence  $\mathbf{c}$ , i.e. for every  $k \in K$  one has  $\mathbf{c} = \psi_k(\mathbf{m})$ , whereas to disclose from the sequence of cipher-blocks, one uses the decryption functions  $\mathbf{m} = \phi_k(\psi_k(\mathbf{m}))$ . Since the complete encryption scheme is a symmetric algorithm, the encryption and decryption processes use the same enciphering key  $\mathbf{k}$ .

### A. Matrix approach

In a previous work, the ESCA cryptosystem was implemented with a matrix approach [6],[7].

The indexed family of permutations  $\Psi$ . In the encryption process we have

$$\mathbf{c} = \psi_k(\hat{\mathbf{m}}) = [(\hat{\mathbf{P}} \times \mathbf{k}) + (\hat{\mathbf{Q}} \times \hat{\mathbf{m}})] \bmod 2 \quad (1)$$



# A Secure Compression Scheme for Real-time Applications Using 2D-WT and Cellular Automata

M. T. Ramírez-Torres, J. S. Murguía, M. Mejía Carlos, and  
J. A. Aboytes-González

Universidad Autónoma de San Luis Potosí,  
Coordinación Académica Región Altiplano Oeste e IICO, San Luis Potosí,  
Mexico

tulio.torres@alumnos.uaslp.edu.mx,  
ondeleto@uaslp.mx,  
marcela.mejia@uaslp.mx,  
j.a.a.g.85@hotmail.com  
<http://salinas.uaslp.mx>

**Abstract.** In this work is presented a numerical implementation of a system that combines a compression scheme with an improved encryption procedure, which is applied to digital images. For the compression stage is considered the two-dimensional Haar wavelet transform, where an energy criterion is contemplated. On the other hand, the encryption scheme regarded is based on the synchronization of the cellular automaton rule 90, this system presents a good performance to encrypt images and it is resistant to cryptanalysis attacks such as the Chosen/Known-plaintext attack. The numerical conjunction of these procedures could be an appealing option for real-time applications such as video communications, video-surveillance among others.

**Keywords:** Cellular automata, encryption system, two-dimensional wavelet transform, compression

## 1 Introduction

Nowadays, there exists a great interest in the protection and manipulation of the data. Due to the great advances in technology, each time is required to have better and more efficient algorithms for confidential and secure data handling. This information may vary depending on the application area and in many cases is necessary processing it in real time. For example, now is very common in different countries that the police install surveillance video cameras on the cities. If the information transmitted from these cameras is not encrypted the confidentiality of data is exposed in the links allowing access to third parties without being detected. But if an encryption processes is added, the latency of the data transmission could increase and the information will not be available on time.



# The Hurst exponents of *Nitzschia* sp. diatom trajectories observed by light microscopy

J.S. Murguía<sup>a</sup>, H.C. Rosu<sup>b,\*</sup>, A. Jimenez<sup>b</sup>, B. Gutiérrez-Medina<sup>b</sup>,  
J.V. García-Meza<sup>c</sup>

<sup>a</sup> Facultad de Ciencias, Universidad Autónoma de San Luis Potosí, Álvaro Obregón 64, 78000 San Luis Potosí, S.L.P., Mexico

<sup>b</sup> IPICYT, Instituto Potosino de Investigación Científica y Tecnológica, Camino a la presa San José 2055, Col. Lomas 4a Sección, 78216 San Luis Potosí, S.L.P., Mexico

<sup>c</sup> Instituto de Metalurgia, Geomicrobiología, Universidad Autónoma de San Luis Potosí, Álvaro Obregón 64, 78000 San Luis Potosí S.L.P., Mexico

## HIGHLIGHTS

- We determine Hurst parameters for digitally recorded 2D trajectories of a diatom species.
- The WT-DFA scaling method is used.
- We thus give statistical evidence for the persistent character of diatom motion.

## ARTICLE INFO

### Article history:

Received 20 April 2014

Received in revised form 19 September 2014

Available online 28 September 2014

### Keywords:

Diatom

Trajectory

Time series

Wavelet

Hurst exponent

## ABSTRACT

We present the results of an experiment with light microscopy performed to capture the trajectories of live *Nitzschia* sp. diatoms. The time series corresponding to the motility of this kind of cells along ninety-five circular-like trajectories have been obtained and analyzed with the scaling statistical method of detrended fluctuation analysis optimized via a wavelet transform. In this way, we determined the Hurst parameters, in two orthogonal directions, which characterize the nature of the motion of live diatoms in light microscopy experiments. We have found mean values of these directional Hurst parameters between 0.70 and 0.63 with overall standard errors below 0.15. These numerical values give evidence that the motion of *Nitzschia* sp. diatoms is of persistent type and suggest an active cell motility with a kind of memory associated with long-range correlations on the path of their trajectories. For the collected statistics, we also find that the values of the Hurst exponents depend on the number of abrupt turns that occur in the diatom trajectory and on the type of wavelet, although their mean values do not change much.

© 2014 Elsevier B.V. All rights reserved.

## 1. Introduction

Ubiquitous in aquatic habitats, diatoms are photosynthetic unicellular microalgae that exist in both planktic and benthic lifestyles. The *Nitzschia* species is a common genus of benthic diatoms that exhibits a paired mechanism of cell adhesion and

\* Corresponding author. Tel.: +52 444 8342000x718.

E-mail addresses: [ondeleto@uaslp.mx](mailto:ondeleto@uaslp.mx) (J.S. Murguía), [hcr@ipicyt.edu.mx](mailto:hcr@ipicyt.edu.mx) (H.C. Rosu), [andres.jimenez@ipicyt.edu.mx](mailto:andres.jimenez@ipicyt.edu.mx) (A. Jimenez), [bgutierrez@ipicyt.edu.mx](mailto:bgutierrez@ipicyt.edu.mx) (B. Gutiérrez-Medina), [jviridiana@gmail.com](mailto:jviridiana@gmail.com) (J.V. García-Meza).

<http://dx.doi.org/10.1016/j.physa.2014.09.046>

0378-4371/© 2014 Elsevier B.V. All rights reserved.

## Two-dimensional DFA scaling analysis applied to encrypted images

C. Vargas-Olmos

*Facultad de Ciencias, Universidad Autónoma de San Luis Potosí (UASLP)  
Instituto de Investigación en Comunicación Óptica  
Álvaro Obregón 64, 78000 San Luis Potosí, S.L.P., México  
[cv\\_olmos@cactus.iico.uaslp.mx](mailto:cv_olmos@cactus.iico.uaslp.mx)*

J. S. Murguía\*

*Facultad de Ciencias, Universidad Autónoma de San Luis Potosí  
Álvaro Obregón 64, 78000 San Luis Potosí, S.L.P., México  
[ondeleto@uaslp.mx](mailto:ondeleto@uaslp.mx)*

M. T. Ramírez-Torres<sup>†</sup> and M. Mejía Carlos<sup>‡</sup>

*Instituto de Investigación en Comunicación Óptica, UASLP  
Álvaro Obregón 64, 78000 San Luis Potosí, S.L.P., México  
<sup>†</sup>[tulio.torres@alumnos.uaslp.edu.mx](mailto:tulio.torres@alumnos.uaslp.edu.mx)  
<sup>‡</sup>[mmejia@cactus.iico.uaslp.mx](mailto:mmejia@cactus.iico.uaslp.mx)*

H. C. Rosu

*IPICyT, Instituto Potosino de Investigación Científica y Tecnológica  
Apartado Postal 3-74 Tangamanga, 78231 San Luis Potosí, México  
[hcr@ipicyt.edu.mx](mailto:hcr@ipicyt.edu.mx)*

H. González-Aguilar

*Facultad de Ciencias, Universidad Autónoma de San Luis Potosí  
Álvaro Obregón 64, 78000 San Luis Potosí, S.L.P., México  
[hernan@fc.uaslp.mx](mailto:hernan@fc.uaslp.mx)*

Received 20 October 2014

Accepted 25 November 2014

Published 2 January 2015

The technique of detrended fluctuation analysis (DFA) has been widely used to unveil scaling properties of many different signals. In this paper, we determine scaling properties in the encrypted images by means of a two-dimensional DFA approach. To carry out the image encryption, we use an enhanced cryptosystem based on a rule-90 cellular automaton and we compare the results obtained with its unmodified version and the encryption system AES. The numerical results show that the encrypted images present a persistent behavior which is close to

\*Corresponding author.

## DIRECTIONAL COMPLEXITY AND ENTROPY FOR LIFT MAPPINGS

VALENTIN AFRAIMOVICH

Instituto de Investigación en Comunicación Óptica  
Universidad Autónoma de San Luis Potosí  
Karakorum 1470, Lomas 4a 78220, San Luis Potosi, S.L.P, Mexico

MAURICE COURBAGE

Laboratoire Matière et Systèmes Complexes (MSC)  
UMR 7057 CNRS et Université Paris 7-Denis Diderot  
10, rue Alice Domon et Léonie Duquet 75205 Paris Cedex 13, France

LEV GLEBSKY

Instituto de Investigación en Comunicación Óptica  
Universidad Autónoma de San Luis Potosí  
Karakorum 1470, Lomas 4a 78220, San Luis Potosi, S.L.P, Mexico

**ABSTRACT.** We introduce and study the notion of a directional complexity and entropy for maps of degree 1 on the circle. For piecewise affine Markov maps we use symbolic dynamics to relate this complexity to the symbolic complexity. We apply a combinatorial machinery to obtain exact formulas for the directional entropy, to find the maximal directional entropy, and to show that it equals the topological entropy of the map.

**1. Introduction.** There is a well-developed theory of rotation vectors (numbers) and rotation sets (see, for instance, [11] and reference therein). One considers a map  $f : M \rightarrow M$  generating a dynamical system and an observable  $\phi : M \rightarrow \mathbb{R}^d$  that classically is a displacement but might be an arbitrary function. The rotation vector of  $x$  is the Birkhoff average

$$\lim_{n \rightarrow \infty} \frac{1}{n} \sum_{i=0}^{n-1} \phi(f^i x),$$

provided that the limit exists, say, equals  $v$ . Then we may say that  $x$  moves in the direction  $v$ . A natural question arises: how many points move in the direction  $v$  if one measures them in terms of the topological entropy. The authors of [11] have mentioned several attempts to answer the question and have described their own approach. All of them including one of [16] are based on the thermodynamic formalism, in particular, on the variational principle. In our article we use purely topological (metric) approach to describe points moving to the prescribed direction.

---

2010 *Mathematics Subject Classification.* 37E10, 37E45.

*Key words and phrases.* Rotation interval, space-time window, directional complexity, directional entropy.

An essential part of this work has been written during V.A. and L.G. stay at the Nizhny Novgorod University supported by the grant RNF 14-41-00044. The authors also thank the referee for useful suggestions.

## Characterization of Si<sub>3</sub>N<sub>4</sub>/Si(111) thin films by reflectance difference spectroscopy

Luis Felipe Lastras-Martínez<sup>1\*</sup>, Nicolás Antonio Ulloa-Castillo<sup>1</sup>, Rafael Herrera-Jasso<sup>1</sup>, Raúl Eduardo Balderas-Navarro<sup>1,2\*</sup>, Alfonso Lastras-Martínez<sup>1</sup>, Mahesh Pandikunta<sup>3</sup>, Oleg Ledyayev<sup>3</sup>, Vladimir Kuryatkov<sup>3</sup>, and Sergey Nikishin<sup>3\*</sup>

<sup>1</sup>Instituto de Investigación en Comunicación Óptica, Universidad Autónoma de San Luis Potosí, Alvaro Obregón 64, 78000 San Luis Potosí, S.L.P., México

<sup>2</sup>Paul-Drude-Institut für Festkörperelektronik, Hausvogteiplatz 57, Berlin, Germany

<sup>3</sup>Nano Tech Center, Texas Tech University, Lubbock, TX 79409, U.S.A.

E-mail: lflm@cactus.iico.uaslp.mx; rbn@cactus.iico.uaslp.mx; sergey.a.nikishin@ttu.edu

Received August 10, 2014; accepted October 19, 2014; published online January 14, 2015

Si<sub>3</sub>N<sub>4</sub> has become an important material with great technological and scientific interests. The lattice symmetry and the crystallinity quality of Si<sub>3</sub>N<sub>4</sub> thin films are fundamental parameters that must be determined for different applications. In order to evaluate the properties of Si<sub>3</sub>N<sub>4</sub> films, we used reflectance difference spectroscopy/reflectance anisotropy spectroscopy (RDS/RAS) to measure the optical anisotropy of Si<sub>3</sub>N<sub>4</sub> thin films (1–2 nm) grown by nitridation of two different Si(111) substrates, one with a 4.2° miscut off towards the [11 $\bar{2}$ ] direction and another one with a nonintentional miscut. We demonstrate that, by modifying the measurement optical setup, we could increase the RD sensitivity and clearly display the optical response corresponding to the hexagonal symmetry of the Si<sub>3</sub>N<sub>4</sub> thin layer. Our results are in good agreement with reflection high energy electron diffraction (RHEED) measurements for both misoriented and oriented substrates. © 2015 The Japan Society of Applied Physics

### 1. Introduction

III–nitride (III–N)-based optoelectronic devices on Si substrates are very attractive owing to the low cost and large area of these wafers and the possibility of integration with other devices in the same platform.<sup>1)</sup> However, both the high thermal expansion coefficient difference and lattice constant mismatch between Si and III–N compounds lead to the cracking of III–N epitaxial layers.<sup>2)</sup> Molecular beam epitaxy (MBE) with a reflection high-energy electron diffraction (RHEED) system ensures in situ control of the growth process. The first crack-free thick AlN and GaN layers on Si(111)<sup>3,4)</sup> were grown by ammonia MBE, where the Si–N–Al interface<sup>5)</sup> was formed under in situ RHEED monitoring.

Plasma-assisted MBE (PAMBE) also yields high-quality III–N on Si(111).<sup>6)</sup> Both MBE approaches require the fabrication of a high-quality buffer (interfacial) Si<sub>3</sub>N<sub>4</sub> layer on silicon. This coherent Si<sub>3</sub>N<sub>4</sub>/Si(111) interface is formed by silicon wafer nitridation by which crystalline Si<sub>3</sub>N<sub>4</sub> films can be obtained.<sup>7–11)</sup> More recently, it has been found that the intentional growth of a Si<sub>3</sub>N<sub>4</sub> buffer layer on Si can be better controlled during PAMBE because the growth chamber is free of background ammonia and has a small amount of active nitrogen before plasma ignition.<sup>11–13)</sup> Note that the growth of Si<sub>3</sub>N<sub>4</sub> layers is conducted with a background pressure in the growth chamber of around  $1.33 \times 10^{-3}$  Pa. This ambient condition shortens the lifetime of the RHEED electron gun. Thus, the development and application of in situ monitoring methods that are less sensitive to the ambient conditions are important tasks.

Reflectance difference spectroscopy/reflectance anisotropy spectroscopy (RDS/RAS)<sup>14)</sup> is an optical modulation technique that is very sensitive to surface and crystal symmetries. In comparison with RHEED, which uses high-energy electrons (around 10 keV) that activate a chemical reaction between Si and residual carbon- and oxygen-containing molecules, RDS is a very low power optical method that does not activate any chemical process during in situ monitoring. It has recently been demonstrated that RDS is a powerful tool for the study of the first stages of epitaxial growth.<sup>15,16)</sup>

Additionally, RDS can be used in vacuum or in air to characterize the sample under in situ or ex situ conditions.

In the present work, we report the results of ex situ RD measurements carried out on Si(111) substrates and Si<sub>3</sub>N<sub>4</sub>/Si(111) heterostructures. Two Si(111) substrates were used: one with an  $\approx 4.2^\circ$  misoriented miscut towards the [11 $\bar{2}$ ] direction and another one with a nonintentional miscut ( $\pm 0.5^\circ$ ). RD spectra revealed hexagonal symmetry for Si<sub>3</sub>N<sub>4</sub> thin films grown on both substrates. Because of the negligible oxidation rate of Si<sub>3</sub>N<sub>4</sub> thin layers at room temperature,<sup>17)</sup> we anticipate that RDS can also be used for the in situ monitoring of Si nitridation during the MBE process.

By following the evolution of the RD line shape around the optical transitions of Si<sub>3</sub>N<sub>4</sub> during the growth process, it is possible to perform a structural analysis to determine the crystallinity and symmetry of the layer. RD constitutes an attractive tool for the in situ monitoring of the growth process and can be used alone or in conjunction with most common monitoring techniques such as RHEED.

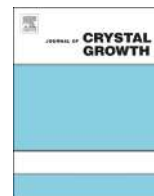
### 2. Experimental procedure

Ultrathin silicon nitride films were fabricated on low-resistance n-type Si(111) substrates. The experiments were carried out in the growth chamber of a GEN10 PAMBE system equipped with a UNI-Bulb RF nitrogen plasma source and a RHEED system. Note that we have already reported a good agreement between RHEED and low-energy electron diffraction investigation of Si nitridation during ammonia MBE.<sup>18)</sup> All two-inch silicon substrates were initially prepared by wet chemical etching<sup>3)</sup> that allows the formation of the hydrogen-saturated Si(111) surface with  $1 \times 1$  reconstruction at room temperature, as shown in Fig. 1(a). Radiative annealing of these substrates under ultrahigh-vacuum conditions at  $\approx 650^\circ\text{C}$  leads to the formation of the  $7 \times 7$  surface structure corresponding to the bare, hydrogen-free Si(111) plane, as shown in Fig. 1(b). Afterwards, the substrate temperature was raised to  $T_t \approx 830^\circ\text{C}$  until the surface reconstruction from  $7 \times 7$  to  $1 \times 1$  occurred. This transition temperature provides a convenient calibration point of the substrate temperature.<sup>19)</sup> On the basis of recent



Contents lists available at ScienceDirect

Journal of Crystal Growth

journal homepage: [www.elsevier.com/locate/jcrysgr](http://www.elsevier.com/locate/jcrysgr)

## Reflectance-difference spectroscopy as a probe for semiconductor epitaxial growth monitoring

A. Lastras-Martínez<sup>a,\*</sup>, J. Ortega-Gallegos<sup>a</sup>, L.E. Guevara-Macías<sup>a</sup>, O. Nuñez-Olvera<sup>a</sup>,  
R.E. Balderas-Navarro<sup>a</sup>, L.F. Lastras-Martínez<sup>a</sup>, L.A. Lastras-Montaña<sup>b</sup>,  
M.A. Lastras-Montaña<sup>c</sup>

<sup>a</sup> Instituto de Investigación en Comunicación Óptica, Universidad Autónoma de San Luis Potosí, Alvaro Obregón 64, San Luis Potosí, SLP 78000, México

<sup>b</sup> IBM T. J. Watson Research Center, Yorktown Heights, NY 10598, USA

<sup>c</sup> Department of Electrical and Computer Engineering, University of California, Santa Barbara, Santa Barbara, CA 93106, USA

### ARTICLE INFO

Communicated by A. Brown

#### Keywords:

A.1 Characterization  
A.1 Surface processes  
A.3 Molecular beam epitaxy  
B.2 Semiconducting III–V materials

### ABSTRACT

We report on real-time reflectance-difference (RD) spectroscopic measurements carried out during the homoepitaxial growth of GaAs under As overpressures in the range from  $P_{As} = 6 \times 10^{-7} - 5 \times 10^{-6}$  Torr. We found that the time-dependent RD spectrum is described in terms of two basic line shapes. One of these components is associated to the orthorhombic surface strain due to surface reconstruction while the second one has been assigned to surface composition. Results reported in this paper render RD spectroscopy as a powerful tool for the real-time monitoring of surface strains and its interplay with surface composition during growth.

© 2015 Elsevier B.V. All rights reserved.

## 1. Introduction

Reflectance-difference spectroscopy (RDS) is a noninvasive, contrasting technique that suppresses the bulk isotropic component of the optical reflectance spectrum of cubic semiconductors enhancing its surface-associated component. Both its noninvasive character and surface specificity make RDS a very attractive tool for monitoring the epitaxial growth of zincblende semiconductors, as it was first reported by Aspnes and collaborators [1]. The interpretation of reflectance-difference (RD) spectra, nevertheless, poses some challenges as the surface may become anisotropic for a number of physical mechanisms [2], including surface electric fields [3],  $\alpha$  and  $\beta$  dislocations [4], surface reconstruction strains [5,6] and surface dimers [7,8]. At the same time, time-resolved RD spectra measured during epitaxial growth would lead to a great deal of information on the kinetics of epitaxial growth, provided we can resolve them into their different components and determine the time-evolution of such components during growth.

Previously we reported on real-time RDS of homoepitaxial GaAs (001) grown by molecular beam epitaxy (MBE) [9]. For the growth we employed a As overpressure ( $P_{As}$ ) of  $1 \times 10^{-6}$  which led to a rich surface reconstruction evolution as growth progressed as well as to

considerable changes in RD spectrum line shape. We showed that the time-evolution of RD spectra during growth is well described in terms of two independent components, each with a specific physical origin. In this paper we report on the results of a study carried out within a range of As overpressures and demonstrate that our previous results can be extended to more general growth conditions.

## 2. Experimental details and results

Epitaxial growth was carried out on (001) GaAs substrates in a solid-source MBE chamber (Riber 32P). Epitaxial growth was carried out under four As overpressures ( $P_{As}$ ) ranging from  $6 \times 10^{-7}$  to  $5 \times 10^{-6}$  Torr at a growth rates from 0.14 to 0.23 ML/s as determined from RHEED oscillations. Growth substrate temperature was 520 °C in all cases. Epitaxial growth was initiated/interrupted by opening/closing the Ga shutter and lasted for about 45 s. Time-resolved spectroscopic RD measurements were performed with a rapid RD, 32-channel spectrometer attached to the epitaxial growth chamber. More details on the RD spectrometer are given elsewhere [10]. In order to correlate RD changes with surface reconstruction changes, RHEED patterns were acquired concurrently with RD spectra.

To prevent components associated to dislocations in the measured RD spectra, a 0.3  $\mu\text{m}$  thick GaAs buffer layer was grown prior to carrying out the experiments. Further, to avoid electro-optical contributions that may hinder the analysis of the RD line shapes, we did not intentionally dope the GaAs films.

\* Corresponding author.

E-mail addresses: [alm@cactus.iico.uaslp.mx](mailto:alm@cactus.iico.uaslp.mx),  
[alastras@gmail.com](mailto:alastras@gmail.com) (A. Lastras-Martínez).

<http://dx.doi.org/10.1016/j.jcrysgr.2015.02.061>  
0022-0248/© 2015 Elsevier B.V. All rights reserved.

# Finite temperature orbital and spin magnetism of small Fe linear chains

R Garibay-Alonso<sup>1</sup>, I Guillén-Escamilla<sup>2</sup>, M Reyes-Reyes<sup>3</sup>  
and R López-Sandoval<sup>4</sup>

<sup>1</sup> Departamento de Ingenierías, CU-Tonalá, Universidad de Guadalajara, Morelos 180, CP 45400, Tonalá, Mexico

<sup>2</sup> Departamento de Ciencias Exactas y Naturales, CU-Valles, Universidad de Guadalajara, Carretera Guadalajara-Ameca Km. 45, Mexico

<sup>3</sup> Instituto de Investigación en Comunicación Óptica, Universidad Autónoma de San Luis Potosí, Alvaro Obregón 64, San Luis Potosí, México

<sup>4</sup> Instituto Potosino de Investigación Científica y Tecnológica, Camino a la presa San José 2055, CP 78216, San Luis Potosí, Mexico

E-mail: [raul.garibay@live.com](mailto:raul.garibay@live.com)

Received 6 April 2015

Accepted for publication 26 May 2015

Published 23 June 2015



## Abstract

The finite temperature spin and orbital magnetism of  $N \leq 10$  Fe<sub>N</sub> linear chains is theoretically studied in the framework of a spin fluctuation theory based on a realistic *d*-band model Hamiltonian, which includes the spin–orbit coupling interaction in a non-perturbative way. Spin and orbital magnetic moments are calculated as a function of the temperature by using an exchange Monte Carlo method that takes into account in a full way the short-range magnetic order. The finite temperature anisotropy effects on the spin and orbital cluster moment values are analysed by considering magnetization directions perpendicular to and along the chain axis. The temperature dependence of the orbital cluster moment follows a general trend similar to that of the spin one and shows clear anisotropy effects at low and intermediate temperatures, before total thermal disorder appears. Interesting anisotropy effects driven by thermal spin fluctuations are also observed for the spin results in most of the systems.

Keywords: iron clusters, spin–orbit coupling effects, temperature dependence, Monte Carlo simulation

(Some figures may appear in colour only in the online journal)

## 1. Introduction

Currently, scientific research in the field of modern materials has become relevant due to the quantitative or qualitative new physical and chemical properties derived from the low dimensionality or nano-scale of the materials [1–16]. Among all these new properties, a very important mention is deserved for the magnetic properties of low dimensional (LD) transition metal (TM) systems used in the development of new recording technologies for high density magnetic information storage. Additionally, from the point of view of pure scientific knowledge, the study of the magnetic properties of LD TM systems provides the opportunity for understanding how the electronic properties make impact on the shape of

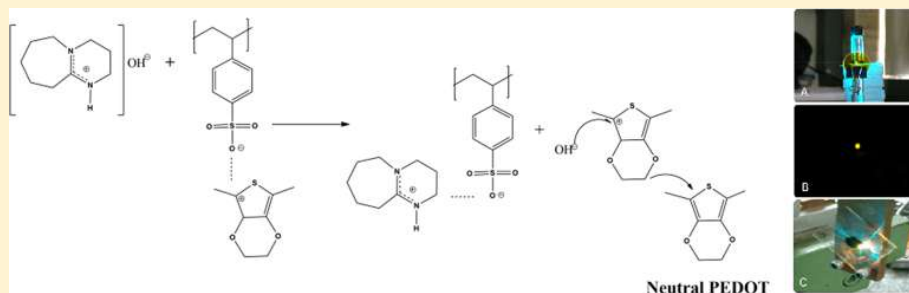
the magnetic order in a material, its magnetic anisotropy, its orbital magnetism, etc, as well as the temperature evolution of all these properties.

In the case of ferromagnetic TM systems with reduced dimensionality, the effects on the magnetic anisotropy and orbital magnetization introduced by the spin–orbit coupling (SOC) are known to be significant and even outstanding in some circumstances [17–31]. For instance, we can mention from the literature the significant enhancement of the ground state orbital magnetic moments and magnetic anisotropy energy in ferromagnetic TM clusters [20–23]. Other ground state results that deserve special attention due to the remarkable effects of the SOC interaction on the magnetic anisotropy energy are those related to the study of the magnetism of

## Visible Luminescence of Dedoped DBU-Treated PEDOT:PSS Films

Isidro Cruz-Cruz,<sup>†,‡</sup> Marisol Reyes-Reyes,<sup>†</sup> Israel A. Rosales-Gallegos,<sup>†</sup> Andrei Yu Gorbachev,<sup>†</sup> José M. Flores-Camacho,<sup>†</sup> and Román López-Sandoval<sup>\*,‡</sup><sup>†</sup>Instituto de Investigación en Comunicación Óptica, Universidad Autónoma de San Luis Potosí, Álvaro Óbregon 64, San Luis Potosí 78000, Mexico<sup>‡</sup>Advanced Materials Department, IPICYT, Camino a la Presa San José 2055, Col. Lomas 4a sección, San Luis Potosí 78216, Mexico

## Supporting Information



**ABSTRACT:** Dedoping of PEDOT:PSS by a simple and physical process has been performed by the addition of 1,8-diazabicyclo[5.4.0]undec-7-ene (DBU), a strong organic base, in the PEDOT:PSS aqueous dispersion. The DBU-treated PEDOT:PSS samples showed a strong absorption band at 600 nm ( $\pi-\pi^*$  transition) and a small band at 900 nm (polaronic band), which indicates that some PEDOT chains were being reduced. The dedoping efficiency depended of the amount of DBU added to the aqueous PEDOT:PSS dispersion. The DBU-treated PEDOT:PSS aqueous dispersions and films showed a strong yellow emission, visible with the naked eye, when they were excited with a 488 nm laser. In addition, the same emission features were observed using another reducing agent like sodium hydroxide (NaOH), which indicates that the emission originates from neutral PEDOT chains rather than artifacts. Finally, Raman and FTIR spectroscopies were used to figure out the mechanism responsible for the PEDOT reduction. The reduction of PEDOT chains is due to the formation of hydroxide anions, which come from the interaction of DBU with water present in the PEDOT:PSS aqueous solution and interact with the oxidized thiophene molecules, resulting in a neutralization of the PEDOT backbone.

## INTRODUCTION

Organic compounds have attracted a great interest over the past years due to the possibility of obtaining flexible, stable, and low-cost electronic devices.<sup>1</sup> One of these compounds that have attracted great interest is the conductive material poly(3,4-ethylenedioxythiophene) doped with the counteranion poly(styrenesulfonate) (PEDOT:PSS).<sup>2</sup> As is well-known, PEDOT is considered a promising material in applications where the electronic transport is crucial since, in its oxidized state, it has excellent conductivity and high transparency in the visible spectrum, among other properties.<sup>3,4</sup> In the case of the polymeric complex PEDOT:PSS, which is available commercially as an aqueous dispersion, PSS improves its processability for the fabrication of thin films, but reduces the conductivity down to around 0.1 S/cm. In this regard, many efforts have been performed in order to improve its conductivity and the importance of the molecular rearrangement in the thin films was discussed widely,<sup>5–22</sup> because better molecular arrangement promotes an increase in the crystallinity degree and improves the charge carriers delocalization. In particular, oxidizing agents have been used to increase the PEDOT:PSS

conductivity by the partial replacement of some segments of  $\text{PSS}^{-1}$  by ionic groups such as  $\text{SO}_4^{-2}$  or  $\text{HSO}_4^{-1}$  and the corresponding elimination of the insulating PSS from the thin films.<sup>20,21</sup> Thus, the majority of the applications are related with PEDOT in its oxidized state (*p*-doped). However, in this work, we performed the partial reduction of this polymer to its neutral state ( $\text{PEDOT}^0$ ), which shows enough stability.

As reported in the literature, it is possible to modulate the electrical, thermoelectric, and optical properties of PEDOT:PSS<sup>23–26</sup> by using reducing agents like polyethylenimine,<sup>24</sup> hydrazine,<sup>25</sup> and sodium hydroxide (NaOH).<sup>26</sup> In the former two cases, it was possible to obtain a low oxidized form of PEDOT,<sup>24,25</sup> whereas, in the latter, no change in the doped state of the polymer was observed, but only a change in the relative population between polarons and bipolarons.<sup>26</sup> In the present work, the use of 1,8-diazabicyclo[5.4.0]undec-7-ene (DBU) as a reducing agent in PEDOT:PSS is reported. DBU is

Received: April 27, 2015

Revised: July 23, 2015

Published: August 11, 2015





SEARCH

ADVANCED SEARCH

HOME

PROCEEDINGS

JOURNALS

eBOOKS

TOPIC COLLECTIONS

LIBRARIANS

Optical Engineering: [Journal Home](#) [Current Issue](#) [All Issues](#)[Optical Engineering](#) | [Volume 55](#) | [Issue 3](#) | [Lasers, Fiber Optics, and Communications](#) >< [Previous Article](#)[Next Article](#) >

Lasers, Fiber Optics, And Communications

## Acousto-optic interaction in biconical tapered fibers: shaping of the stopbands

*Gustavo Ramírez-Meléndez ; Miguel Ángel Bello-Jiménez ; Christian Cuadrado-Laborde ; Antonio Díez ; José Luis Cruz ; Amparo Rodríguez-Cobos ; Raúl Balderas-Navarro ; Miguel Vicente Andrés Bou*[\[+\] Author Affiliations](#)*Opt. Eng.* 55(3), 036105 (Mar 08, 2016). doi:10.1117/1.OE.55.3.036105

History: Received November 13, 2015; Accepted February 16, 2016

Text Size: [A](#) [A](#) [A](#)[Article](#) [Figures](#) [Tables](#) [References](#)

### Abstract

Abstract | [Introduction](#) | [Numerical Modeling of the Acousto-Optic Interaction in a Tapered Fiber](#) | [Configuration Under Discussion and Results](#) | [Conclusions](#) | [Acknowledgments](#) | [References](#)

Some tools below are only available to our subscribers or users with an online account.



PDF



Email



Share



Get Citation



Get Permissions



Article Alerts



Slideset (.ppt)

### Related Content

Customize your page view by dragging & repositioning the boxes below.

Related Journal Articles



Related Proceedings Articles



Related Book Chapters



Topic Collections



Advertisement

# Experimental Investigation of Fused Biconical Fiber Couplers for Measuring Refractive Index Changes in Aqueous Solutions

Marco V. Hernández-Arriaga, Miguel A. Bello-Jiménez, A. Rodríguez-Cobos,  
and Miguel V. Andrés, *Member, IEEE*

**Abstract**—A detailed experimental study of a simple and compact fiber optic sensor based on a fused biconical fiber coupler is presented, in which the sensitivity is improved by operating the coupler beyond the first coupling cycle. The sensor is demonstrated to perform high sensitivity measurements of refractive index changes by means of variation of sugar concentration in water. The device is operated to achieve a linear transmission response, allowing a linear relation between the sugar concentration and the output signal. The initial sensitivity was measured as 0.03 units of normalized transmission per unit of sugar concentration (g/100 mL), with a noise detection limit of a sugar concentration of 0.06 wt% of sugar concentration. Improvements in sensitivity were studied by operating the coupler beyond their first coupling cycles; achieving an improved sensitivity of 0.15 units of normalized transmission per unit of sugar concentration, and a minimum detection limit of 0.012 wt% of sugar concentration. From this result, the minimum detectable refractive index change is estimated as  $2 \times 10^{-5}$  refractive index unit.

**Index Terms**—Fiber optic sensor, fused biconical fiber coupler, refractive index sensor.

## I. INTRODUCTION

FIBER-OPTIC couplers have attracted considerable attention in recent years for their ability to detect small changes in the refractive index (RI) of liquid solutions. A fiber coupler is a four-port device with a transmission spectrum that is strongly affected by the refractive index of the surrounding medium due to the evanescent field that is generated along the coupling region [1]. This effect has proven to be useful for sensing applications [2]. Recent approaches of fiber-coupler based RI sensors include fused biconical fiber couplers [3]–[7], optical microfibers [8]–[12], photonic crystal fibers [13], [14], and specially designed

two-core optical fibers [15], [16], all of them offering the advantages of high sensitivity, *in situ* measurements, compact size, and immunity to external electromagnetic interference. Most of these sensors are codified in wavelength and the achieved sensitivities are in the range of 1,125 to 30,100 nanometer (nm) per refractive index unit (RIU), with a minimum detection limit of  $4 \times 10^{-4}$  to  $4 \times 10^{-7}$  RIU, respectively.

From the point of view of implementation, the necessity of expensive equipment, such as optical spectrum analyzers, for measuring the shift in wavelength heavily affects the use of fiber-coupler based RI sensors. Thus, it is worthwhile to consider an alternative scheme based on the dependence of the power coupling on the surrounding medium. The two complementary outputs of a fiber coupler enable a straightforward normalization, i.e. the ratio between the difference and the addition, which automatically compensates for power fluctuations. In earlier works the dependence of the power coupling of traditional fused biconical tapered couplers on the external RI has been presented and it has been proposed that it is possible to use such a structure to develop a fiber based refractometer [1], [17]. Tazawa et al. [2] have implemented this power measurement approach to demonstrate a biosensor with estimated  $4 \times 10^{-6}$  RIU detection limit. Recently, it has been demonstrated that modal interferometers based on integrated waveguides provide one of the best resolutions ever reported ( $2.5 \times 10^{-7}$  RIU) [18]. A fused biconical couplers is, in fact, a modal interferometer in which the phase difference between the symmetric and antisymmetric supermodes determine the power distribution at the output fibers. Small changes of the external RI do not modify substantially the coupling coefficient, but they generate a significant phase difference between supermodes. In terms of fiber-coupler based RI sensors, this last point deserves particular attention for the detection of slight changes in the refractive index of aqueous solutions. Although several schemes have reported this effect [1], [2], [17], they did not study the conditions for an optimal performance of the reported device. Here our purpose is the experimental analysis of a fused biconical fiber coupler, operated beyond the first coupling cycle, with a power transmission that depends on the surrounding medium.

The objective is not only to gain insights into the dynamics of this kind of device, but also looking forwards an improvement of its performance. Based on this motivation, the

Manuscript received July 10, 2015; revised August 26, 2015; accepted August 27, 2015. Date of publication September 16, 2015; date of current version December 10, 2015. This work was supported in part by Promep under Grant DSA/103.5/14/10476 and in part by the Consejo Nacional de Ciencia y Tecnología under Grant 206425 and Grant 222476. The associate editor coordinating the review of this paper and approving it for publication was Dr. Anna G. Mignani.

M. V. Hernández-Arriaga, M. A. Bello-Jiménez, and A. Rodríguez-Cobos are with the Instituto de Investigación en Comunicación Óptica, Universidad Autónoma de San Luis Potosí, San Luis Potosí 78210, Mexico (e-mail: dmxsol@hotmail.com; m.bello@cactus.iico.uaslp.mx; roca@cactus.iico.uaslp.mx).

M. V. Andrés is with the Departamento de Física Aplicada y Electromagnetismo, Institute of Materials Science, Universidad de Valencia, Valencia 46100, Spain (e-mail: miguel.andres@uv.es).

Digital Object Identifier 10.1109/JSEN.2015.2475320

# Experimental Investigation of Fused Biconical Fiber Couplers for Measuring Refractive Index Changes in Aqueous Solutions

Marco V. Hernández-Arriaga, Miguel A. Bello-Jiménez, A. Rodríguez-Cobos,  
and Miguel V. Andrés, *Member, IEEE*

**Abstract**—A detailed experimental study of a simple and compact fiber optic sensor based on a fused biconical fiber coupler is presented, in which the sensitivity is improved by operating the coupler beyond the first coupling cycle. The sensor is demonstrated to perform high sensitivity measurements of refractive index changes by means of variation of sugar concentration in water. The device is operated to achieve a linear transmission response, allowing a linear relation between the sugar concentration and the output signal. The initial sensitivity was measured as 0.03 units of normalized transmission per unit of sugar concentration (g/100 mL), with a noise detection limit of a sugar concentration of 0.06 wt% of sugar concentration. Improvements in sensitivity were studied by operating the coupler beyond their first coupling cycles; achieving an improved sensitivity of 0.15 units of normalized transmission per unit of sugar concentration, and a minimum detection limit of 0.012 wt% of sugar concentration. From this result, the minimum detectable refractive index change is estimated as  $2 \times 10^{-5}$  refractive index unit.

**Index Terms**—Fiber optic sensor, fused biconical fiber coupler, refractive index sensor.

## I. INTRODUCTION

FIBER-OPTIC couplers have attracted considerable attention in recent years for their ability to detect small changes in the refractive index (RI) of liquid solutions. A fiber coupler is a four-port device with a transmission spectrum that is strongly affected by the refractive index of the surrounding medium due to the evanescent field that is generated along the coupling region [1]. This effect has proven to be useful for sensing applications [2]. Recent approaches of fiber-coupler based RI sensors include fused biconical fiber couplers [3]–[7], optical microfibers [8]–[12], photonic crystal fibers [13], [14], and specially designed

two-core optical fibers [15], [16], all of them offering the advantages of high sensitivity, *in situ* measurements, compact size, and immunity to external electromagnetic interference. Most of these sensors are codified in wavelength and the achieved sensitivities are in the range of 1,125 to 30,100 nanometer (nm) per refractive index unit (RIU), with a minimum detection limit of  $4 \times 10^{-4}$  to  $4 \times 10^{-7}$  RIU, respectively.

From the point of view of implementation, the necessity of expensive equipment, such as optical spectrum analyzers, for measuring the shift in wavelength heavily affects the use of fiber-coupler based RI sensors. Thus, it is worthwhile to consider an alternative scheme based on the dependence of the power coupling on the surrounding medium. The two complementary outputs of a fiber coupler enable a straightforward normalization, i.e. the ratio between the difference and the addition, which automatically compensates for power fluctuations. In earlier works the dependence of the power coupling of traditional fused biconical tapered couplers on the external RI has been presented and it has been proposed that it is possible to use such a structure to develop a fiber based refractometer [1], [17]. Tazawa et al. [2] have implemented this power measurement approach to demonstrate a biosensor with estimated  $4 \times 10^{-6}$  RIU detection limit. Recently, it has been demonstrated that modal interferometers based on integrated waveguides provide one of the best resolutions ever reported ( $2.5 \times 10^{-7}$  RIU) [18]. A fused biconical couplers is, in fact, a modal interferometer in which the phase difference between the symmetric and antisymmetric supermodes determine the power distribution at the output fibers. Small changes of the external RI do not modify substantially the coupling coefficient, but they generate a significant phase difference between supermodes. In terms of fiber-coupler based RI sensors, this last point deserves particular attention for the detection of slight changes in the refractive index of aqueous solutions. Although several schemes have reported this effect [1], [2], [17], they did not study the conditions for an optimal performance of the reported device. Here our purpose is the experimental analysis of a fused biconical fiber coupler, operated beyond the first coupling cycle, with a power transmission that depends on the surrounding medium.

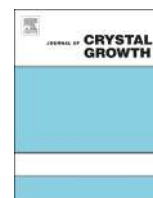
The objective is not only to gain insights into the dynamics of this kind of device, but also looking forwards an improvement of its performance. Based on this motivation, the

Manuscript received July 10, 2015; revised August 26, 2015; accepted August 27, 2015. Date of publication September 16, 2015; date of current version December 10, 2015. This work was supported in part by Promep under Grant DSA/103.5/14/10476 and in part by the Consejo Nacional de Ciencia y Tecnología under Grant 206425 and Grant 222476. The associate editor coordinating the review of this paper and approving it for publication was Dr. Anna G. Mignani.

M. V. Hernández-Arriaga, M. A. Bello-Jiménez, and A. Rodríguez-Cobos are with the Instituto de Investigación en Comunicación Óptica, Universidad Autónoma de San Luis Potosí, San Luis Potosí 78210, Mexico (e-mail: dmxsol@hotmail.com; m.bello@cactus.iico.uaslp.mx; roca@cactus.iico.uaslp.mx).

M. V. Andrés is with the Departamento de Física Aplicada y Electromagnetismo, Institute of Materials Science, Universidad de Valencia, Valencia 46100, Spain (e-mail: miguel.andres@uv.es).

Digital Object Identifier 10.1109/JSEN.2015.2475320



# Bulk lattice parameter and band gap of cubic $\text{In}_x\text{Ga}_{1-x}\text{N}$ (001) alloys on MgO (100) substrates



V.D. Compeán García<sup>a</sup>, I.E. Orozco Hinostroza<sup>b</sup>, A. Escobosa Echavarría<sup>c</sup>, E. López Luna<sup>a</sup>, A.G. Rodríguez<sup>a</sup>, M.A. Vidal<sup>a,\*</sup>

<sup>a</sup> Coordinación para la Innovación y Aplicación de la Ciencia y Tecnología (CIACyT), Universidad Autónoma de San Luis Potosí (UASLP), Álvaro Obregón 64, 78000 San Luis Potosí, Mexico

<sup>b</sup> Instituto Potosino de Investigación Científica y Tecnológica, Camino a la Presa San José 2055, Col. Lomas 4<sup>a</sup> Sección, 78216 San Luis Potosí, Mexico

<sup>c</sup> Electric Engineering Department, Centro de Investigación y Estudios Avanzados del IPN, Apartado Postal 14-740, 07000 México D.F., Mexico

## ARTICLE INFO

### Article history:

Received 9 September 2014

Received in revised form

11 February 2015

Accepted 13 February 2015

Communicated by: M. Weyers

Available online 25 February 2015

### Keywords:

A3. Molecular beam epitaxy

B1. Nitrides

B2. Semiconducting III–V materials

## ABSTRACT

$\text{In}_x\text{Ga}_{1-x}\text{N}$  (001) ternary alloys were grown on GaN/MgO (100) substrates in a plasma assisted molecular beam epitaxy system. We determined the in-plane [001] and in-growth [110] lattice parameters, as well as the bulk lattice parameter of the alloys for different In concentrations by high resolution X-ray diffraction. The In concentration was determined assuming Vegard's law for the alloy lattice parameter. The optical energy gap of  $\text{In}_x\text{Ga}_{1-x}\text{N}$  has been determined by transmittance measurements from absorption edges for several In concentrations. Our results show that the alloys have a direct band gap for all In concentrations and a bowing parameter  $b=1.84$ .

© 2015 Elsevier B.V. All rights reserved.

## 1. Introduction

GaN and InN in cubic phase have a band gap of 3.2 and 0.61 eV at room temperature [1,2] and a lattice parameters  $a=4.51$  Å [1] and 5.01 Å [2,3], respectively. The ternary alloy between GaN and InN has a great potential, among other wide and narrow bandgap III–V semiconductors, for fabrication of devices emitting in the blue–green–red spectral region [4–7] and multijunction solar cell devices. Therefore, InGaN has attracted attention in recent years due to the possibility of tuning its bandgap energy from UV (GaN) to IR (InN) only by varying the In molar fraction.

While the most stable and studied phase of III–N compounds is the hexagonal (wurtzite) structure, GaN and InN can also have the cubic zincblende structure as a metastable phase [8,9]. Nitrides with the cubic structure have several advantages compared to those with the hexagonal phase, for instance, a higher crystalline symmetry of the cubic nitrides that results in more isotropic properties and no spontaneous polarization induced–electric fields in the direction parallel to the  $c$ -axis. In addition, it is expected that cubic nitrides have superior electronic properties such as higher carrier mobilities, higher drift velocities, better doping efficiencies. Since the bandgap of  $\beta$ -InGaN is lower than that of

hexagonal InGaN with the same In molar fraction, it is possible to achieve visible light emission at a given wavelength with lower In molar fraction using  $\beta$ -InGaN.

Although several research groups have grown  $\beta$ -InGaN with low In content [10–17], the growth of cubic  $\beta$ -InGaN over the complete range of In concentration has not been accomplished. These limitations can be stem from several factors: (i) very narrow range of Ga, In and N fluxes to obtain ternary alloys for different In concentrations, in a plasma assisted molecular beam epitaxial system (PA-MBE), (ii) instability of molecular fluxes during the growth that leads to changes in the arrival rate of surface atoms species and therefore change of concentration or stoichiometry of layers, (iii) the strong tendency to incorporate the more stable hexagonal phase in the growth process, especially when dealing with substrates with high lattice-mismatch.

In this work, we report the growth of cubic  $\beta$ -InGaN(001) homogeneous epilayers on MgO (100) substrates by PA-MBE, and the characterization of the optical band gap and structural properties for several In concentrations in all range from  $x=0$  to  $x=1$ .

## 2. Experimental details.

Before growing  $\beta$ -InGaN ternary alloys, the MgO (100) substrate was cleaned in a sequential trichloroethylene and acetone ultrasonic

\* Corresponding author.

# Determination of the Thermal Expansion Coefficient of Single-Wall Carbon Nanotubes by Raman Spectroscopy

L. I. ESPINOSA-VEGA, A. G. RODRÍGUEZ, H. NAVARRO-CONTRERAS, and M. A. VIDAL

*Coordinación para la Innovación y la Aplicación de la Ciencia y la Tecnología (CIACYT) Universidad Autónoma de San Luis Potosí, San Luis Potosí, México*

Received 20 September 2013, Accepted 24 October 2013

We have examined the effect of high temperature on single-wall carbon nanotubes under air and nitrogen ambient by Raman spectroscopy. We observe the temperature dependence of the radial breathing mode and the G-band modes. The thermal expansion coefficient ( $\beta$ ) of the bundled nanotubes is obtained experimentally using the estimated volume from Raman scattering.  $\beta$  behaves linearly with temperature from  $0.33 \times 10^{-5} \text{ K}^{-1}$  to  $0.28 \times 10^{-5} \text{ K}^{-1}$  in air and from  $0.58 \times 10^{-5} \text{ K}^{-1}$  to  $0.47 \times 10^{-5} \text{ K}^{-1}$  in nitrogen ambient, respectively. The temperature dependence of the radial breathing mode Raman frequencies is consistent with a pure temperature effect.

**Keywords:** nanotubes, Raman spectroscopy, thermal expansion

## Introduction

Research on single-wall carbon nanotubes (SWCNTs) has been of great interest due to their potential applications given their electronic, mechanical, and thermal properties.<sup>[1]</sup> For certain applications, it is important to know the effect of high temperature on the properties of nanotubes. Raman scattering is one of the useful analysis techniques for the characterization of carbon nanostructures and investigation of their properties.<sup>[2–7]</sup> The Raman spectra from the SWCNTs have unique features, such as the G-band, D-band, and the radial breathing mode (RBM) peaks, which are related to the conductivity, the quality, and the diameter distribution of the SWCNTs. These measurements are usually obtained at room temperature but the temperature-dependent Raman frequency shift of carbon nanomaterials has also been reported.<sup>[2–7]</sup> The Raman spectra of SWCNTs can present some significant changes with increasing temperature such as frequency shifts, increase or decrease of the modes intensity, and the G-peaks broadening. A few authors have noted that the frequency decreases with increasing temperature for all the Raman peaks of straight nanotubes and rings in SWCNT bundles.<sup>[4]</sup> Raravikar et al. report a softening of the radial and tangential band frequencies with temperature and estimate the contribution of the factors that may be responsible for the observed temperature dependence of

the RBM frequency.<sup>[2]</sup> Maoshuai et al. obtain the Raman spectra of carbon nanobuds and compare them to those of SWCNT and show the thermal stability of these nanostructures.<sup>[8]</sup>

In this paper, we present the Raman Spectroscopy of SWCNTs when heated under two different ambient conditions: air and nitrogen. We show that the experimental data of the Raman shifts allow us to determine the thermal expansion coefficient of the nanotubes. The experimental coefficient is in good agreement with calculated values of the linear thermal expansion coefficient and X-ray measurements.<sup>[2,9]</sup> In air, the process is reversible up to a critical temperature between 855 and 875 K. If the nanotubes are heated above this temperature, the RBM and G phonon line-shapes change abruptly, and the process is no longer reversible. On the other hand, if the nanotubes are heated in nitrogen the phonon line-shapes of the Raman spectra do not deteriorate permanently with temperature, and the process remains reversible up to 1075 K. The irreversibility may be caused by oxygen adsorption when the nanotubes are heated in air, as revealed energy-dispersive X-ray spectroscopy (EDS) measurements.

## Experimental Details

The SWCNT bundles under study were purchased from Nano-Lab, Waltham, MA, USA. According to the vendor specifications, the nanotubes diameter is 1–1.5 nm with an average length of 1  $\mu\text{m}$  and approximately 90% pure. Raman scattering measurements were carried out in SWCNTs at different temperatures. The Raman scattering measurements were done using a Jobin-Yvon T64000 spectrometer

---

Address correspondence to A. G. Rodríguez, Coordinación para la Innovación y la Aplicación de la Ciencia y la Tecnología (CIACYT) Universidad Autónoma de San Luis Potosí, Álvaro Obregón 64, San Luis Potosí, S. L. P. 78000, México. E-mail: angel.rodriguez@uaslp.mx

# A multichannel reflectance anisotropy spectrometer for epitaxial growth monitoring

D Ariza-Flores<sup>1,2</sup>, J Ortega-Gallegos<sup>1</sup>, O Núñez-Olvera<sup>1</sup>,  
R E Balderas-Navarro<sup>1</sup>, L F Lastras-Martínez<sup>1</sup>, L E Guevara-Macías<sup>1</sup>  
and A Lastras-Martínez<sup>1</sup>

<sup>1</sup> Instituto de Investigación en Comunicación Óptica, Universidad Autónoma de San Luis Potosí, Alvaro Obregón 64, San Luis Potosí, SLP 78000, Mexico

<sup>2</sup> Cátedras Conacyt, Av. Insurgentes 1582, Crédito Constructor, Delegación Benito Juárez, DF 03940, Mexico

E-mail: [david.ariza@cactus.iico.uaslp.mx](mailto:david.ariza@cactus.iico.uaslp.mx)

Received 11 July 2015, revised 10 September 2015

Accepted for publication 14 September 2015

Published 12 October 2015



## Abstract

We report on a reflectance anisotropy (RA) spectrometer capable of measuring reflectance spectra on the 100 ms time-scale and sensitivity in the upper  $10^{-4}$  range. A multichannel lock-in amplifier was used to acquire 32 wavelengths RA spectra covering the 2.25–3.85 eV photon energy range, where the  $E_1$  and  $E_1 + \Delta_1$  transitions of GaAs and other technologically relevant III–V semiconductor are located. The RA spectra recorded during the first stages of the GaAs homoepitaxial deposition are presented for the first 0.38 monolayers of growth, showing significant changes in the lineshape with low noise. Thanks to the capabilities of this instrument, it is possible to observe in detail, in terms of the evolution of RA spectra, the processes carried out during the migration of surface reconstruction between two stable phases present in the homoepitaxial growth of GaAs.

Keywords: reflectance anisotropy spectroscopy, reflectance difference spectroscopy, surface processes, molecular beam epitaxy, optical characterization, GaAs homoepitaxy

(Some figures may appear in colour only in the online journal)

## 1. Introduction

Reflectance anisotropy (RA) spectroscopy (RAS, also termed reflectance difference spectroscopy (RDS)) is a non-invasive surface optical characterization technique based on the difference in reflectivity for two orthogonal polarized light beams [1]. For non-centrosymmetric crystals, this spectroscopy yields information on the near-surface region due to the breaking of cubic symmetry within the first atomic monolayers (ML's) [2, 3]. Taking advantage of its surface-specific nature, single-wavelength RA measurements have been successfully applied to the real-time monitoring of molecular beam epitaxy (MBE) growth of both III–V semiconductors [4–6] and Group IV semiconductors [7, 8], as well as to epitaxial growth under

moderate pressures, such as metal-organic chemical vapor deposition (MOCVD) [9, 10].

Single-wavelength RA measurements, nevertheless, hardly exploit the full spectroscopic potential of RAS and therefore a fundamental knowledge of detailed surface phenomena is lost. RA real-time spectroscopic measurements are thus highly desirable. The dynamics of surface phenomena taking place during epitaxial growth, on the other hand, demands subsecond spectrum acquisition times while typical acquisition times for monochannel spectrometers are considerably larger than one second [11], thus preventing the use of single-channel scanning spectrometers for this application. To this end, some efforts to achieve a faster RA spectral response have been reported by using multichannel spectrometers. For

## Characterization of Si<sub>3</sub>N<sub>4</sub>/Si(111) thin films by reflectance difference spectroscopy

Luis Felipe Lastras-Martínez<sup>1\*</sup>, Nicolás Antonio Ulloa-Castillo<sup>1</sup>, Rafael Herrera-Jasso<sup>1</sup>, Raúl Eduardo Balderas-Navarro<sup>1,2\*</sup>, Alfonso Lastras-Martínez<sup>1</sup>, Mahesh Pandikunta<sup>3</sup>, Oleg Ledyayev<sup>3</sup>, Vladimir Kuryatkov<sup>3</sup>, and Sergey Nikishin<sup>3\*</sup>

<sup>1</sup>Instituto de Investigación en Comunicación Óptica, Universidad Autónoma de San Luis Potosí, Alvaro Obregón 64, 78000 San Luis Potosí, S.L.P., México

<sup>2</sup>Paul-Drude-Institut für Festkörperelektronik, Hausvogteiplatz 57, Berlin, Germany

<sup>3</sup>Nano Tech Center, Texas Tech University, Lubbock, TX 79409, U.S.A.

E-mail: lflm@cactus.iico.uaslp.mx; rbn@cactus.iico.uaslp.mx; sergey.a.nikishin@ttu.edu

Received August 10, 2014; accepted October 19, 2014; published online January 14, 2015

Si<sub>3</sub>N<sub>4</sub> has become an important material with great technological and scientific interests. The lattice symmetry and the crystallinity quality of Si<sub>3</sub>N<sub>4</sub> thin films are fundamental parameters that must be determined for different applications. In order to evaluate the properties of Si<sub>3</sub>N<sub>4</sub> films, we used reflectance difference spectroscopy/reflectance anisotropy spectroscopy (RDS/RAS) to measure the optical anisotropy of Si<sub>3</sub>N<sub>4</sub> thin films (1–2 nm) grown by nitridation of two different Si(111) substrates, one with a 4.2° miscut off towards the [112] direction and another one with a nonintentional miscut. We demonstrate that, by modifying the measurement optical setup, we could increase the RD sensitivity and clearly display the optical response corresponding to the hexagonal symmetry of the Si<sub>3</sub>N<sub>4</sub> thin layer. Our results are in good agreement with reflection high energy electron diffraction (RHEED) measurements for both misoriented and oriented substrates. © 2015 The Japan Society of Applied Physics

### 1. Introduction

III–nitride (III–N)-based optoelectronic devices on Si substrates are very attractive owing to the low cost and large area of these wafers and the possibility of integration with other devices in the same platform.<sup>1)</sup> However, both the high thermal expansion coefficient difference and lattice constant mismatch between Si and III–N compounds lead to the cracking of III–N epitaxial layers.<sup>2)</sup> Molecular beam epitaxy (MBE) with a reflection high-energy electron diffraction (RHEED) system ensures in situ control of the growth process. The first crack-free thick AlN and GaN layers on Si(111)<sup>3,4)</sup> were grown by ammonia MBE, where the Si–N–Al interface<sup>5)</sup> was formed under in situ RHEED monitoring.

Plasma-assisted MBE (PAMBE) also yields high-quality III–N on Si(111).<sup>6)</sup> Both MBE approaches require the fabrication of a high-quality buffer (interfacial) Si<sub>3</sub>N<sub>4</sub> layer on silicon. This coherent Si<sub>3</sub>N<sub>4</sub>/Si(111) interface is formed by silicon wafer nitridation by which crystalline Si<sub>3</sub>N<sub>4</sub> films can be obtained.<sup>7–11)</sup> More recently, it has been found that the intentional growth of a Si<sub>3</sub>N<sub>4</sub> buffer layer on Si can be better controlled during PAMBE because the growth chamber is free of background ammonia and has a small amount of active nitrogen before plasma ignition.<sup>11–13)</sup> Note that the growth of Si<sub>3</sub>N<sub>4</sub> layers is conducted with a background pressure in the growth chamber of around  $1.33 \times 10^{-3}$  Pa. This ambient condition shortens the lifetime of the RHEED electron gun. Thus, the development and application of in situ monitoring methods that are less sensitive to the ambient conditions are important tasks.

Reflectance difference spectroscopy/reflectance anisotropy spectroscopy (RDS/RAS)<sup>14)</sup> is an optical modulation technique that is very sensitive to surface and crystal symmetries. In comparison with RHEED, which uses high-energy electrons (around 10 keV) that activate a chemical reaction between Si and residual carbon- and oxygen-containing molecules, RDS is a very low power optical method that does not activate any chemical process during in situ monitoring. It has recently been demonstrated that RDS is a powerful tool for the study of the first stages of epitaxial growth.<sup>15,16)</sup>

Additionally, RDS can be used in vacuum or in air to characterize the sample under in situ or ex situ conditions.

In the present work, we report the results of ex situ RD measurements carried out on Si(111) substrates and Si<sub>3</sub>N<sub>4</sub>/Si(111) heterostructures. Two Si(111) substrates were used: one with an  $\approx 4.2^\circ$  misoriented miscut towards the [112] direction and another one with a nonintentional miscut ( $\pm 0.5^\circ$ ). RD spectra revealed hexagonal symmetry for Si<sub>3</sub>N<sub>4</sub> thin films grown on both substrates. Because of the negligible oxidation rate of Si<sub>3</sub>N<sub>4</sub> thin layers at room temperature,<sup>17)</sup> we anticipate that RDS can also be used for the in situ monitoring of Si nitridation during the MBE process.

By following the evolution of the RD line shape around the optical transitions of Si<sub>3</sub>N<sub>4</sub> during the growth process, it is possible to perform a structural analysis to determine the crystallinity and symmetry of the layer. RD constitutes an attractive tool for the in situ monitoring of the growth process and can be used alone or in conjunction with most common monitoring techniques such as RHEED.

### 2. Experimental procedure

Ultrathin silicon nitride films were fabricated on low-resistance n-type Si(111) substrates. The experiments were carried out in the growth chamber of a GEN10 PAMBE system equipped with a UNI-Bulb RF nitrogen plasma source and a RHEED system. Note that we have already reported a good agreement between RHEED and low-energy electron diffraction investigation of Si nitridation during ammonia MBE.<sup>18)</sup> All two-inch silicon substrates were initially prepared by wet chemical etching<sup>3)</sup> that allows the formation of the hydrogen-saturated Si(111) surface with  $1 \times 1$  reconstruction at room temperature, as shown in Fig. 1(a). Radiative annealing of these substrates under ultrahigh-vacuum conditions at  $\approx 650^\circ\text{C}$  leads to the formation of the  $7 \times 7$  surface structure corresponding to the bare, hydrogen-free Si(111) plane, as shown in Fig. 1(b). Afterwards, the substrate temperature was raised to  $T_t \approx 830^\circ\text{C}$  until the surface reconstruction from  $7 \times 7$  to  $1 \times 1$  occurred. This transition temperature provides a convenient calibration point of the substrate temperature.<sup>19)</sup> On the basis of recent



## OPEN

SUBJECT AREAS:  
MATHEMATICS AND  
COMPUTING  
STATISTICAL PHYSICSReceived  
3 December 2014Accepted  
11 February 2015Published  
13 March 2015Correspondence and  
requests for materials  
should be addressed to  
J.E.-G. (jesquivel@fc.  
uaslp.mx)

# On a growth model for complex networks capable of producing power-law out-degree distributions with wide range exponents

J. Esquivel-Gómez<sup>1,2</sup>, P. D. Arjona-Villicaña<sup>3</sup>, E. Stevens-Navarro<sup>2</sup>, U. Pineda-Rico<sup>2</sup>,  
R. E. Balderas-Navarro<sup>1</sup> & J. Acosta-Eliás<sup>2</sup><sup>1</sup>Instituto de Investigación en Comunicación Óptica, Universidad Autónoma de San Luis Potosí (UASLP), México, <sup>2</sup>Facultad de Ciencias, Universidad Autónoma de San Luis Potosí (UASLP), México, <sup>3</sup>Facultad de Ingeniería, Universidad Autónoma de San Luis Potosí (UASLP), México.

The out-degree distribution is one of the most reported topological properties to characterize real complex networks. This property describes the probability that a node in the network has a particular number of outgoing links. It has been found that in many real complex networks the out-degree has a behavior similar to a power-law distribution, therefore some network growth models have been proposed to approximate this behavior. This paper introduces a new growth model that allows to produce out-degree distributions that decay as a power-law with an exponent in the range from 1 to  $\infty$ .

Among the topological properties of real complex networks (CN), one of the most studied is the out-degree distribution. This property describes the probability that a node in the network has a particular number of outgoing links. It has been found that in many real CN the out-degree behaves as a power-law distribution ( $P(k) \propto k^{-\gamma}$ )<sup>1-7</sup>. In order to approximate this type of out-degree distribution, some growth models for CN have been proposed. For example, Dorogovtsev *et.al.*<sup>8</sup> and Bollobás *et.al.*<sup>9</sup> have each developed a model capable of producing out-degree distributions that decay as a power-law with exponent  $\gamma = 2 + \frac{n_r + n + B}{m}$  and  $\gamma = 1 + \frac{1 + \delta_{out}(\alpha + \beta)}{\beta + \gamma}$ , respectively. Hence in both models the  $\gamma$  exponent is greater than 2. Esquivel *et.al.*<sup>10</sup> proposed a model that produces out-degree distributions that decay as a power-law where the  $\gamma$  exponent value is in the range between 0 and 1.

The previous models are not able to produce out-degree distributions with  $\gamma$  exponents in the range between 1 and 2. However, there are real CN where the  $\gamma$  exponent value is within this interval. For example, the social network of Flickr users<sup>6</sup>, the Any Beat network<sup>7</sup>, the online social network Epinions<sup>6</sup> and the network of flights between airports of the world (OpenFlights)<sup>6</sup> where the  $\gamma$  exponent for the out-degree distribution of these CN is close to 1.74, 1.71, 1.69 and 1.74 respectively.

This paper introduces a new model for growth of directed CN that allows to obtain out-degree distributions that decay as a power-law with exponents in the range  $1 < \gamma < \infty$ . That is, the proposed model is able to generate all exponent values found in documented real CN<sup>1-7</sup>.

It has been demonstrated that the growth and evolution of CN is influenced by local processes that shape its topological and dynamical properties<sup>11</sup>. The model proposed in here incorporates two local processes for adding new nodes to the network: a random out-degree selection and a copy of an already present out-degree value. In many large networks the maximum degree of a node (the degree of a node is the sum of its incoming and outgoing links) is much smaller than the number of nodes<sup>6</sup>. Thus, the proposed model assumes that the probability that a new node  $n_{new}$  selects a random out-degree decreases as the network grows. This probability is expressed as  $N^{-\alpha}$  where  $N$  is the total number of nodes in the network (including  $n_{new}$ ) and  $\alpha$  is a constant greater than 0. In other words, the probability that new nodes have an out-degree close to  $N$  tends to zero as  $N \gg 1$ .



## On the growth of directed complex networks with preferential attachment: Effect upon the prohibition of multiple links

J. Esquivel-Gómez\* and R. E. Balderas-Navarro†

*Instituto de Investigación en Comunicación Óptica  
Universidad Autónoma de San Luis Potosí (UASLP), Mexico*

\*jesquivel@fc.uaslp.mx

†rbn@cactus.iico.uaslp.mx

Edgardo Ugalde

*Instituto de Física*

*Universidad Autónoma de San Luis Potosí (UASLP), Mexico*

ugalde@ifisica.uaslp.mx

J. Acosta-Eliás

*Facultad de Ciencias*

*Universidad Autónoma de San Luis Potosí (UASLP), Mexico*

jacosta@uaslp.mx

Received 22 July 2014

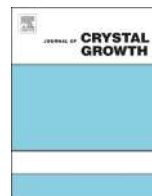
Accepted 15 October 2014

Published 25 November 2014

Several real-world directed networks do not have multiple links. For example, in a paper citation network a paper does not cite two identical references, and in a network of friends there exists only a single link between two individuals. This suggests that the growth and evolution models of complex networks should take into account such feature in order to approximate the topological properties of this class of networks. The aim of this paper is to propose a growth model of directed complex networks that takes into account the prohibition of the existence multiple links. It is shown through numerical experiments that when multiple links are forbidden, the exponent  $\gamma$  of the in-degree connectivity distribution,  $P(k_{\text{in}}) \sim k_{\text{in}}^{-\gamma}$ , takes values ranging from 1 to  $\infty$ . In particular, the proposed multi-link free (MLF) model is able to predict exponents occurring in real-world complex networks, which range  $1.05 < \gamma < 3.51$ . As an example, the MLF reproduces some topological properties exhibited by the network of flights between airports of the world (NFAW); i.e.  $\gamma \approx 1.74$ . With this result, we believe that the multiple links prohibition might be one of the local processes accounting for the existence of exponents  $\gamma < 2$  found in some real complex networks.

*Keywords:* Complex networks; power-laws; preferential attachment.

PACS Nos.: 11.25.Hf, 123.1K.



# Reflectance-difference spectroscopy as a probe for semiconductor epitaxial growth monitoring



A. Lastras-Martínez<sup>a,\*</sup>, J. Ortega-Gallegos<sup>a</sup>, L.E. Guevara-Macías<sup>a</sup>, O. Nuñez-Olvera<sup>a</sup>,  
R.E. Balderas-Navarro<sup>a</sup>, L.F. Lastras-Martínez<sup>a</sup>, L.A. Lastras-Montaño<sup>b</sup>,  
M.A. Lastras-Montaño<sup>c</sup>

<sup>a</sup> Instituto de Investigación en Comunicación Óptica, Universidad Autónoma de San Luis Potosí, Alvaro Obregón 64, San Luis Potosí, SLP 78000, México

<sup>b</sup> IBM T. J. Watson Research Center, Yorktown Heights, NY 10598, USA

<sup>c</sup> Department of Electrical and Computer Engineering, University of California, Santa Barbara, Santa Barbara, CA 93106, USA

## ARTICLE INFO

Communicated by A. Brown  
Available online 21 February 2015

### Keywords:

A.1 Characterization  
A.1 Surface processes  
A.3 Molecular beam epitaxy  
B.2 Semiconducting III–V materials

## ABSTRACT

We report on real-time reflectance-difference (RD) spectroscopic measurements carried out during the homoepitaxial growth of GaAs under As overpressures in the range  $P_{As} = 6 \times 10^{-7} - 5 \times 10^{-6}$  Torr. We found that the time-dependent RD spectrum is described in terms of two basic line shapes. One of these components is associated to the orthorhombic surface strain due to surface reconstruction while the second one has been assigned to surface composition. Results reported in this paper render RD spectroscopy as a powerful tool for the real-time monitoring of surface strains and its interplay with surface composition during growth.

© 2015 Elsevier B.V. All rights reserved.

## 1. Introduction

Reflectance-difference spectroscopy (RDS) is a noninvasive, contrasting technique that suppresses the bulk isotropic component of the optical reflectance spectrum of cubic semiconductors enhancing its surface-associated component. Both its noninvasive character and surface specificity make RDS a very attractive tool for monitoring the epitaxial growth of zincblende semiconductors, as it was first reported by Aspnes and collaborators [1]. The interpretation of reflectance-difference (RD) spectra, nevertheless, poses some challenges as the surface may become anisotropic for a number of physical mechanisms [2], including surface electric fields [3],  $\alpha$  and  $\beta$  dislocations [4], surface reconstruction strains [5,6] and surface dimers [7,8]. At the same time, time-resolved RD spectra measured during epitaxial growth would lead to a great deal of information on the kinetics of epitaxial growth, provided we can resolve them into their different components and determine the time-evolution of such components during growth.

Previously we reported on real-time RDS of homoepitaxial GaAs (001) grown by molecular beam epitaxy (MBE) [9]. For the growth we employed a As overpressure ( $P_{As}$ ) of  $1 \times 10^{-6}$  which led to a rich surface reconstruction evolution as growth progressed as well as to

considerable changes in RD spectrum line shape. We showed that the time-evolution of RD spectra during growth is well described in terms of two independent components, each with a specific physical origin. In this paper we report on the results of a study carried out within a range of As overpressures and demonstrate that our previous results can be extended to more general growth conditions.

## 2. Experimental details and results

Epitaxial growth was carried out on (001) GaAs substrates in a solid-source MBE chamber (Riber 32P). Epitaxial growth was carried out under four As overpressures ( $P_{As}$ ) ranging from  $6 \times 10^{-7}$  to  $5 \times 10^{-6}$  Torr at a growth rates from 0.14 to 0.23 ML/s as determined from RHEED oscillations. Growth substrate temperature was 520 °C in all cases. Epitaxial growth was initiated/interrupted by opening/closing the Ga shutter and lasted for about 45 s. Time-resolved spectroscopic RD measurements were performed with a rapid RD, 32-channel spectrometer attached to the epitaxial growth chamber. More details on the RD spectrometer are given elsewhere [10]. In order to correlate RD changes with surface reconstruction changes, RHEED patterns were acquired concurrently with RD spectra.

To prevent components associated to dislocations in the measured RD spectra, a 0.3  $\mu\text{m}$  thick GaAs buffer layer was grown prior to carrying out the experiments. Further, to avoid electro-optical contributions that may hinder the analysis of the RD line shapes, we did not intentionally dope the GaAs films.

\* Corresponding author.

E-mail addresses: [alm@cactus.iico.uaslp.mx](mailto:alm@cactus.iico.uaslp.mx),  
[alastras@gmail.com](mailto:alastras@gmail.com) (A. Lastras-Martínez).

# Adsorption of carbon monoxide on small aluminum oxide clusters: Role of the local atomic environment and charge state on the oxidation of the CO molecule

J. C. Ornelas-Lizcano and R. A. Guirado-López<sup>a)</sup>

Instituto de Física “Manuel Sandoval Vallarta,” Universidad Autónoma de San Luis Potosí,  
Alvaro Obregón 64, 78000 San Luis Potosí, México

(Received 3 November 2014; accepted 14 March 2015; published online 26 March 2015)

We present extensive density functional theory (DFT) calculations dedicated to analyze the adsorption behavior of CO molecules on small  $Al_xO_y^\pm$  clusters. Following the experimental results of Johnson *et al.* [J. Phys. Chem. A **112**, 4732 (2008)], we consider structures having the bulk composition  $Al_2O_3$ , as well as smaller  $Al_2O_2$  and  $Al_2O$  units. Our electron affinity and total energy calculations are consistent with aluminum oxide clusters having two-dimensional rhombus-like structures. In addition, interconversion energy barriers between two- and one-dimensional atomic arrays are of the order of 1 eV, thus clearly defining the preferred isomers. Single CO adsorption on our charged  $Al_xO_y^\pm$  clusters exhibits, in general, spontaneous oxygen transfer events leading to the production of  $CO_2$  in line with the experimental data. However, CO can also bind to both Al and O atoms of the clusters forming aluminum oxide complexes with a  $CO_2$  subunit. The vibrational spectra of  $Al_xO_y + CO_2$  provides well defined finger prints that may allow the identification of specific isomers. The  $Al_xO_y^+$  clusters are more reactive than the anionic species and the final  $Al_2O^+ + CO$  reaction can result in the production of atomic Al and carbon dioxide as observed from experiments. We underline the crucial role played by the local atomic environment, charge density distribution, and spin-multiplicity on the oxidation behavior of CO molecules. Finally, we analyze the importance of coadsorption and finite temperature effects by performing DFT Born-Oppenheimer molecular dynamics. Our calculations show that CO oxidation on  $Al_xO_y^+$  clusters can be also promoted by the binding of additional CO species at 300 K, revealing the existence of fragmentation processes in line with the ones experimentally inferred. © 2015 AIP Publishing LLC. [<http://dx.doi.org/10.1063/1.4916320>]

## I. INTRODUCTION

Aluminum oxide nanostructures have received a lot of attention in the last years due to their broad range of applications in materials, chemistry, and physics. In the solid state, the  $Al_2O_3$  compound is highly abundant in nature, the most stable phase being specified by the  $\alpha$ - $Al_2O_3$  corundum structure.<sup>1</sup> However, aluminum oxide is well known to be characterized by a remarkable structural diversity due to the existence of the so-called transition aluminas, which are metastable  $Al_2O_3$  polymorphs characterized by complex atomic structures.<sup>2</sup> It is important to precise that the  $\alpha$ -phase is not the most stable atomic configuration for nanostructured alumina. For example, in the case of thin films, Franchy<sup>3</sup> have assigned well defined features of the infrared spectra to a  $\gamma$ - $Al_2O_3$  crystalline structure. Furthermore, in the case of ultrathin NiAl films, extensive *ab initio* calculations and scanning tunneling microscopy experiments<sup>4</sup> have obtained atomic arrangements different from known bulk alumina structures.

In the small cluster regime, experiment and theory have been also nicely combined to explain the mass spectra of anionic aluminum oxide clusters,<sup>5</sup> electronic affinity measurements,<sup>6</sup> vibrational and photoelectron spectroscopy data,<sup>7</sup> as

well as the reactivity of  $Al_xO_y$  species towards various types of small gaseous molecules (e.g., molecular oxygen, methane, water, methanol, and carbon monoxide).<sup>8</sup> From the previous data, it has been concluded that aluminum oxide clusters exhibit a large variety of one-, two-, and three-dimensional structures, the lowest energy isomers being strongly dependent on cluster size, ionization state, oxygen content, and the presence of chemisorbed species on their surface. In the very small cluster regime, we would like to underline the existence of various closed in energy isomers, where rhombus-like and linear atomic arrays compete to define the ground state structure,<sup>7</sup> having energy differences varying in the range of 0.05-0.36 eV for different spin multiplicities and basis sets (see Tables I and VII of Ref. 7). In addition, Santambrogio and co-workers<sup>9</sup> have found the unexpected existence of conical configurations for  $(Al_2O_3)_{1-4}(AlO)^+$  systems, while Rahane and collaborators<sup>10</sup> have revealed that, for  $(Al_2O_3)_n$  ( $n = 1-10$ ) spheroidal particles, the lowest energy isomers show preference for having elementary units consisting of 4-membered  $Al_2O_2$  and 6-membered  $Al_3O_3$  rings.

Despite the previously described structural complexity of  $Al_xO_y$  systems as a function of dimensionality, we must precise that, in all cases, the interaction of Al atoms with the oxygen species is known to be of ionic character, the valence electrons of aluminum being transferred to O atoms. For example, in the

<sup>a)</sup>Electronic address: [guirado@ifisica.uaslp.mx](mailto:guirado@ifisica.uaslp.mx)

# Formation and Atomic Structure of Hierarchical Boron Nitride Nanostructures

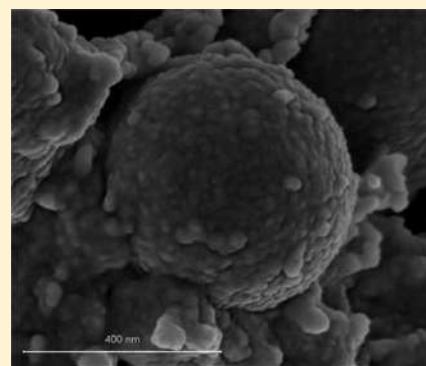
R. A. Silva-Molina,<sup>†</sup> E. Muñoz-Sandoval,<sup>‡</sup> R. Gámez-Corrales,<sup>§</sup> and R. A. Guirado-López<sup>\*,†</sup>

<sup>†</sup>Instituto de Física “Manuel Sandoval Vallarta”, Universidad Autónoma de San Luis Potosí, Álvaro Obregón 64, 78000, San Luis Potosí, SLP, México

<sup>‡</sup>Advanced Materials Department, IPICYT, Camino a la Presa San José 2055, Col. Lomas 4a. sección, San Luis Potosí 78216, SLP, México

<sup>§</sup>Departamento de Física, Universidad de Sonora, Apartado Postal 5-088, 83190, Hermosillo, Sonora, México

**ABSTRACT:** We report a combined experimental and theoretical study of boron nitride (BN) nanostructures synthesized by ball milling methodology. The BN nanostructures were obtained using *h*-BN powder under low-vacuum conditions and steel balls of different sizes. The HRTEM images of our samples show the formation of spheroidal BN nanoparticles with diameters as small as  $\sim 7$  nm which self-assemble into different hierarchical nanostructures such as two-dimensional layered materials, spheroidal configurations, and one-dimensional solid BN chains. The Raman spectra reveal an intense absorption band in the  $300\text{--}600\text{ cm}^{-1}$  region, which is absent in the spectra of BN nanotubes, previously synthesized BN nanoparticles, and in all bulk boron nitride polymorphs. Density functional theory calculations show that the Raman spectra are consistent with the formation of fullerene-like BN particles which also exhibit an intense absorption band in the  $200\text{--}800\text{ cm}^{-1}$  range dominated by a complex mixture of tangential, stretching, and radial breathing modes. Finally, by means of electron-beam irradiation experiments additional structural transformations can be induced on our hierarchical BN particles consisting in the formation of nanoholes of the order of 5 nm. Our here-reported BN nanostructures might lead to a wide range of potential applications.



## 1. INTRODUCTION

One of the most studied bulk layered materials in the past years is boron nitride in its hexagonal form due to its properties suitable for a wide range of applications.<sup>1–4</sup> The hexagonal *h*-BN structure is the most stable among BN polymorphs (when compared to the cubic and wurtzite BN), and within each layer, boron and nitrogen atoms are strongly bonded whereas the layers are held together by weak van der Waals forces similar to graphite. Consequently, *h*-BN is employed as a lubricant (at both low and high temperatures)<sup>5</sup> as well as protective and optical coatings.<sup>6</sup> Boron nitride ceramics are also typically used as parts of high-temperature equipment<sup>7</sup> and, in the electronics industry, as substrates for semiconductors as well as a structural material for seals.<sup>8</sup>

Other forms of boron nitride have been reported in the literature motivated by the increasing efforts intended to achieve the nanostructuring of BN. Boron nitride nanotubes were predicted in 1994<sup>9</sup> and experimentally synthesized in 1995.<sup>10</sup> The properties of BN nanotubes were found to be different from those obtained for carbon nanotubes. While the latter can be metallic or semiconducting depending on the rolling direction and radius, the former ones are defined by an insulating behavior with a wide bandgap of  $\sim 5.5$  eV, being independent of tube diameter, helicity, length, and number of walls.<sup>11</sup> Boron nitride nanotubes are characterized by a high thermal and chemical stability which defines them also as

promising materials to be used in hazardous and high-temperature environments.<sup>12</sup>

Spheroidal BN nanoparticles have also attracted the interest of the scientific community since they exhibit a higher surface area than nanomaterials with other morphologies. In addition, the production of BN particles with reduced diameters will allow its effective inclusion in different types of matrices forming various kinds of composite materials. The elaboration of BN nanoparticles has been undertaken by two main approaches: bottom-up and top-down methodologies. The former procedure involves the synthesis of BN nanostructures from boron- and nitrogen-containing molecular precursors using the chemical vapor deposition (CVD) method.<sup>13</sup> In the latter, mechanical cleavage, sonication-assisted exfoliation, and BN nanotube unzipping are the most employed approaches. With the use of the previous methodologies a large variety of BN nanoparticles with different sizes and morphologies have been produced, and interesting trends have been revealed. For example, Tang et al.<sup>14</sup> synthesized spherical boron nitride nanoparticles by the chemical vapor deposition reaction of trimethoxyborane [B(OMe)<sub>3</sub>] with ammonia, followed by high-temperature annealing. The as-synthesized BN spheres had

Received: July 21, 2015

Revised: October 23, 2015

## DIRECTIONAL COMPLEXITY AND ENTROPY FOR LIFT MAPPINGS

VALENTIN AFRAIMOVICH

Instituto de Investigación en Comunicación Óptica  
Universidad Autónoma de San Luis Potosí  
Karakorum 1470, Lomas 4a 78220, San Luis Potosi, S.L.P, Mexico

MAURICE COURBAGE

Laboratoire Matière et Systèmes Complexes (MSC)  
UMR 7057 CNRS et Université Paris 7-Denis Diderot  
10, rue Alice Domon et Léonie Duquet 75205 Paris Cedex 13, France

LEV GLEBSKY

Instituto de Investigación en Comunicación Óptica  
Universidad Autónoma de San Luis Potosí  
Karakorum 1470, Lomas 4a 78220, San Luis Potosi, S.L.P, Mexico

**ABSTRACT.** We introduce and study the notion of a directional complexity and entropy for maps of degree 1 on the circle. For piecewise affine Markov maps we use symbolic dynamics to relate this complexity to the symbolic complexity. We apply a combinatorial machinery to obtain exact formulas for the directional entropy, to find the maximal directional entropy, and to show that it equals the topological entropy of the map.

**1. Introduction.** There is a well-developed theory of rotation vectors (numbers) and rotation sets (see, for instance, [11] and reference therein). One considers a map  $f : M \rightarrow M$  generating a dynamical system and an observable  $\phi : M \rightarrow \mathbb{R}^d$  that classically is a displacement but might be an arbitrary function. The rotation vector of  $x$  is the Birkhoff average

$$\lim_{n \rightarrow \infty} \frac{1}{n} \sum_{i=0}^{n-1} \phi(f^i x),$$

provided that the limit exists, say, equals  $v$ . Then we may say that  $x$  moves in the direction  $v$ . A natural question arises: how many points move in the direction  $v$  if one measures them in terms of the topological entropy. The authors of [11] have mentioned several attempts to answer the question and have described their own approach. All of them including one of [16] are based on the thermodynamic formalism, in particular, on the variational principle. In our article we use purely topological (metric) approach to describe points moving to the prescribed direction.

---

2010 *Mathematics Subject Classification.* 37E10, 37E45.

*Key words and phrases.* Rotation interval, space-time window, directional complexity, directional entropy.

An essential part of this work has been written during V.A. and L.G. stay at the Nizhny Novgorod University supported by the grant RNF 14-41-00044. The authors also thank the referee for useful suggestions.

## Sequential memory: Binding dynamics

Valentin Afraimovich,<sup>1</sup> Xue Gong,<sup>2,a)</sup> and Mikhail Rabinovich<sup>3</sup>

<sup>1</sup>*IICO-UASLP, Karakorum 1470, Lomas 4a, San Luis Potosi, SLP 78210, Mexico*

<sup>2</sup>*Department of Mathematics, Ohio University, Athens, Ohio 45701, USA*

<sup>3</sup>*BioCircuits Institute, University of California San Diego, 9500 Gilman Dr., La Jolla, California 92093-0328, USA*

(Received 22 July 2015; accepted 22 September 2015; published online 13 October 2015)

Temporal order memories are critical for everyday animal and human functioning. Experiments and our own experience show that the binding or association of various features of an event together and the maintaining of multimodality events in sequential order are the key components of any sequential memories—episodic, semantic, working, etc. We study a robustness of binding sequential dynamics based on our previously introduced model in the form of generalized Lotka-Volterra equations. In the phase space of the model, there exists a multi-dimensional binding heteroclinic network consisting of saddle equilibrium points and heteroclinic trajectories joining them. We prove here the robustness of the binding sequential dynamics, i.e., the feasibility phenomenon for coupled heteroclinic networks: for each collection of successive heteroclinic trajectories inside the unified networks, there is an open set of initial points such that the trajectory going through each of them follows the prescribed collection staying in a small neighborhood of it. We show also that the symbolic complexity function of the system restricted to this neighborhood is a polynomial of degree  $L - 1$ , where  $L$  is the number of modalities. © 2015 AIP Publishing LLC.

[<http://dx.doi.org/10.1063/1.4932563>]

**Human mental functions like perception, cognition, and social interaction depend upon coordinated brain network activity. Such a coordination operates within noisy, overlapping modes of these networks on different levels of a cognitive hierarchy. Usually, the performance of cognitive task, for example, memory recall or generation of ideas, is a sequential dynamical process of switching among different information items or cognitive modes in a winnerless competitive manner. In fact, while we are thinking about a sequence of episodes or complex objects, the mind unifies several representing operations with different features of such episodes or objects. This is a binding process. For successful performance, the binding dynamics has to be stable or robust against noise. Mathematical aspects of this problem are considered in this paper.**

maintenance of information in mind, and the manipulation of this information for the purpose of achieving an immediate goal. The simplest example is remembering a phone number while picking up and dialing a phone. Working memory is also important for comprehending long written or spoken sentences, performing and holding in mind a string of new information or a series of movements. Declarative memories typically include information about time and place of an event, as well as detailed information about the event itself.

SM dealing with sequential order of thoughts or events provides the functional backbone to high-level cognition. Maintenance in SM is assumed to depend on the persistence of functional networks that represent memory information content. Imaging methods for measuring and analyzing population-level brain patterns show that activity of memory networks is highly dynamic.<sup>2</sup> Corresponding to the performance of the SM, brain dynamics involves different partially overlapping brain functional networks. Their interconnections change in time according to the performance stage, and can be stimulus-driven or induced by an intrinsically generated goal. Such brain activity can be described by spatiotemporal discrete patterns or sequentially changing dynamical modes.

At first glance, such a dynamics seems at odds with the very nature of keeping information items in SM. How can we recall a stable order of thoughts, episodes, etc., in mind while the brain activity is constantly changing? The answer to this question can be very useful for the understanding of different mental disorders and for the role of emotions in sequential memory binding.<sup>3</sup>

This paper is based on models that authors have developed before. In the paper Ref. 4 in 2001 and after this in Ref. 5, it was suggested a new paradigm for neuro-cognitive science—dynamical encoding of environmental or

### I. INTRODUCTION

There are several types of sequential memory (SM), which can be divided into the kinds of memory that are expressed explicitly, that is, by direct conscious access to information (declarative memory), and the kinds of memory that are expressed implicitly through changes in behavioral or physiological responses in the absence of conscious access (non-declarative memory). One particular form of declarative memory is episodic memory—the ability to encode and retrieve the sequence of events in our daily personal activities. Such memory is supported by cooperation of many cortical and subcortical structures.<sup>1</sup> Another type of sequential memory is working memory that is involved in the short-term

<sup>a)</sup>Electronic mail: [xg345709@ohio.edu](mailto:xg345709@ohio.edu)

# Two-dimensional heteroclinic attractor in the generalized Lotka–Volterra system

Valentin S Afraimovich<sup>1</sup>, Gregory Moses<sup>2</sup> and Todd Young<sup>2</sup>

<sup>1</sup> Universidad Autonoma de San Luis Potosi, IICO, Mexico

<sup>2</sup> Department of Mathematics, Ohio University, OH, USA

E-mail: [gm192206@ohio.edu](mailto:gm192206@ohio.edu)

Received 21 November 2014, revised 15 September 2015

Accepted for publication 3 March 2016

Published 5 April 2016



CrossMark

Recommended by Dr Dmitry Turaev

## Abstract

We study a simple dynamical model exhibiting sequential dynamics. We show that in this model there exist sets of parameter values for which a cyclic chain of saddle equilibria,  $O_k$ ,  $k = 1, \dots, p$ , have two-dimensional unstable manifolds that contain orbits connecting each  $O_k$  to the next two equilibrium points  $O_{k+1}$  and  $O_{k+2}$  in the chain ( $O_{p+1} = O_1$ ). We show that the union of these equilibria and their unstable manifolds form a two-dimensional surface with a boundary that is homeomorphic to a cylinder if  $p$  is even and a Möbius strip if  $p$  is odd. If, further, each equilibrium in the chain satisfies a condition called ‘dissipativity’, then this surface is asymptotically stable.

Keywords: heteroclinic orbits, Lotka–Volterra equations, unstable manifolds  
Mathematics Subject Classification numbers: 34A34

(Some figures may appear in colour only in the online journal)

## 1. Background

In the last decade it has become clear that typical processes in many neural and cognitive networks are realized in the form of sequential dynamics (see [5, 23, 14, 24, 26, 25, 2] and references therein). The dynamics are exhibited as sequential switching among metastable states, each of which represents a collection of simultaneously activated nodes in the network, so that at most instants of time a single state is activated. Such dynamics are consistent with the winner-less competition principle [2, 26]. In the phase space of a mathematical model of such a system each state corresponds to an invariant saddle set and the switchings are determined by trajectories joining these invariant sets. In the simplest case these invariant sets may be saddle equilibrium points coupled by heteroclinic trajectories, and they form a heteroclinic



# Nanostructure formation during relatively high temperature growth of Mn-doped GaAs by molecular beam epitaxy



A. Del Río-De Santiago<sup>a</sup>, V.H. Méndez-García<sup>a</sup>, I. Martínez-Velis<sup>b</sup>, Y.L. Casallas-Moreno<sup>b</sup>, E. López-Luna<sup>a</sup>, A. Yu Gorbachev<sup>c</sup>, M. López-López<sup>b</sup>, E. Cruz-Hernández<sup>a,\*</sup>

<sup>a</sup> CIACyT-UASLP, Sierra Leona Av. # 550, Lomas 2a Secc, San Luis Potosí, S.L.P. 78210, México

<sup>b</sup> Physics Department, CINVESTAV-IPN, Apdo. Postal 14470 D. F. México, México

<sup>c</sup> IICO-UASLP, Av. Karakorum 1470, Lomas 4a. Sección, San Luis Potosí, S.L.P. 78210, México

## ARTICLE INFO

### Article history:

Received 31 July 2014

Received in revised form 29 January 2015

Accepted 29 January 2015

Available online 7 February 2015

### Keywords:

MBE

GaMnAs

Nanostructures

Photoluminescence

Electrical properties

High temperature

## ABSTRACT

In the present work, we report on molecular beam epitaxy growth of Mn-doped GaAs films at the relatively high temperature (HT) of 530 °C. We found that by increasing the Mn atomic percent, Mn%, from 0.01 to 0.2, the surface morphology of the samples is strongly influenced and changes from planar to corrugated for Mn% values from 0.01 to 0.05, corresponding to nanostructures on the surface with dimensions of 200–300 nm and with the shape of leave, to nanowire-like structures for Mn% values above 0.05. From reflection high-energy electron diffraction patterns, we observed the growth mode transition from two- to three-dimensional occurring at a Mn% exceeding 0.05. The optical and electrical properties were obtained from photoluminescence (PL) and Hall effect measurements, respectively. For the higher Mn concentration, besides the Mn related transitions at approximately 1.41 eV, PL spectra sharp peaks are present between 1.43 and 1.49 eV, which we related to the coexistence of zinc blende and wurtzite phases in the nanowire-like structures of this sample. At Mn% of 0.04, an increase of the carrier mobility up to a value of  $1.1 \times 10^3 \text{ cm}^2/\text{Vs}$  at 77 K was found, then decreases as Mn% is further increased due to the strengthening of the ionized impurity scattering.

© 2015 Elsevier B.V. All rights reserved.

## 1. Introduction

Since the first successful growth of GaMnAs by molecular-beam epitaxy (MBE) showing ferromagnetic behavior [1–3], this diluted magnetic semiconductor (DMS) has received extensive attention because of the interest in the integration of both carrier induced ferromagnetism and spin-electronics with the existing semiconductor technology. However, these potential applications have been limited because of the low solubility of the Mn atoms, on the order of  $10^{18} \text{ cm}^{-3}$  or less, in the GaAs semiconductor matrix [4,5]. So far, the low-temperature (LT) MBE technique, below 300 °C, is the best method for the preparation of such materials with Mn concentrations many times higher than solubility. Unfortunately, LT-MBE and a high Mn concentration are characterized by a high content of point defects, such as As antisites and Mn interstitials [6,7] and by the poor crystallinity. Even when these defects can be reduced by optimizing the growth LT conditions or by post-growth annealing processes [7,8], the number of defects remains

elevated relative to GaAs films grown at relatively high temperature (HT) MBE (>500 °C). Successful growth of high crystalline quality GaMnAs at HT possesses a high potential for incorporating the ferromagnetic GaMnAs layers into GaAs-based microelectronic and optoelectronic devices. However, by growing at HT, precipitation of MnAs clusters in a GaMnAs matrix has been observed [9,10]. In addition, due to the inherent inhibition of uniform growth of GaMnAs with high Mn concentrations, little work has been published regarding HT MBE [11–13]. Despite this drawback, the number of As<sub>Ga</sub> in GaMnAs has been found to be reduced by increasing the substrate temperature ( $T_S$ ) [12,13]. Moreover, by growing at intermediate temperatures (IT), from 325 to 500 °C, some authors have been able to improve the optical properties of Mn-doped GaAs layers compared to LT GaMnAs [14,15]. In this paper, to gain more insight into relatively HT GaMnAs, we present a study of Mn-doped GaAs layers prepared by varying the nominal Mn atomic percent (Mn%) from 0.01 to 0.2 at a temperature of 530 °C.

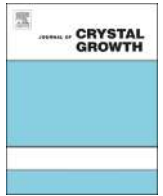
## 2. Experimental

The samples were grown by MBE using solid sources onto epitaxially grown GaAs (001) substrates. After growing a five-period AlAs

\* Corresponding author. Tel.: +52 4448262300.

E-mail address: [esteban.cruz@uaslp.mx](mailto:esteban.cruz@uaslp.mx) (E. Cruz-Hernández).





# Si-doped AlGaAs/GaAs(6 3 1)A heterostructures grown by MBE as a function of the As-pressure



Víctor-Hugo Méndez-García<sup>a,\*</sup>, S. Shimomura<sup>b</sup>, A.Yu. Gorbachev<sup>c</sup>,  
E. Cruz-Hernández<sup>a</sup>, D. Vázquez-Cortés<sup>b</sup>

<sup>a</sup> Center for the Innovation and Application of Science and Technology, Universidad Autónoma de San Luis Potosí, Av. Sierra Leona # 550, Col. Lomas 2a Sección, C.P. 78210 San Luis Potosí, Mexico

<sup>b</sup> Graduate School of Science and Engineering, Ehime University, 3 Bukyo-cho, Matsuyama 790-8577, Ehime, Japan

<sup>c</sup> Instituto de Investigación en Comunicación Óptica, Universidad Autónoma de San Luis Potosí, Av. Karakorum # 1470, Col. Lomas 2a Secc., C.P. 78210 San Luis Potosí, Mexico

## ARTICLE INFO

Available online 2 April 2015

### Keywords:

A1. Atomic force microscopy  
A1. Impurities  
A1. Characterization  
A3. Molecular beam epitaxy  
B2. Semiconducting gallium compounds

## ABSTRACT

The effects of doping with silicon (Si) AlGaAs layers grown by molecular beam epitaxy on GaAs (6 3 1)-oriented substrates as a function of the arsenic pressure ( $P_{As}$ ) is presented and compared with layers grown on (1 0 0) oriented substrates. The surface texture of the AlGaAs (6 3 1) films is composed by nanogrooves, whose dimensions depend on  $P_{As}$ . On the contrary, the MBE growth on the (1 0 0) plane resulted on rough surfaces, without evidence of formation of terraces. Mobility and carrier density of AlGaAs:Si layers grown on substrates (6 3 1) were studied as a function of  $P_{As}$ . The doping type conversion from p-type to n-type as a function of the As pressure is corroborated for high index samples. All the films grown on (1 0 0) exhibited silicon n-type doping. These observations were related with the amphotericity of Si, where it acts as a donor impurity occupying Al or Ga-sites or as an acceptor when it takes an As-site, depending on the competition that the Si atoms encounters with As for any of these sites. The acceptor and donor lines close to the AlGaAs transition observed by photoluminescence spectroscopy (PL) were affected by the incorporation of Si. When increasing  $P_{As}$  the energy of the main PL peak is redshifted for n-type AlGaAs layers, but it is shifted back towards high energy once the conduction type conversion takes place. X-ray diffraction patterns revealed high crystalline quality for samples grown at the highest  $P_{As}$ .

© 2015 Elsevier B.V. All rights reserved.

## 1. Introduction

Recently nanotechnology is generating new technological developments and it is envisaged as the most powerful and promising engine for the development of the society. In this emerging area, nanostructured materials are investigated for applications in electronics, optoelectronic and electro-mechanical devices. For example, semiconductor nanowires (NWRs) have emerged as one of the most versatile building blocks for integration of nanoscale devices with current technology. In addition, NWRs has been used for the investigation of basic aspects of one-dimensional systems (1D) [1–4]. In this direction, the growth of semiconductor materials on high-index substrates is a very important subject since it has been proved that, under suitable growth conditions, nanoscale step arrays and

nanogrooves can be self-assembled and later employed as templates for the synthesis of high quality semiconductor NWRs. Recently, highly ordered nanoscale step arrays were obtained in the homoepitaxial growth of GaAs on (6 3 1) oriented substrates [5], opening opportunities to the self-assembling of 1D arrays. Nevertheless, for the further application of these 1D systems, several challenges must be overcome. For example, the obtaining of n- and p-type doped AlGaAs layers is an essential step for the application of NWRs in optoelectronic devices. Si is known to be amphoteric dopant in III–V compounds [6,7]. For example in GaAs, Si behaves as donor or acceptor depending on the lattice site occupation: a Si atom occupying an As (Ga) site acts like an acceptor (donor). In the growth on high index substrates, the doping type strongly depends on both, growth conditions and on the particular substrate orientation [6–11].

In this work the Si doping of AlGaAs layers grown on (6 3 1)-oriented substrates as a function of the  $As_4$ -beam equivalent pressure ( $P_{As}$ ) is studied. The electrical properties obtained by

\* Corresponding author.

E-mail address: [victor.mendez@uaslp.mx](mailto:victor.mendez@uaslp.mx) (V.-H. Méndez-García).

## Terahertz harvesting with shape-optimized InAlAs/InGaAs self-switching nanodiodes

Irving Cortes-Mestizo,<sup>1</sup> Victor H. Méndez-García,<sup>1</sup> Joel Briones,<sup>2</sup>  
Manuel Perez-Caro,<sup>3</sup> Ravi Droopad,<sup>3</sup> Stefan McMurtry,<sup>4</sup> Michel Hehn,<sup>4</sup>  
François Montaigne,<sup>4</sup> and Edgar Briones<sup>1,2,a</sup>

<sup>1</sup>CIACyT, Universidad Autónoma de San Luis Potosí, San Luis Potosí 78210 SLP, México

<sup>2</sup>Department of Mathematics and Physics, ITESO, Jesuit University of Guadalajara, Tlaquepaque, 45604 Jalisco, Mexico

<sup>3</sup>Ingram School of Engineering, Texas State University, San Marcos, TX 78666, USA

<sup>4</sup>Institut Jean Lamour, CNRS, Université de Lorraine, F-54506 Vandoeuvre Les Nancy, France

(Received 25 August 2015; accepted 16 November 2015; published online 24 November 2015)

In this letter, self-switching nanochannels have been proposed as an enabling technology for energy gathering in the terahertz (THz) regime. Such devices combine their diode-like behavior and high-speed of operation in order to generate DC electrical power from high-frequency signals. By using finite-element simulations, we have improved the sensitivity of L-shaped and V-shaped nanochannels based on InAlAs/InGaAs samples. Since those devices combine geometrical effects with their rectifying properties at zero-bias, we have improved their performance by optimizing their shape. Results show nominal sensitivities at zero-bias in the order of 40 V<sup>-1</sup> and 20 V<sup>-1</sup>, attractive values for harvesting applications with square-law rectifiers. © 2015 Author(s). All article content, except where otherwise noted, is licensed under a Creative Commons Attribution 3.0 Unported License. [<http://dx.doi.org/10.1063/1.4936792>]

### I. INTRODUCTION

Self-switching diodes (SSDs) are planar semiconductor structures at the core of new advances in terahertz detection and generation.<sup>1-4</sup> The novel functionalities that those devices exhibit such as the ability to detect extremely weak signals without applied bias,<sup>5,6</sup> their high sensitivity<sup>7</sup> and their capability to operate in the terahertz regime<sup>5,8</sup> make the SSD concept a rewarding tool that have opened a broad range of applications.<sup>9</sup> In this regard, an area of emerging interest where SSDs find potential applications is energy harvesting of long wave thermal infrared emission emitted by Earth.<sup>10-12</sup> Earth's emitting thermal radiation represents a source of renewable energy, which covers the 7 – 20 μm spectral range<sup>13</sup> and also longer wavelengths, this range can be easily reached by increasing the SSD's mobility in low temperature process. The recently explored alternative to generate renewable energy from thermal radiation is the use of high-speed rectifiers coupled to terahertz and infrared antennas, known as rectennas.<sup>11</sup> These devices convert the free-propagating infrared radiation into DC power by employing a rectification mechanism. The efficiency of the rectennas is directly related to the performance of the employed rectifier.<sup>11</sup> In this context, novel functionalities like the high sensitivity without applied bias, make the SSDs good candidates for the development of high-speed rectifiers, able to recover the longer wavelengths of the thermal emission of Earth (>20μm) and also some other artificial thermal sources such as engines or furnaces.

Self-switching diodes are obtained by simply tailoring a narrow asymmetrical channel on a semiconductor. The channels asymmetry results in a remarkably diode-like behavior induced by the surface charges at flanges.<sup>14,15</sup> The SSDs can be understood as a two-dimensional field-effect transistor with gate and drain short-circuited where flanges act as a double lateral-gate terminal.<sup>6</sup> The basic

<sup>a</sup> Author to whom correspondence should be addressed. Electronic mail: [edgar.briones@uaslp.mx](mailto:edgar.briones@uaslp.mx), [edgarbriones@iteso.mx](mailto:edgarbriones@iteso.mx)





## Thermoluminescent properties of ZnS:Mn nanocrystalline powders



Arturo Agustín Ortiz-Hernández<sup>a,\*</sup>, Víctor Hugo Méndez García<sup>b,1</sup>,  
María Leticia Pérez Arrieta<sup>c,2</sup>, José Juan Ortega Sígala<sup>c,2</sup>, José de Jesús Araiza Ibarra<sup>c,2</sup>,  
Héctor Rene Vega-Carrillo<sup>d,3</sup>, Ciro Falcony Guajardo<sup>e,4</sup>

<sup>a</sup> DICIM-UASLP, Doctorado en Ingeniería y Ciencia de Materiales, Universidad Autónoma de San Luis Potosí, Sierra Leona No. 530 Col. Lomas 2da. Sección, C.P. 78210 San Luis Potosí, Mexico

<sup>b</sup> CIACYT-UASLP, Coordinación para la Innovación y Aplicación de la Ciencia y la Tecnología, Universidad Autónoma de San Luis Potosí, Sierra Leona No. 530 Col. Lomas 2da. Sección, C.P. 78210 San Luis Potosí, Mexico

<sup>c</sup> UAF-UAZ, Unidad Académica de Física, Universidad Autónoma de Zacatecas, Calzada Solidaridad esquina con Paseo la Bufa s/n, C.P. 98060 Zacatecas, Mexico

<sup>d</sup> UAEN-UAZ, Unidad Académica de Estudios Nucleares, Universidad Autónoma de Zacatecas Calle Ciprés #10, Fraccionamiento La Peñuela, C.P. 98068 Zacatecas, Mexico

<sup>e</sup> Departamento de Física, Cinvestav IPN, Apartado Postal 14-740, C.P. 07000 México D.F., Mexico

### HIGHLIGHTS

- Nanocrystals in powder of ZnS:Mn were synthesized using the co-precipitation method.
- The integrated TL spectra has a linear behavior on the dose range 5–100 mGy of  $\gamma$ -radiation.
- The kinetic parameters were obtained by the CGCD procedure.
- Results support the possible use of nanocrystalline ZnS:Mn as a new  $\gamma$ -dose nanoTLD.

### ARTICLE INFO

#### Article history:

Received 29 July 2014

Received in revised form

4 January 2015

Accepted 6 February 2015

Available online 13 February 2015

#### Keywords:

NanoTLD

Dosimetry

Thermoluminescence

ZnS:Mn nanocrystalline

Glow curve analysis

### ABSTRACT

Thermoluminescent ZnS nanocrystals doped with  $Mn^{2+}$  ions were synthesized by chemical co-precipitation method. From X-ray diffraction studies it was observed that the synthesized nanoparticles have cubic zinc blende structure with average sizes of about 40–50 nm. Morphology was analyzed by TEM. Photoluminescence studies showed two transitions, one of them close to 396 nm and other close to 598 nm, which is enhanced with increasing dopant concentration, this behavior was also observed in the cathodoluminescence spectrum. The thermoluminescence gamma dose-response has linear behavior over dose range 5–100 mGy, the glow curve structure shows two glow peaks at 436 K and at 518 K that were taken into account to calculate the kinetic parameters using the Computerized Glow Curve Deconvolution procedure.

© 2015 Elsevier Ltd. All rights reserved.

### 1. Introduction

During the last four decades the application of thermoluminescent dosimetry (TLD) in radiation protection has grown steadily in parallel with the worldwide progress (Azorin, 2013). Thermoluminescent dosimetry is the dominant dosimetric method for the measurement of doses in the medical physics personnel dosimetry and environmental monitoring (Azorin, 2013; Bos, 2006). In the search for materials with good dosimetric response, semiconductor nanocrystals have attracted large interest, specially the II–VI semiconductor compounds because they are easy to synthesize in the size range required being that in the nanometer size regimen. In the nanometer size regimen, which is

\* Corresponding author.

E-mail addresses: [icearturoortiz@hotmail.com](mailto:icearturoortiz@hotmail.com) (A.A. Ortiz-Hernández), [victor.mendez@uaslp.mx](mailto:victor.mendez@uaslp.mx) (V.H. Méndez García), [mlp.arrieta@gmail.com](mailto:mlp.arrieta@gmail.com) (M.L. Pérez Arrieta), [jjosila@hotmail.com](mailto:jjosila@hotmail.com) (J.J. Ortega Sígala), [araizaib@hotmail.com](mailto:araizaib@hotmail.com) (J.d.J. Araiza Ibarra), [hvegacarrillo@yahoo.com.mx](mailto:hvegacarrillo@yahoo.com.mx) (H.R. Vega-Carrillo), [cfalcony@fis.cinvestav.mx](mailto:cfalcony@fis.cinvestav.mx) (C. Falcony Guajardo).

<sup>1</sup> Tel.: +52 4448262300 x 8473.

<sup>2</sup> Tel.: +52 4929241314.

<sup>3</sup> Tel.: +52 4929227043 x 119.

<sup>4</sup> Tel.: 747 3800 x 6171.